PERFORMANCE STUDY OF A PV/T ASSISTED AIR SOURCE HEAT PUMP SYSTEM WITH A NOVEL ABSORBER IN SOLAR COLLECTOR

Xinru Wang MPhil. (Hons)

Thesis submitted to the University of Nottingham

for the degree of Doctor of Philosophy

Oct 2020

Abstract

Photovoltaic/thermal (PV/T) systems play an important role in solar system development, reducing pollution, and meeting the rapid increase in energy demand. PV/T can significantly improve energy transfer efficiency, hence improving its performance attracted extensive research attention. Different structures of the solar collector are proposed. To reduce the investment and cost of the experiment, several prediction studies are also conducted, as modeling its performance is meaningful for the optimization and design of the system.

In this thesis, we study a photovoltaic/thermal assisted air source heat pump (PV/T-ASHP) system with a novel absorber of the solar collector in Beijing. It is shown that for the whole year the electricity self-sufficiency is over 50 % and the heat self-sufficiency is 30.7 % in extreme conditions for the heating systems (e.g., December). Ambient temperature and solar irradiation change highly affect the performance of the whole system. In extreme weather e.g., a sunny day in December, the average COP is higher than 3.5. The payback time for this system is 9.5 years, and it reduces equivalent to 6.8 t of carbon dioxide (CO_2) emission per year. Based on the experiment results, we then predict the performance using an ANN. It is seen that the more considered factor, the higher the performance of the prediction model. It is also seen that in this case, an ANN with two hidden layers performs better than that of one hidden layer. Furthermore, the comparison results suggest that in practice it is required to find the best suitable ANN network before application.

Acknowledgements

I would like to express my sincere gratitude to my supervisors Dr. Liang Xia, Pro. Ruibin Bai and Pro. Yupeng Wu for their technical support and patient guidance which was significant and contribute a lot for this thesis. Moreover, I would like to thank Dr. Song pan and Jinshun Wu, who provide me with the valuable support and help me in both academic and financial aspects, especially when I was down, he inspired me a lot to insist and pursue the research work.

I would also like to express my appreciation to the ABE research group of Dalarna university in Sweden including Dr. Xingxing Zhang, Dr. Mengjie Han, Dr Yujiao Wang and so on, who gave me help during the first year of PhD including academic and life aspects.

I would like to thank my friends, close and far away in Dalarna and UNNC for their advice, understanding, encouragement, patience and supports to sustain me through the downs and depression during this difficult period. Furthermore, I would like to express the special appreciation to Miss Wan Wu for her help in experimental aspect.

Last but not least, I would like to give my great thanks to me beloved family for standing by me side all the time. Their love, patience and understanding support me to pursuit my PhD degree, without them, the life is by no means with happiness, color and journey.

Thanks again for everyone who had help me during my whole PhD period.

Contents

List of Figures

List of Tables

Nomenclature

Abbreviations	
ASHP	Air source heat pump
(BI)PV	(Building integrated) Solar photovoltaic
(BI)PV/T	(Building integrated) solar Photovoltaic/thermal
COP	Coefficient of performance
DA-SA	Direct expansion solar assisted
DHW	Domestic hot water
DMHP	Dual source multi-functional heat pump
DX-SA-ASHP	Direct solar assisted air source heat pump
EER	Energy efficiency ratio
EEV	Electronic expansion valve
EIF	Emission intensity factor
EPBT	Energy payback time
EROI	Energy returned in invested
FPC	Flat plate collectors

GHG	Greenhouse gases
HE	Heat exchanger
HP	Heat pump
HVAC	Heat, ventilation & air conditioning
IDX-SA-(ASHP)	Indirect solar assisted (air source heat pump)
IX-SAMHP	Indirect expansion solar-assisted multi-functional heat pump
LCA	Life cycle assessment
LCC	Life cycle cost
PCM	Phase change material
PV+AC	Photovoltaic + air conditioning unit
PV-ASHP	Photovoltaic assisted air source heat pump
PV/T	Photovoltaic/solar thermal
PV/T-ASHP	Photovoltaic/solar thermal assisted air source heat pump
PV-LHP	Photovoltaic loop heat pipe
RFHW	Floor heating without water

SAHP	Solar assisted heat pump
SF	Solar fraction
SIASHP	Solar integrated sir source heat pump
SPF	Seasonal performance factor
SRCD	Standard reverse-cycle defrosting
ST	Solar thermal
ST-ASHP	Solar thermal assisted air source heat pump
TCC	Tolerable capital cost
TES	Thermal energy storage
TRESE	Triple-sleeve energy storage exchanger
TRTHE	Triple tube heat exchanger
TS VC	Two-stage variable capacity
TTCC	Total tolerable capital cost
WH	Water heater
WSHP	Water source heat pump

Chapter 1: Introduction

1.1 Motivation for the project

The photovoltaic/thermal (PV/T) assisted air source heat pump (ASHP) systems have attracted more attention due to the rapid increase in energy demand. In this thesis, we built a PV/T-ASHP system with a novel absorber for solar collectors to enhance their performance and to develop a new structure for future marketable applications.

1.2 Overview

Recently, the concerns about the environmental effects of energy consumption have been significantly increased. The growing concerns encourage the versatile development of renewable and clean energy systems which can reduce the environmental pollution caused by fossil fuels, e.g., oil, and coal [1]. And the global renewable energy power capacity increased rapidly from 2007 to 2017 [2] . The total installed renewable power capacity at the end of 2017 is the highest in China, which is nearly 30% of the world's renewable power capacity-approximately 647 GW including 313 GW of hydropower. Among all renewable and sustainable energies, such as wind energy, soil energy, nuclear energy, solar energy is often considered the most important due to its accessibility throughout the world [3]. The renewable power capacity in China

accounts for 75% of global capacity in 2017 and China continues to be the leader in solar-based energy production in the world. Solar photovoltaic (PV) is the top source of new power capacity in several major markets, including China, and India.

Renewable energy systems based on solar energy are either based on solar-thermal energy or PV. Solar thermal converts solar energy into heat whereas PV converts solar energy into electric energy [4]. However, in the PV system, besides the electricity produced by the cells the solar energy also increases the cell surface's temperature. This may reduce the cells' efficiency in producing electric energy. Therefore, the heat produced by PV cells needs to be managed to reduce the surface temperature and to improve the performance of the cells. To address this issue, one approach is to combine PV with the solar thermal system, i.e., PV/T systems. PV/T systems enable dual usage of solar energy and produce both electricity and heat. PV/T improves the efficiency of the PV cells, and further produces more energy than either solar thermal, or PV system [5].

There are several different designs for thermal absorbers, the common designs include a sheet-and-tube structure, a rectangular tunnel with or without fins/grooves, flat plate tube, micro-channel heat pipe array/ heat mat, extruded heat exchanger, roll-bond heat exchanger, and cotton wick structure [6]. The sheet-and-tube absorber needs a lower investment due to the established industry and also provides high efficiency [7] [8], however, these absorbers are complex [9], and their heavyweights limit their applications [10]. Compared with other absorbers, the rectangular tunnel with or without fins/grooves has a lower weight and requires less investment [11] [12], but the heat transfer

efficiency is also lower [13] [14] [15] [16] [17]. For a flat plate tube, the resistance is high, although the contact between PV cells and absorber is simple [18] [19]. The micro-channel heat pipe also called heat mat, improves the heat transfer performance, but the heat transfer resistance is also increased [20] [21] [22]. Although extruded heat exchanger requires special design, its performance is high [23]. The roll-bond heat exchanger and cotton wick structure absorbers are limited in the application [24] [25] [26] [27] [28]. Currently, extruded heat exchanger is becoming a promising solution. Different arrangements and combinations can also create various flow channels [23]. However, only a few related studies are investigating the performance of such absorbers. Xu et al. [23] developed a super thin-conductive thermal absorber to regulate the PV working temperature by retrofitting the existing PV panel into the PV/T panel. The schematic structure of the thermal absorber and the associated prototypes were also shown in [23]. They found that the hybrid PV/T panel enhances the electrical return of PV panels by nearly 3.5% and increases the overall energy output by nearly 324.3%. The laboratory testing results demonstrated that the PV/T panel achieves an electrical efficiency of about 16.8% (relatively 5% improvement comparing to the stand-alone PV panel), and yields an extra amount of heat with a thermal efficiency of nearly 65%. Shen et al. [29] proposed a novel compact solar thermal façade (STF) with an internally extruded pin-fin flow channel. They showed that this construction of STF is beneficial for further design, optimization, and application including the provision of hot water, space heating/cooling, increased ventilation, or even electricity in the buildings.

1.3 Aims and objectives

There are still some issues that need to be addressed in the solar-assisted ASHP system. The main issues are as the following.

Experimental studies of (BI)PV/T-ASHP are only reported in a few papers, whereas most of the existing works are focused on the system concept and mainly used simulations for performance analysis. Nevertheless, (BI)PV/T-ASHP has not yet been largely applied and there still exist practical problems such as deployment and operation. Such issues have to be solved before the versatile development of this technology. Besides, optimization of the systems is required including the structure optimization of some components in the whole system [40], the operation mode optimization as its running mode should be dynamically adjusted as well as the capacity optimization for each component [54].

There is also a lack of standardized indicators to evaluate system performance [107]. Although COP and SPF are adopted in most papers, the process and the evaluation parameters are different from each other. Moreover, few papers [98] considered the environmental and economic parameters. Common standards and official certifications can help users to make better choices and make a comparison among different solar assisted ASHP systems.

This thesis aims to develop a solar collector based on a PV/T-ASHP system with a novel structure absorber. A pilot study of this PV/T-ASHP system is also

built for an office building and its performances including the electric and thermal are evaluated and analyzed in practical conditions.

The objectives of this thesis are:

- To develop a novel absorber structure for the solar collector by comparing different designs and choosing the best design;
- To build a practical PV/T-ASHP system for an office building and monitor its operation over a year;
- To test the solar collector performance by using experiment and validated simulation results;
- To analyze the system performance for a year of operation and evaluate its effectiveness in terms of environmental and economic impact ;
- To use an artificial neural network to predict the performance of the PV/T collector.

1.4 Thesis outline and content

Chapter 2 presents the literature review of the existing related researches on solar assisted air source heat pump system. The main related systems include solar thermal assisted system, photovoltaic assisted system, and the combination PV/T assisted system. The overall content of Chapter 2 is divided into simulation researches and experimental researches. The advantages and disadvantages of these systems are compared and the researches gap and future work directions are presented.

Chapter 3 presents the experiment setup. The design process of the PV/T system is also described, especially the absorber design. The absorber design choice is based on the simulation results by comparing six different structures. Furthermore, the setup of the whole system including the main devices and the measurement equipment is presented. The working principle and the detailed system information, e.g., the location and the installation information are also provided.

Chapter 4 presents the related experiment research on the thermal performance of PV/T collector. The performance of the PV/T-ASHP system during the heating season is measured and based on the results, the thermal performance of the PV/T collector is analyzed. To clarify the parametric study, a Matlab model is built to simulate the environmental factors such as solar radiation, temperature, and their impact on the thermal performance of the PV/T collector.

Chapter 5 presents the performance of the PV/T-ASHP system in 2019. The electric and thermal performance of the system is evaluated and analyzed for each month of the PV/T-ASHP system operation. Then the economic impact and payback time of this system is evaluated and its impact on the environment is also evaluated.

Chapter 6 presents the prediction of the performance of the PV/T collector using an artificial neural network (ANN). First, the related ANN researches on PV/T are reviewed and then the method of ANN is described. Different factors are considered and different ANN constructions are investigated and compared. Finally, the prediction results are analyzed and compared.

Chapter 7 presents the conclusions of this thesis. The main results of this case study of the PV/T-ASHP system are concluded and summarized in this chapter. Besides, a few future research directions including the experiment, the system, and the prediction method on the PV/T assisted air source heat pump system are described.

Chapter 2: Literature review and background

Solar energy and heat pump systems have been investigated for several decades, which are capable to increase the share of renewable energy. Many articles have been published on these two topics, however, literatures on solar assisted air source heat pump (ASHP) system of different technologies (solar thermal, photovoltaic and hybrid thermal/photovoltaic) are lacking, and thus leading to a practical challenge to evaluate different solar assisted ASHP systems in various scenarios [6]. The ASHP systems assisted by solar energy resources have drawn wide attentions owing to their great feasibility in buildings for space heating/cooling and hot water purposes. This review thus conducts a comprehensive review of the prevailing solar assisted ASHP systems, including their system boundaries, system configurations, performance indicators, research methodologies and major research findings.

We will concentrate the R&D work of three most prevailing solar assisted ASHP systems, including solar thermal assisted ASHP (ST-ASHP), photovoltaic combined ASHP (PV-ASHP) and photovoltaic/thermal (PV/T-ASHP). The entire article focused on the system level and organized as follows: section 2.1 introduces the system boundaries and assessment indicators of solar energy assisted ASHP systems. Section 2.2 reviewed the existing researches in recently near ten years papers. In section 2.3, promising research directions for

enlarging popular market application are discussed. Finally, salient conclusions are drawn in section 2.4.

2.1 System boundaries and performance indicators

2.1.1 System boundaries

System boundaries are important to understand the system and evaluate their performance in an equivalent condition. While in many studies, researchers do not clearly define the system boundaries of solar assisted ASHP systems, which makes it difficult to distinguish the different systems. Within IEA SHC Task 44/HPP Annex 38 (T44A38), the various system boundaries of solar and heat pump systems were introduced [30], shown in Figure 2- 1. Heat sources are identified in green, while purchased energy electricity is in grey. The red boxes on the right represent the energy supplied to users.

For conventional ASHP system, the heat pump gains heat from air and electricity from grid. In theoretical working principle, conventional ASHP system can supply heating, cooling and hot water for users, but with the climate limitations, ASHP systems generally need auxiliary heaters to meet the user demand in severe conditions. Solar assisted ASHP system can use both air and solar energy as the energy sources. The system configuration is explained in section 2.2 and the definitions of system boundaries shown in Figure 2- 1. There are also other sources heat pump system, like ground, water and so on, in this paper, we only show the air source heat pump system.

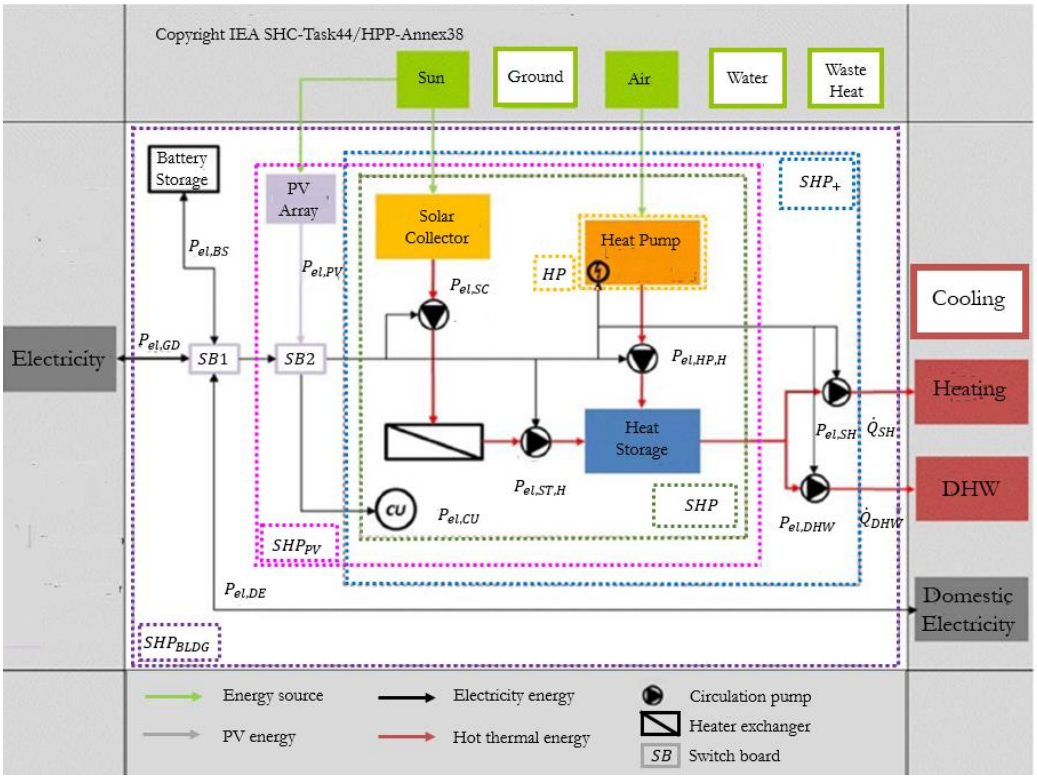

Figure 2- 1 Different system boundaries (figure based on the ongoing Task 53 [30] work).

According to the Task 53 [31], the definitions of solar assisted air source heat pump system boundaries (Figure 2- 1) mainly contain five types. The origin air source heat pump system is shown in orange dashed line (HP), which contains heat pump only. Adding solar collector system, which is concluded in green dashed line, the system is called solar assisted air source heat pump system (SHP), while above two system types are both without circulation water pump. System boundary SHP+ does include these pumps (blue dashed line). Solar assisted air source heat pump system with PV arrays (SHP_{PV}) is shown in red dashed line. It includes the PV array but without battery storage. With battery storage system, the system boundary is called solar assisted air source heat pump system (SHP_{BLDG}) for building heating, DHW and electricity (purple

dashed line) [32]. Corresponding to Task 53, in this paper, SHP+ is recorded ST-ASHP system, SHP_{PV} boundary is the PV-ASHP system and SHP_{BLDG} is the PV/T-ASHP system.

2.1.2 System configuration

There are many different ways of categorization of solar assisted ASHP system. In Figure 2-1, the system boundaries are identified on a component level, e.g. heat pump, or on a system level. Among them, the solar heat pump (SHP+) system includes the circulation pumps, while SHP and HP does not, which is used for comparing the assessment of the system environmental impact in operation [30]. Besides that, they can also be divided based on the type of heat demand to be served, e.g. heating, DHW [33]. In addition, the interaction way of the heat pump and the solar assisted system is another common categorization. This paper categorizes the solar assisted ASHP systems according to the evaporator component, including ST-ASHP, PV-ASHP, and PV/T-ASHP.

2.1.2.1 ST-ASHP system

For ST-ASHP system, the solar thermal collector convert solar irradiation into thermal energy that could be used directly by users or supply to ASHP. ASHP produce heat/cold for users. ST-ASHP system could supply different types of energy such as heating, cooling, hot water even the steam.

Based on the generation method, the ST-ASHP system can be categorized into direct expansion solar assisted (DX-SA) and indirect expansion solar assisted system (IDX-SA). In DX-ST-ASHP, the heat pump and solar thermal system

work together as one combined system and solar thermal collector acts as the system evaporator. Indirect expansion solar thermal and air source heat pump (IDX-ST-ASHP) systems can generally be classified in parallel, serial, regenerative (Figure 2- 2) and complex system concepts by the interaction between solar thermal and heat pump [30, 34]. The serial type is common in solar and ground source heat pump combination system, while for solar thermal assisted air source heat pumps system, a statistical analysis on market-available ST-ASHP systems can be found in Ruschenburg et al. [35, 36]. Their main result indicated that the parallel systems are the market-dominating system concepts (61% of the surveyed systems) [36]. In parallel configuration (Figure 2-2 (a)), solar collector and air source heat pump independently supply heating and/or DHW, or cooling to users.

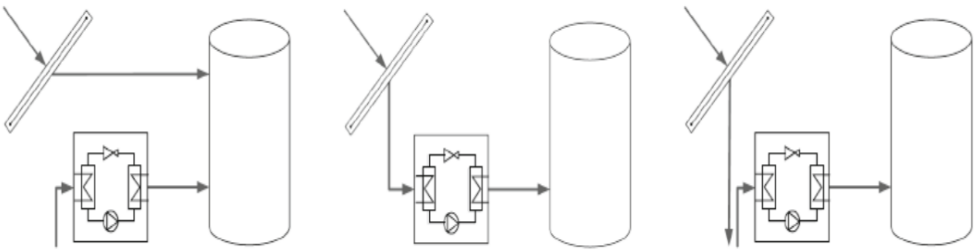

(a) (b) (c)

Figure 2- 2 Classification of solar thermal and heat pump systems in parallel, serial and regenerative system concepts: (a) parallel; (b) serial; (c) regenerative [33,34]

ST-ASHP system commonly use two types of media: liquid and air. Based on media temperature, ST-ASHP is divided into two types. Low and medium temperature is less than 100 ℃,while the other is high temperature [35]. While

the common temperature used in real application of ST-ASHP system usually is the low and medium temperature types.

2.1.2.2 PV-ASHP system

Solar photovoltaic (PV) [37] can directly convert sunlight into electricity without any heat engine to interfere. The ASHP partially covered by the electricity produced by PV in the buildings is called PV-ASHP system. Nowadays, there is also another popular type of the PV which integrated with the building such as the roofing, window and so on, called building-integrated photovoltaic (BIPV) systems. PV-ASHP system could supply heating, cooling and electricity to buildings. The principle of PV/T-ASHP system is that the electricity produced by the PV can be supplied to the ASHP which supply the heating or cooling to the building, when the PV cannot meet the demand, the ASHP can gain electricity from the grid. Meanwhile, the overcome electricity produced by PV can also be added to the grid in the electricity producing time, e.g. midday in the sunny days when the load of building is also small.

PV-ASHP system could be classified direct expansion and indirect expansion types. Moreover, it can also be classified by the array types [38]. While the common classification is based on the lighting absorbing materials. The most common material is silicon which include silicon, amorphous silicon and crystalline silicon and there are other materials such as cadmium telluride and cadmium sulphide, organic and polymer cells and hybrid photovoltaic cell and some other cells.

2.1.2.3 PV/T-ASHP system

Normally, PV module only converts 4-17% of incoming solar radiant into electricity, which varies along with the material and working conditions, and as a result, much more solar energy is converted into heat. Over high ambient temperature could reduce the efficiency of the PV and cause damage to the structure to the modules [35]. PV/T can produce electricity as well as heat, which can cool the surface temperature of cells. Like the BIPV system, the PV/T integrated with building called BIPV/T system, which can save the space than two separated arrays of PV and solar thermal collectors. Combined with ASHP, PV/T-ASHP system can supply heating and domestic hot water (DHW), even cooling for buildings in the future.

While in PV/T-ASHP system, as PV/T collectors can not only provide heat, but also produce electricity, the common type is in serial connection, as the PV/T collectors are used to regenerate the heat exchanger [39]. PV/T systems can be divided into five types: air cooled system, water cooled system, both water and air cooled, using PCM PV/T system and using heat pipes in PV/T system [40]. And more recently, using PCM in PV/T system is concentrated [41]. And based on the integrated fabric of the building, the BIPV/T system can be divided into wall integrated, window integrated, roof integrated and façade integrated systems. For the whole PV/T-ASHP system, according to the application, there are heating, DHW intents types.

2.1.3 System performance indicators

With a variety of goals and system boundaries, there are many different performance indicators to evaluate the solar assisted ASHP systems. In this section, the performance of solar assisted ASHP system is regarded from a boarder concept including energy, economy and environment aspects, within certain boundaries under given operating conditions for a defined time.

2.1.3.1 Energetic performance indicators

Coefficient of performance (COP) and energy efficiency ratio (EER) are usually used as the energetic performance indicators for heat pump unit under defined operating conditions, as the EER is used for cooling application in European [30]. While seasonal performance factor (SPF) is used to express the overall system efficiency including all auxiliary components, e.g. storages. There are also other figures, e.g. collector thermal efficiency, and the component performance figures such as thermal output of collector, in this paper, they are not listed, as they are not common in the reviewed solar assisted ASHP system papers.

COP or EER [42, 43] is evaluated by measuring the temperature of the inlet and outlet of the heat transfer media and the electricity consumption, as written in Eq. (2-1).

$$COP_{sys} = \frac{Q_t}{P_{el}} \tag{2-1}$$

Where, COP_{sys} is the overall performance of system, Q_t is the heat gained in system, P_{el} is the power consumption.

System energy efficiency ratio (EER_{SYS}) can be calculated from the energy efficiency ratio of the unit (EER_{UNIT}) and the Solar Contribution (SC) by Eq. (2-2).

$$EER_{SYS} = EER_{UNIT} \frac{100 - SC(\%)}{100} \tag{2-2}$$

Seasonal performance factor (SPF) is the ratio of overall useful supplied energy to users to the overall electricity used during operation, which is defined in Eq. (2-3). Where. Q_{SH} is the heat amount for space heating, Q_{DHW} is the heat amount for domestic hot water.

$$\text{SPF} = \frac{Q_{SH} + Q_{DHW}}{P_{el}} \tag{2-3}$$

EER is used for cooling application, while for heating and hot water, COP and SPF are commonly used. So the definition of COP and SPF not including EER in Eq. (2-1) and (2-3) for electricity for different system boundaries is concluded in [32]. However, there are very limited information that can be found on the EER, COP or SPF at building level in existing literatures, which thus need more attention in the future.

Table 2- 1 Definition of SPF/COP and the total power for different system boundaries in Figure 2- 1 [32]

System boundary	Definition of COP/SPF	Total Electrical power
HP	COP_{HP}/SPF_{HP}	$P_{el} = P_{el,HP} + P_{el,AS}$
SHP	COP_{SHP}/SPF_{SHP}	$P_{el} = P_{el,HP} + P_{el,AS} + P_{el,SC} + P_{el,ST,H} + P_{el,HP,H} + P_{el,CU}$
SHPPV	$COP_{SHP,PV}/SPF_{SHP,PV}$	$P_{el} = P_{el,HP} + P_{el,AS} + P_{el,SC} + P_{el,ST,H} + P_{el,HP,H} + P_{el,CU} - (P_{el,SHP} \cap P_{el,PV})$
SHP+	COP_{SHP+}/SPF_{SHP+}	$P_{el} = P_{el,HP} + P_{el,AS} + P_{el,SC} + P_{el,ST,H} + P_{el,HP,H} + P_{el,CU} + P_{el,SH} + P_{el,DHW}$

Where, electricity use $P_{el,HP}$ and $P_{el,\mathrm{AS}}$ are the total electrical energy use of the heat pump compressor and fans (system boundary HP). $P_{el,SC}$ is the total electrical energy use of solar circuit, $P_{el,EH}$ is the total electrical energy use of auxiliary electrical heater (if included, not in this case). $P_{el,CU}$ is the total electrical energy use of control units, while the others are all circulation pump consumption. $P_{el,\mathrm{ST,H}}$ and $P_{el,\mathrm{ST,C}}$ are the total electrical energy use of hot and cold storage circulation pumps. $P_{el,\mathrm{SH}}$ and $P_{el,DHW}$ are electric space heat and DHW circulation pump consumption. $P_{el,SHP} \cap P_{el,PV}$ is the intersection electric power of heat pump consumption and PV generation.

2.1.3.2 Economic performance indicators

In terms of economic aspect, the capital investment is always considered. Christos et al [44] compared the net present value of all investment including the capital cost and the electricity consumption of solar assisted ASHP with WSHP and fan coil system. Evangelos et al [45, 46] also considered the total cost to examine the system. Besides investment, the payback time, the energy saving also compared by [45].

Life cycle cost (LCC) in Eq.(2-4) are used to compare different systems. Stefano Poppi et al [47] developed an economic model based on a comparative cost-analysis between the system variations and the reference system for simulation.

$$\mathrm{LCC} = C_{system} + C_{installation} + C_{maintenance} + C_{energy\ usage} \qquad (2\text{-}4)$$

Accurate estimation of solar assisted ASHP system's initial investment is difficult because the installed costs can vary significantly depending on the scope of the plant equipment, geographical area, competitive market conditions, special site requirements, and prevailing labour rates. Thus, an alternative approach to conventional economic feasibility analysis is adopted, which involves the calculation of the ‘‘tolerable capital cost” (TCC) of the upgrades [48]. TCC is the capital cost for an energy saving upgrade that will be recovered based on the annual savings, the number of years allowed for payback, and the estimated annual interest and fuel cost escalation rates.

Other papers concentration on the payback time, and the energy payback time (EPBT) [49, 50] and energy returned on energy invested (EROI) [43] for the

solar assisted ASHP life cycle assessment (LCA). LCA is a methodology to assess the environmental impact of a product or service over its whole life cycle, which may include processes from the extraction of raw materials to recycling or disposal [51].

$$\text{EPBT(year)} = \frac{Embedded\ (primary) energy\ (MJ/m^2)}{Annual\ (primary) energy\ \ (MJ/(m^2 \cdot year))} \quad (2\text{-}5)$$

$$\text{EROI} = \frac{\text{lifetime energy output}}{\text{Embedded energy}} \quad (2\text{-}6)$$

However, compared with energetic performance indicators, the economic performance indicators are less popular. Most of the papers that mentioned the economic performance only simplified compared the investment or showed the payback time. Moreover, different researches referred different contents on economic aspect, which is difficult to make a comparison among different systems.

2.1.3.3 Environmental performance indicators

For environment impact, some papers [52, 53] analysed the greenhouse gases (GHG) especially CO_2 emission reduction. The GHG emissions are evaluated and reported as "equivalent CO_2" (CO_{2e}) emitted per unit input energy, which is determined based on the fuel type and efficiency of the energy conversion devices. The GHG emission associated with electricity use is determined based on the amount of fossil fuel consumption to produce and deliver electricity to a building, which is updated in each time step using the actual fossil fuel

consumption [54]. While CO_2 emission by wood combustion returns to the atmosphere where the CO_2 that was recently removed by photosynthesis as the tree grew [55]. For comparison among different systems, the GHG emission intensity factor (EIF) is defined. The GHG EIF is defined as the level of CO_{2e} emission for generation and delivery of 1 kWh electricity to the end-user. While, usage need to take into account the different electricity generation ways during peak and base periods. Thus, different average and marginal GHG EIFs are developed to address electricity generation within the base and peak periods [55]. Moreover, besides CO_2, the greenhouse gas emission of PV-ASHP like SO_2 and NOx emission was also calculated in some papers [52,55].

Although there are some researches noticed the environmental performance of solar assisted system, the number is few, and most of them only mentioned these results in few sentences. There are a few reason, the first is that there is no standard calculation method for all researches to make a comparison. Second, the measurement for different systems are also different, as different authors focus on different aspects on their own system.

2.2 Simulation researches and the related results

Table 2- 2 summarizes the main research findings of simulation in solar assisted ASHP, including the tools applied, the built model types, the corresponding models' operation conditions, the input and output parameters and their main results.

The simulation models for solar assisted ASHP system include TRNSYS, CFD, self-developed Matlab and mathematic model, in which TRNSYS is dominant. The second most used models are built on various mathematical equations.

In the TRNSYS models, these models are named by the numbers, which can refer to TRNSYS guidline. Type 56 is the most used model for multi-zone buildings and type 832 is commonly used for collector. Heat exchanger is built by different types including type 805, type 91 and type 557a. Heat pump models are type 401 for compressor heat pump, type 655-3, type 665, type 887, and type 841 for CO_2 heat pump. For store devices, type 340, type 534 and type 4 are used. Besides, type 15 is applied for weather data reading and processing, type 6 is used for electrical heater.

The operation conditions can be classified by outdoor environment including air temperature, solar irradiation and operation mode including heating mode, cooling mode and DHW, while for ASHP with phase change material (PCM-ASHP) system, operation modes include charging/discharging mode.

For the input parameters, the surrounding conditions [56], including the location which means the solar and ambient air temperature, are the most important parameters. Moreover, some researchers highlight the components' design and operation parameters. To evaluate the solar assisted ASHP system, COP, SPF, payback time and GHG are often used to assess the system performance.

In the following subsections, we will discuss the detailed simulation R&D status of each type of solar assisted ASHP systems, mainly by choosing several representative cases from this table.

Table 2- 2 Summary of simulation methods and the related results of solar assisted ASHP systems

Ref	System	Tool	Model	Location	Operation Conditions	Input data	Building Types	Evaluation parameters	Results
[57] [58]	parallel ST-ASHP	TRNSYS 17	Type 832 QDT multimode model for collector; Type 340 for store; Type 805- heat exchanger; Type 887-heat pump	Zurich and Carcassonne, Sweden	SFH100 (100 of single family houses) in Carcassonne	location and house model; interest rate, inflation rate and price of electricity;	laboratory	SPF; Total electricity use; Annual DHW discharge energy; collector area; tank volume; UA-value of DHW heat exchanger; Payback time;	▪SPF= 2.84; ▪EPBT= 10 years ▪ system electricity change between 305 and 552 kW h/y when collector area from 5 to 15 m^2; ▪main influence for system including annual DHW discharge energy, collector area, UA-value of DHW heat exchanger and heat pump size;
[59]	Different SAHP (review)	TRNSYS	Type 56-ASHP; Type 655-3-default heat pump	—	—	location and equipment	—	energetic comparison;	▪ASHP system cost lowest investment and highest electricity among solar assisted WSHP and fan coil heating system;

						parameters;		indoor temperature distribution; financial evaluation;	
[60]	parallel ST-ASHP/ST-GSHP	TRNSYS	Type 56-building; Type 832-collector; Type 401-compressor HP; Type 557a-borehole heat exchanger; Type 340-multiport storage tank	Helsinki, Strasbourg, Athens	solar heating/ CO_2 heat pump heating mode	Location;	building type SFH45 (TRNSYS)	SPF;	▪The design of SHP systems depending on the boundary conditions of the specific application; ▪COP of ASHP= 3.66
[61]	solar combined CO_2 heat pump	TRNSYS	Type 71-solar collector; Type 841-CO_2 heat pump; Type 4- storage tank; Type 534- operation tank;	Shanghai, China	—	Taiyuan, Shanghai	residential building	volume of storage tank and operation tank;	▪the optimization values: storage tank volume=2.21 m^3 and operation tank volume= 0.3 m^3 ▪the optimized system can save 14.2% electricity and solar fraction can reach 71.1%.

[62]	PV-LHP/SAHP	mathematical model	—	Qinhuangdao, China	solar/air source heat pump	solar irradiation and ambient air temperature	residential buildings	operation performance of under typical working conditions; economic feasibility analyses;	▪solar energy utilization efficiency decreased with solar irradiation growth and ambient temperature decrease; ▪ monthly average COP of heat pump modes= 3.10; ▪The annual solar heating ratio of the system is up to 57.8%. ▪ Life cycle cost of the PV-LHP/SAHP could be reduced by 29.6% than ASHP.
[63]	ST-ASHP	TRNSYS 17	Type 1-quadratic efficiency collector; Type 3- pump; Type 2b-controller; Type 15-weather data reading and processing	Taipei and Kaohsiung	—	setting parameters for components	lab-scale system	SPF and solar fraction; Payback time;	▪The overall efficiency of a DHW system improved, while the cost is also increased; ▪ EPBT= 5 years; ▪ SPF= 4.56 / 4.93 in Taibei and Kaohsiung
[64]	DX-SHPWH	mathematical model	—	Xi'an, China	the solar radiation ranges; ambient air temperature	component parameters	--	heating capacity; COP;	▪Solar irradiation and ambient air temperature have a great effect on the system performance;

					superheating degrees of the two evaporators;				▪The COP on average increases by 14.1%; ▪Given solar radiation of 500W/m2, the COP=4.98 and Qc = 605 W
[65]	ST-ASHP	TRNSYS	one-node model	Geneva (Switzerland).	(i) direct solar heat production; (ii) storage discharge, (iii) activation of the HP, with surplus production (iv) direct electric heating	hourly weather data; hourly load demand;	multifamily buildings	SPF;	▪SPF of system achieved maximize 4.4 and when temperature distributed, the SPF is 3.1-4.1; ▪SPF of system achieves 5 is potential ▪investment and roof area reality condition are not considered;
[66]	PV-ASHP; PVT-WSHP;	TRNSYS	Type 56-building; Type 655-3-heat pump;	Greece	heating mode	undefined parameter; the collecting area and storage	commercial building	monthly load; COP; energy consumption;	▪lower energy consumption than ASHP and fan coil heating system; ▪Indoor temperature is better in solar driven heat pump system;

						tank volume			▪The COP is near 4 and for the conventional air source systems close to 2.5.
[67]	ASHP vs. ASHP BIPV/T	TRNSYS	Type 568-BIPV/T system; Type 56-multi-zone building; Type 687-a window model;	Anchorage, southern Alaska, USA	the ambient air supplied to HP the warm air coming out of BIPV/T was supplied into HP	irradiation	residential building	COP;	▪COP improved for average ambient temperature above -3° C; ▪COP did not be improved, when average ambient temperatures were above 10 ° C or below -10 ° C; ▪ The maximum COP of BIPV-ASHP= 5.31;
[68]	BIPV/T-ASHP	TRNSYS	—	Toronto, Canada	cooling/heating/ DHW/floor heating	air flow rate	test hut	COP;	▪An integrated BIPV/T+ASHP thermal energy system increases the overall performance; ▪the seasonal COP could be increased from 2.74 to 3.45. ▪The heat pump electricity consumption is reduced by 20% for winter.

[69]	BIPV/T-ASHP	TRNSYS 17	Type 567-BIPV/T; Type 56-building model; Type 665-ASHP;	Ontario, Canada	heating mode	outdoor temperature	Archetype Sustainable House	COP; saving in energy and cost; GHG emission reduction;	▪ The heat pump electricity consumption is reduced by 20% for winter ▪GHG emission reduced and energy consumption got saving; ▪COP increased from 2.74 to 3.45;
[70] [71]	PV/T-ASHP	CFD	Gambit; Fluent	Shenyang, China	steady state RNG k-ε turbulence model	inlet and outlet velocity	residential building	efficiency of BIPV/T; COP;	▪ COP of heat pump unit reached 4.6; ▪Thermal efficiency of BIPV/T-ASHP integrated heating system was relatively high in low temperature environment;

2.2.1 ST-ASHP system

From above Table 2- 2, in terms of ST-ASHP system, researchers using simulation aim to optimize the system, such as the structure, operation and efficiency, or to verify the performance of system, as some experiments cannot achieve in real projects. Weather data mainly containing temperature, solar radiation and seasonal change are the most important input parameters for simulation. The output parameters contain SPF, COP and tank volume and so on.

Most of the simulation studies focus on the optimization performance of the ST-ASHP system. Many researches compared their own proposed system with original ASHP system. For example, Jonas et al [60] developed and validated a tool--SHP-SimFrame in TRNSYS to simulate the solar heat pump system (SHP), especially solar thermal heat pump. Kim et al [72] carried out three indirect solar assisted heat pump systems including the serial type solar assisted heat pump, solar assisted heat pump with hybrid solar collectors and parallel solar assisted heat pump system with flat plate solar thermal collectors. Zhang et al [73] studied the structural parameters on the performance of a direct expansion solar assisted heat pump including the solar collector area, the collector thickness and the pipe length and internal diameter of condenser. And they got the optimized structural parameters for their system.

To make the table clearer, we chose several researches including the media studies except R22 and a few typical studies with new equipment. Almost all

the simulation papers through software are conducted in TRNSYS software. i.e. Chen et al [61] used TRNSYS to optimize the ST-ASHP using CO_2 as heat pump refrigerant. The simulated results showed the optimized system has a high performance with the solar fraction can reach 71.1%, except Jonas et al [60], they developed and validated a tool 'SHP-SimFrame' in TRNSYS to simulate the solar heat pump system (SHP), especially solar thermal heat pump. They also only used the simulation method to compare the performance of the ST-ASHP system against the conventional ASHP system under various boundary conditions, but the conclusion was not representative, as the simulation parameters changed, the conclusion would also change.

Besides the simulation software method, Li et al [63] and Deng et al [64] developed their own mathematic models to simulate performance of ST-ASHP systems, respectively. Both of them calculated the COP value and found that solar irradiation and ambient air temperature have a great effect on the system performance. They indicated that the solar efficiency decreases with the growth of solar irradiation and decreases of ambient temperature. For detail information, Li et al [71] set up the parameters for components in TRNSYS and calculated SPF and SF of the system. It is proved that the overall efficiency of a DHW system was improved by the combination of a solar collector and heat pump. Deng et al [64] proposed a modified direct expansion solar assisted air source heat pump water heater system, which is illustrated in Figure 2-3. The proposed system mainly contained a flat-plate solar collector, an evaporator, a compressor, a hot water tank with heat exchanger as a condenser, receiver and two electronic expansion valves (EEV). There were two operation modes. When the solar

radiant was high enough to heat the water efficiently, it run on single solar collector mode and. While during the solar radiant was unavailable or low, and evaporating temperature was much lower than ambient air, it worked under combination mode. As a result, at solar radiation of 100 W/m^2, the heating time of this system decreased by 19.8 % compared to renovation when water temperature reaches 55 ℃. Meanwhile, the average system COP increased by 14.1%.

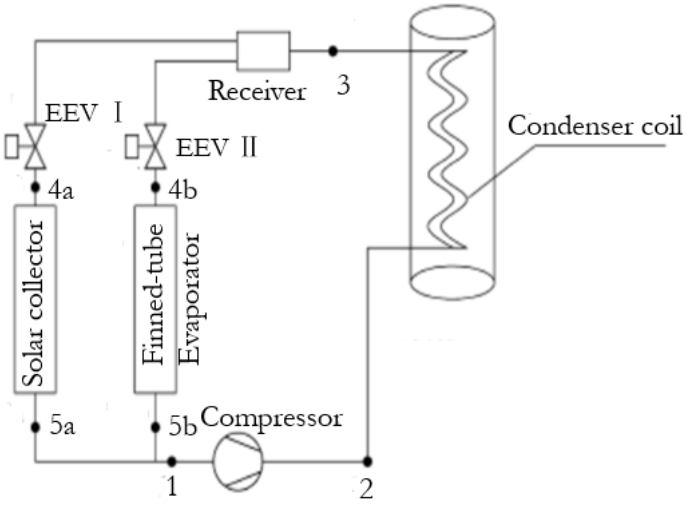

Figure 2-3 Schematic diagram of the new system [64]

While all the results got by simulation were optimized, the performance of these studies were simulated under their defined boundary conditions. Among them, Fraga et al [65] not only simulated the achievable value of SPF, but also calculated the potential SPF value. They developed a simulation model to analyse the potential performance of a ST-ASHP system. SPF of system achieved 4.4 and when temperature distributed the SPF was 3.1-4.1. Moreover, SPF of system achieves five is potential, but considering the envelope, SH

distribution temperature and solar collector area. In real project, the system should take account of real conditions e.g. investment and roof area.

Among all the researches of solar assisted ASHP system, there is one special condition that the performance researches under extreme conditions. The common problem under extreme conditions is that ASHP would be frosting, which also gained many concentrations in recent decades [74, 75]. There are few researches focused on ST-ASHP system that operated under extreme condition, which were not included in above Table 2-2.

Qiu et al [76] compared the integrated heating system of solar energy and air source heat pump system under different working conditions in cold regions. As a result, compared with high temperature and low temperature heating collecting systems, medium temperature had the best performance of this integrated system. Its COP is 55 % higher than other two types when the outdoor temperature is - 25ºC.

2.2.2 PV-ASHP system

For PV-ASHP, it was similar that most authors compared the energetic performance of their proposed system with original system or other system. For example, Evangelos et al [66] compared the ASHP with PV modules and the WSHP with flat plate collectors (FPC) and PVT system. They compared between ASHP with PV and PV/T for space heating. Giuseppe et al [77] set four simulations to compare the energy performance of the ASHP with PV modules system and conventional ASHP system by using the TRNSYS and

Matlab. They assessed the performance in a detached house located in northern Italy with two different cases: one with a PV nodule and the conventional tile without PV. Their work was the application of a title for under-slating ventilation ducts, which was modelled in TRNSYS. They found that solar and air source combined heat pump system demonstrates as the most advantageous case compared to conventional ASHP systems.

While for economic performance, the related studies is few. Evangelos et al [66] examined an ASHP system with PV modules for space heating proposes. Figure 2-4 depicts the system concept. The electricity demand of the heat pump is covered partially by PV panels and partially by grid electricity import. To convert and regulate the voltage and store the momentary supplementary energy, an inverter and batteries are used in this system. They developed the related TRNSYS models and compared the performance, the electricity consumption and financial performance among four systems, which are PV-ASHP systems, water source heat pump with flat plate collectors (FPC-WSHP), water source heat pump with thermal photovoltaic collectors (PV/T-WSHP) and water source heat pump with photovoltaic and flat plate collectors (PV+FPC-WSHP). They concluded that when the electricity cost is between 0.2 €/kWh and 0.23 €/kWh, the use of 20 m2 PV area with an air source heat pump is the most attractive solution financially in Greece.

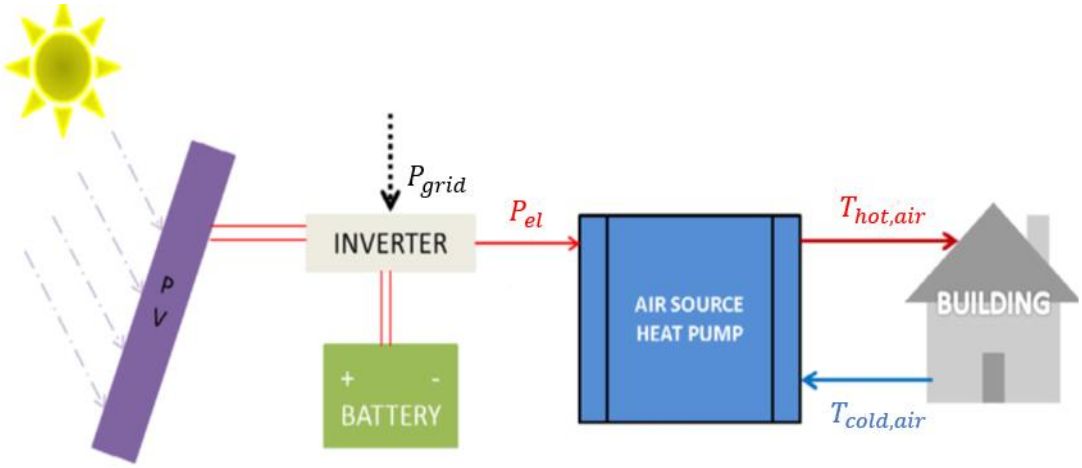

Figure 2-4 Air source heat pump heating system coupled with PV modules [69]

2.2.3 PV/T-ASHP system

Similar with all ASHP multi-system, the simulation tool for PV/T-ASHP system is also TRNSYS. And the performance of PV/T-ASHP system were the main studies contents, the main methods were to change the parameters including the ambient condition or operation modes. They also proposed that, there exist technical problems to hinder the PV/T collector to be large scale used. For example, Raghad et al [68, 69] proved in their TRNSYS model that an integrated BIPV/T+ASHP thermal energy system increases the overall COP and improves the energy efficiency of buildings.

Besides TRNSYS simulation, Cao et al [70] used the CFD simulation to test the performance of the PV/T-ASHP, which mainly studies the outlet temperature of the collector and the COP of the ASHP operated in severe cold region. Simulation time step was set to be 0.25 h, tolerance integration and convergence

were both 0.01. The control scheme was based on the load profile for the system. They obtained the result for supporting heating that the outlet temperature of PV/T collector can reach 76.6℃ and the COP of ASHP unit reached 4.1, which increased even in the low outdoor temperature.

Different from other studies that used simulation software, Getu et al. [67] did the theoretical investigation of the performance of a two-stage variable capacity air source heat pump coupled with a BIPV/T system. They used the simulation method, and the BIPV/T system model was a TRNSYS type 568 component. The main results they found that the results were different along with ambient temperature. The COP of the new system increased obviously when the average temperature was between -3℃ to 10℃; otherwise, there was no significant change.

2.3 Experiment methodologies and the related results

Table 2- 3 summarizes the detailed experimental methods and the related results of solar assist ASHP systems. In this part, we listed the medium used in the experiment studies, the operation modes of the experiments, the practical system performance, the measured parameters and finally the main experiment results.

The most common medium for experiment researches of solar assisted ASHP systems are R410A, R407C and R134 a. R22 is also used in few papers. Unlike simulation, the operation conditions are only based on operation modes for

experiment researches. Operation modes can be divided into heating mode, cooling mode and DHW mode.

Table 2- 3 Summary of experiment methods and the related results of solar assisted ASHP systems

Ref	System	Medium	Operation Mode	Location	Measured Parameters	Building Types	Evaluation Parameters	Main Results
[78]	ST- ASHP	R407c	heating mode	Taiyuan, China	environment condition	experiment room	exergy transfer; COP; energy and exergy efficiency; process quality number; improvement potential;	▪Average exergy efficiency of SIASHP is 77.67, 8% higher than ASHP and the average COP is 2.94, 8.1% more than ASHP; ▪Average process quality number is 59.36, 5.4% higher than ASHP;
[79]	ST-ASHP	R407c	heating mode	Taiyuan, China	condensing temperature	experiment room	integrated part load value (IPLV); seasonal part load value (SPLV); relative size IPLV and SPLV;	▪The higher part load rate, the higher COP; ▪SPLV is no more than IPLV; ▪Average IPLV of SIASHP is 2.54 and SPLV is 2.53, higher 14.9% and 15.5% than ASHP, respectively
[61]	solar combined CO_2 heat pump	—	solar heating/ CO_2 heat	Shanghai, China	ambient conditions	residential building	COP; total heat gain;	▪System COPs of the solar heating and CO_2 HP heating modes can reach 13.5 and 2.18;

			pump heating mode				solar fraction (SC) and SC efficiency;	▪The studied solar assisted system can save 53.6% of the electricity consumption than CO_2 HP;
[80]	Serial SA-ASHP	—	—	Erzurum, Turkey	weather data	residential building	COP; environmental and economic benefits; energy saving ratio; CO_2 reduction ratio; payback period;	▪The average COP of heat pump is 3.8 and solar assisted ASHP is 2.9;
[81]	DMHP	—	heating /cooling mode	--	ambient condition, temperature/ pressure of refrigerant,	enthalpy difference lab	power consumption and COP; exergy analysis; heating capacity and power consumption; water temperature in SWT and DWT	▪ the COP is significantly affected by ambient temperature; ▪ Heating capacity and COP of air source space heating mode are higher than that of solar space heating mode with the outdoor ambient temperature above 4° C; ▪Different components cause most exergy loss in different operation mode
[65] [82]	ST-ASHP	—	space heating/ DHW	Geneva, Switzerland	weather data	Multifamily house	SPF; COP; energy flows;	▪The measured seasonal performance factor of the system is 2.9 for 2012; ▪Several points may have contributed to a relatively low SPF: (i) an unusually low demand for space heating along

							thermal storage;	with an unusually high demand for domestic hot water; (ii) in absence of a load adjusted heat pump; (iii) a single heat distribution circuit with decentralized domestic hot water storage; (iv) no insulation of the unglazed solar collectors
[83]	PV-ASHP	—	heating/ cooling mode	Changsha, central south China	different PV power	office building in university	exergy efficiency/consumption; life expectancy; CO_2 emission reduction;	▪life expectancy of PV-ASHP system in Central south china is about 26 years; ▪Install PV capacity decide by the ASHP required rating power; ▪PV-ASHP has an exergy consumption saving rate of 41.16% for cooling and 35.02% for heating
[84]	PV-AC	R134a	heating mode	Alicante, Spain	irradiation; environment temperature; air mass flow rate;	residential buildings	heat recovered; heat production; COP; energy performance index; primary energy consumption;	▪Average COP of heat pump increases from 3.6 to 3.75; ▪PV cell integrated in the tile can produce more energy than air conditioning required;

[85]	PV module traditional HP system	—	Real operation condition vs. a scaled-down channel (1:5)	Northern Italy	the integral absorptivity and emissivity; the airflow pressure drop	residential building	Air temperature; Energy consumption; Integration angle; COP	▪ air temperature variation ranges from 2 °C to 20 °C leading to a heat recovered between 2 kW and 7 kW in winter and summer time, respectively. ▪ the integration of the PV cell in the tile reduces the thermal energy by 15%. ▪The heat recovered enhances the heat pump COP, reducing the Primary Energy Consumption of a conventional heat pump by 5%, and achieved with limited additional costs.
[70]	PV/T-ASHP	R410 A	cooling mode	Shenyang, China	weather, thermal load, solar irradiance	residential building	power consumption; energy consumption; solar contribution; production factor; load factor; useful thermal energy; EER;	▪System performance depended on the environment including solar radiation, outlet temperature and the unit's load factor; ▪Several technological improvements in the analyzed system have been made to optimize the system performance;
[69]	PV/T-ASHP with TES	—	exergy efficiency/exergy	Toronto, Canada	—	Test hut	model relative error;	▪The relative error of exergy efficiency mode of integrated PV-ASHP for cooling is less than 4.21%;

			consumption cost model					▪The relative error of exergy consumption cost model is 1.5% for cooling and 0.3% for heating;
[86]	PV/T-ASHP	—	hot water	Beijing, China	ambient temperature and solar irradiance	laboratory	COP;	▪COP of heat pump reduced from 5.61 to 1.69 and the average was 3.03. ▪Comprehensive system COP ranged from 6.07 to 1.33, the average was 2.99
[87] [88]	ST-ASHP combined with PCM	—	heating/cooling/water from freezing	Shenyang, China	ambient temperature; solar hot water temperature;	laboratory	COP; Capacity;	▪Ambient temperature had a significant influence on the system performance in cooling mode; ▪In heat pump cycle, solar-heated water temperature had a significant effect on system performance;

Similarly, the outdoor conditions are also essential to the experimental studies, such as temperature and solar irradiation. The most measured parameters include temperature/pressure of compressor/condenser/refrigerant, input power and flow rate. The evaluation parameters are the same as that in simulation, including COP, SPF, power consumption and payback time.

Solar energy assisted ASHP system can save energy and benefit environment using sustainable solar energy [89, 90]. Comparing to the traditional ASHP system, the average COP of solar assisted ASHP systems in experiments can increased from about 1 to almost 3.75. In the following subsection, we will extend the discussions specifically by selecting several researches of each solar assisted ASHP.

2.3.1 ST-ASHP system

Solar thermal assisted ASHP system can save energy and benefit environment using sustainable solar energy [91]. The main evaluation parameters studies by most researches include COP and energy relative parameters such as energy efficiency, energy consumption and energy saving ratio and so on, i.e., Wu et al. [92] carried out the experiment of low-temperature ST-ASHP system for space heating. The solar thermal collectors were connected in parallel with the evaporator. The system has a mean COP of 3.2, when it is designed to supply heating to building in transition season and coldest winter days when the ASHP system cannot meet the demand. Only few papers also contain environmental and economic benefits. For example, Kadir et al. [80] calculated the payback time of the solar thermal

assisted ASHP according to the LPG, electric and fuel oil are 1.4, 2.9 and 3.9 year, respectively.

These studies usually conducted under different conditions, the typical study is Wu et al. [6] and Xu et al. [78, 79]. Wu et al. [6] set experiment to compare the performance of the ASHP and solar assisted ASHP system for domestic hot water (DWH) in different outdoor condition and then simulated two systems for the whole year performance in Shanghai, China. They measured outlet temperature of two different systems in clear and overcast day and night and simulated the month average COP according to the ambient temperature over cast/rainy/snowy days. They concluded that the COP of the ST-ASHP system performs better especially in the winter, when the ambient temperature is low, since the ST-ASHP system draw the heat from the solar can increase the evaporating temperature more remarkably. Xu et al. [78, 79] proposed the solar integrated air source heat pump (SIASHP) with R407c. The system is mainly composed of the SIASHP and capillary copper pipe network without any other large component. They completed the experiment in the laboratory and the first generation of prototype of SIASHP was shown in Figure 2-5. In the system, the R407c absorbs the heat from both solar radiation and air source at the same time in the solar finned tube evaporator and runs through the compressor into the capillary copper pipe network, and then goes by the electronic expansion valve back into the solar finned tube evaporator to complete a whole working cycle. The solar finned tube evaporator bypass regulates the internal refrigerant flow of solar finned tube evaporator to avoid the excessive

overheating of refrigerant into the compressor protecting the safe operation of compressor. The compressor bypass is the standard configuration for the direct current frequency conversion compressor to protect it from liquid hammer when underload. They claimed the average COP of SIASHP with the part load rate of 100% is 2.77, which is 9.8% higher than the 2.52 COP of ASHP and the SIASHP has a dramatically better heating performance with a low level of part load rate in the lab and analyzed the energy efficiency and exergy efficiency of the SIASHP system. Taiyuan and a 130 W/m^2 solar irradiance, the 76.8% exergy efficiency of SIASHP is 7.9% higher than the 71.1% exergy efficiency of ASHP. From 9:00 to 21:00, the 2.89 kWh power consumption of SIASHP is 7.4% lower than the 3.12 kWh of ASHP.

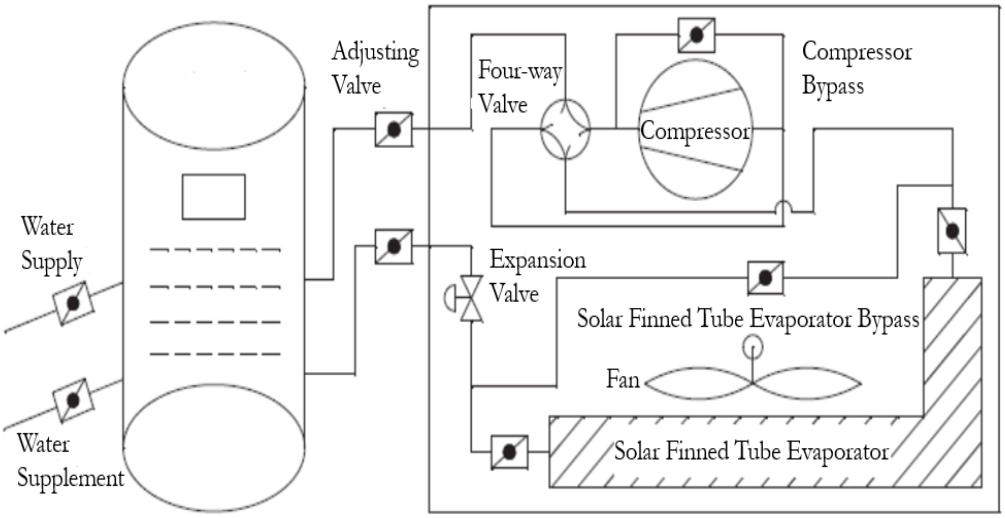

Figure 2-5 Schematic diagram of the SIASHP system [78, 79]

While for mathematic analysis researches, most of them are under stable condition, which is easy to calculate. However, Cai et al. [81] built mathematical model and done the thermodynamic analysis. They tested the performance of the IX-SAMHP system by using numerical analysis and compared the experiment results with simulated model in the space heating mode and space water mode condition. Cai [81] and Ji et al. [93] proposed a novel indirect expansion solar-assisted multi-functional heat pump which composes of the multi-functional heat pump and solar thermal collecting system in Hefei, China. The schematic is shown in Figure 2-6. The system can fulfil space heating, space cooling and water heating with high energy efficiency by utilizing solar energy. The refrigerant circulation loop for the solar space heating is 1-2-9-7-6-5-2-3-1 and for the space cooling plus water heating mode is 1-2-5-6-8-9-3-2-1, while the water circulation loops are 12-14-13-12/13-11-5-13 and 5-10-11-5, respectively. Cai et al. [94] investigate experimentally and theoretically on a novel dual source multi-functional heat pump (DMHP) system. The DMHP system can supply air conditioning and domestic water with air source or solar energy in different working modes. The DMHP system contains indoor units and outdoor units linked by refrigerant circuit and water circuit. The refrigerant circuit is a multi-functional heat pump system consisting of two air heat exchangers, a plate-type heat exchanger, a domestic water tank and a compressor. They tested the influence factor which affect the system including the initial solar water tank, the solar irradiation in the solar water heating mode and solar space heating mode. For the space heating mode, the increase of

the indoor environment temperature decreases the heating capacity and COP. Increasing the initial water temperature in solar water tank can improve the condensing power and evaporation power, as well as the energy consumption and COP of the system. Moreover, the higher solar irradiation can lead to higher heat transfer rate and larger energy consumption. In annual analysis, the DMHP system can obtain relatively high COP of the value above 2.0 throughout the year with the optimal working strategy in three cities under different climate conditions.

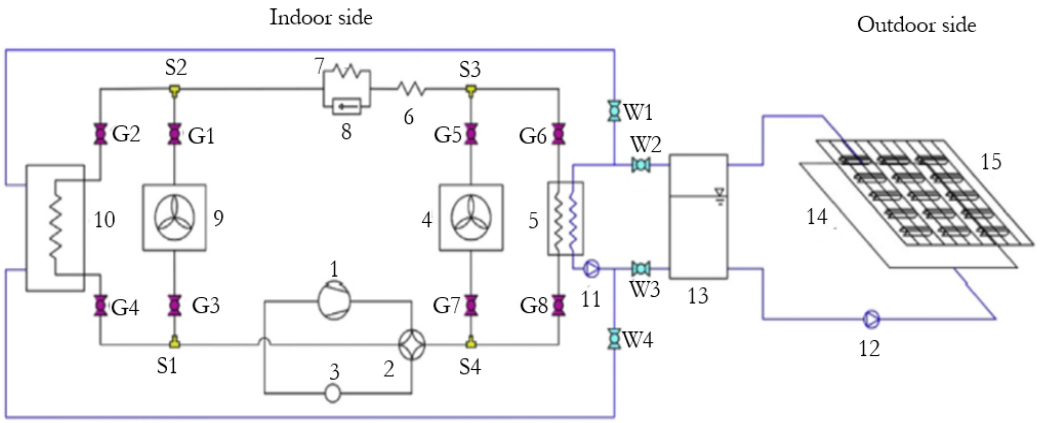

1.compressor 2.reversing valve 3.liquid accumulator 4.outdoor air heat exchanger 5.plate-type heat exchanger 6~7.caillary tube 8.one-way valve 9.indoor air heat exchanger 10.domestic water tank 11~12.water pump 13.solar water tank 14.solar flat-plat collector 15.solar simulator G1~G8 refrigeration valve S1~S4 three-way valve W1~W4 water valve

Figure 2-6 Schematic of the solar-assisted multi-functional heat pump system [94]

One special study among them is that Chen et al [61]. They investigated a solar combi-system consisting of solar collector and a CO_2 heat pump to analyze its performance. Chen et al [61] conducted the experiment study on the performance of a pre-existing solar combi-CO_2 heat pump system. Figure 2-7 shows a schematic

diagram of the system in residential building. The system separates the operation tank from the storage tank. The storage tank acts as the main storage of the captured solar energy and when the temperature level achieved, it delivers energy to the operation tank. The CO_2 heat pump will consume less electricity to maintain the temperature in the small volume operation tank when solar radiation is poor. The operation tank can also be a buffer of heat for whole system with the obvious temperature changes caused by solar radiant. It can weaken the temperature fluctuation. The result showed that the solar assisted system can save electricity consumption at 1790.8 kWh every year with an average COP of 13.5, comparing with CO_2 HP heating system based on year-round operation (COP is 2.18).

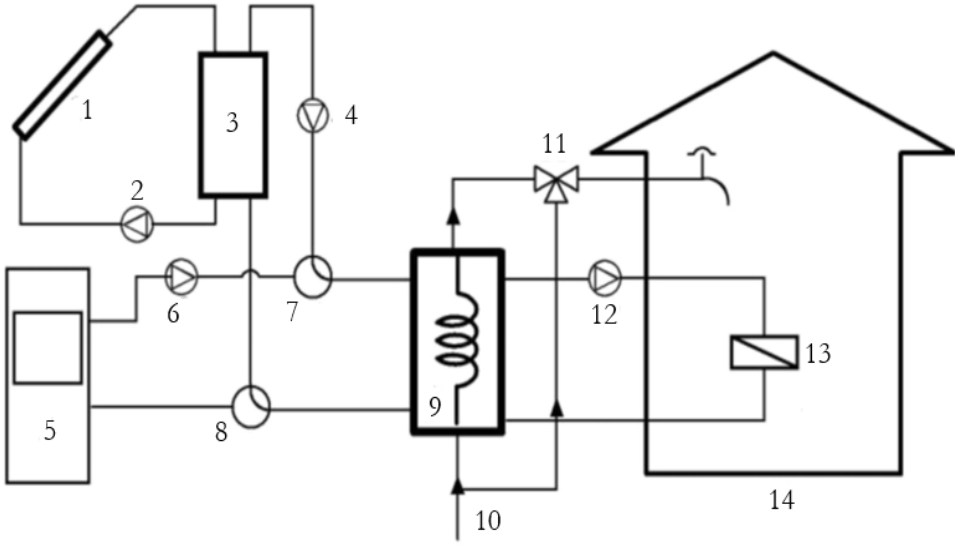

1.Solar collector array 2. solar collector pump 3. storage tank 4. solar collector delivery pump
5.CO_2 heat pump 6.heat pump delivery pump 7.8.switching valve 9.operation tank
10. civil water inlet 11.mixing valve 12.supply pump 13.fan coil units 14.testing room

Figure 2-7 Diagram of solar combi-system with CO_2 HP [61]

For extreme condition studies on the ST-ASHP system, there are only few papers conducted the related research in recent years. The related research mainly concentrated on the performance of the system by controlling different operation modes or under different ambient conditions [95]. Huang et al. [96, 97], experimentally investigated the frosting characteristics of solar collectors with direct expansion air source heat pump system. They conducted the experiment by supporting different temperature, controlling the air humidity and solar irradiation in a lab. As a result, the ambient condition including the temperature, humidity and solar irradiation had a significant on the performance of this system under frosting conditions. The frost occurred when the ambient humidity was 50 % to 70 %, the temperature ranged from 7 ºC to 6 ºC with zero solar irradiation. While the solar irradiation was 100 W/m^2, there was no frosting except the ambient temperature was lower than -3 ºC and the humidity is higher than 90 %. Long et al [98] studied the performance of a dual-solar and sir heat source integrated heat pump evaporator in cold season. The hot water of evaporator had an obvious effect on refrigerant's evaporator temperature and the COP of the heat pump. Liu et al [99] found that the heat capacity and COP of solar assisted air heat pump system increased 62 % and 59 %, compared with air source heat pump system, when the ambient temperature was - 15 ºC.

2.3.2 PV-ASHP system

The common researches for PV-ASHP system also concentrated on the energetic performance, i.e., Giampaolo et al. [85] used the experimental to assess the performance of a PV-ASHP system and validate their simulation model. They adopted a similar approach as in [100] to determine the flow rate and temperature of the air at the outlet of the ventilation channel and combined the generalized. They found that the average COP increased from 3.60 to 3.75, turning into a primary energy reduction with respect to the reference case of 5 %.

Besides the energetic performance, some studies also evaluated the environmental and economic performance. Wang et al. [83]set up an experiment of the integrated PV-ASHP system and tested the system in six cases with different PV powers. Their integrated PV-ASHP system was made up of three sub-systems: a PV system, an electricity storage, an inverter system and an ASHP system, and the experiment located on the top floor of a building. They indicated that the PV-ASHP system could have a saving rate of 41.16 % of exergy consumption per unit investment for cooling and 35.02 % for heating. The life expectancy of the PV-ASHP system could reach about 26 years and it can reduce the 11.10t of CO_2 in the whole life emission and save the operation cost comparing with the ASHP powered by electricity from the national grid.

Besides the conventional PV/T-ASHP system, Aguilar et al [84] conducted an experiment using photovoltaic air conditioning unit (PV+AC). They carried out the

experiment on an air conditioning unit which has been powered using both a PV installation and the grid simultaneously for a whole year with the control system, which is designed to maximize solar contribution in Spain. The PV+AC system consisted of the air conditioning unit with two electrical connections (PV panels and grid) and the PV installation. They test the PV+AC system from May to October in cooling mode in an office located in Alicante (Spain) and the whole system has demonstrated to be 100 % reliable, having undergone no maintenance. Then they optimized the operation mode, regulating the air conditioning unit independently its own operation regime to maximize the PV energy input. The solar contribution obtained in cooling mode from May to October was 64.5 %, while the production factor was 65.1 %. The performance of the system will depend on the solar radiation, outlet temperature and the unit's load factor.

2.3.3 PV/T-ASHP system

For PV/T-ASHP system, few papers done the experiment research, many authors just pay attention to the simulation as the system is complex and difficult to set up in laboratory. And most of the researches focused on the energetic performance. For example, Wang et al. [101] built experiment of the PV/T-ASHP hot water system in laboratory and tested the system. The system was comprised of independently developed flat plate solar PV/T collector based on micro-channel heat pipe array and air source heat pump, which were combined by a new composite evaporator. The COP of heat pump reduced from 5.61 to 1.69 and the average was

3.03. Comprehensive COPsys of PV/T-air composite heat pump system ranged from 6.07 to 1.33, the average was 2.99. Raghad et al [38] design BIPV/T-ASHP system on a test hub and found that the seasonal COP could be increased from 2.74 to a maximum value of 3.45 for direct coupling of BIPV/T+ASHP without the use of diurnal thermal storage. The heat pump electricity consumption is reduced by 20 % for winter. The PV/T-ASHP system usually composed by three parts: (1) PV/T collector or BIPV/T system on facade; (2) heat pump unit; and (3) thermal energy storage (TES) system, including Insulated Concrete Forms walls, ventilated concrete slab, gravel/sand bed and water tank storage. Qu et al. [102] examined a novel solar photovoltaic/thermal integrated dual source heat pump water heating system at different ambient temperature. Besagni et al. [103] focused on the solar-assisted heat pumps for heating and cooling to produce DHW. The system was coupled with PV or PV/T system. They made the examination under different ambient temperature, system parameters and operating modes to compare the performance of the system, main the COP.

One special condition facing by ASHP system in extreme condition is frosting. To avoid the deterioration of heat transfer effect and performance drop of unit due to the evaporator frosting in low temperature condition with the circulated air heated by the air collector, Cao et al. [70] and Li et al. [62] proposed a PV/T-ASHP integration heating system, which aimed to operate safely, stably and efficiently in winter in cold region. PV/T air collectors were arrayed on the building envelop composing an integrated PV/T curtain wall. In the PV/T, up and down sides are

respectively opened outlets and inlets connected to the ASHP unit with air ducts forming a forced circulation in the system. Besides, they assumed that there is almost no overheating during the energy transfer process, freezing, boiling, corrosion and leakage problems. Lu et al. [104] studied the performance of PV/T-AHP system in winter. To improve the performance, they added vapor injection to this system. As a result, the COP was 3.45 when the ambient temperature average was - 1.13 ºC and solar irradiation was 164.03 W/m^2.

2.4 Comparison of different solar assisted ASHP systems

For conventional ASHP system, compared with other source heat pump system, such as, water, ground and so on, the main advantages of ASHP system conclude that the investment is much lower and the installation is much easier than other ground source heat pump system, and the operation and management of ASHP system also easier. However, the disadvantages are also obvious, the ASHP system has a more serious for ambient environment. Water and ground source heat pump systems are more stable and the performance of them are higher than ASHP system, especially under extreme conditions, the frosting is still one of big problems for ASHP system, which seriously affects the performance of ASHP. Auxiliary heat will increase the extra electricity energy consumption.

For solar assisted air source heat pump system, including the ST-ASHP, PV-ASHP and PV/T-ASHP system, compared with ASHP system, the common advantages

for them are obvious. From the system aspect, performance of them are better than ASHP system [105], as the solar assisted systems gain energy from both air and solar, which are both renewable and sustainable. In before reviewed part, the solar assisted air source heat pump system could increase the COP about 30 % to 60 % than ASHP system, under some defined condition, the value is higher. The frosting problem also reduced as the solar supply heat for the ASHP system, as a result, the solar assisted air source heat pump system has a wider spread than ASHP system, special for cold and more extreme regions [21]. Moreover, for the whole energy aspect, the solar assisted air source heat pump system could supply more energy to users and produce more types of energy, i.e., PV-ASHP and PV/T-ASHP system can supply electricity for buildings. Solar assisted air source heat pump system could meet the increasing energy demand better than ASHP system. Besides that, as mentioned above, the solar and air energy are clean and friendly to environment, the solar assisted systems could reduce the environment pollution caused by fossil fuels, i.e. coil, oil. Along these obvious advantages, it is certainly that there are some common weaknesses for all solar assisted air source heat pump systems. Comparing with ASHP system, the investment concluding equipment, installation and maintenance is much higher and the operation and management are much more complex, as the systems are complex.

While only for solar assisted air source heat pump systems, ST-ASHP, PV-ASHP and PV/T-ASHP system, there are also some comparison results of their benefits. Among solar assisted air source heat pump systems, ST-ASHP can avoid frosting

in winter especially in cold regions. Even below ambient temperature, the system performance is still relatedly high. Moreover, the installation requirement is much less strict than PV-ASHP and PV/T-ASHP systems, causing that the payback time is the shortest among three solar assisted air source heat pump system. However, the disadvantage is that most energy produced by ST-ASHP is used only for heat or hot water, and ST-ASHP system is still affected more by the external weather conditions than other two systems, as ST-ASHP system is significantly related with ambient temperature, while other two solar assisted air source heat pump systems mainly rely on the solar radiation. In terms of PV-ASHP system, this system is usually parallel, the PV cell produce electricity supplied to equipment consumption or directly to buildings, while ASHP system supply the heat and hot water (with water tank system) to users. Besides the heat energy, electricity energy can be produced for direct use, which is improved than ST-ASHP system. The performance of the air source heat pump is the best among three solar assisted air source heat pump system, as the energy input is much lower. Of course, more complex system control strategy than ST-ASHP system is also required among PV generation, grid import, battery or TES unit. And electricity storage is still one of difficulties which hinder the widespread use. As for the most complex system among solar assisted air source heat pump systems, PV/T-ASHP system has its own characteristics. It can produce different types of energy including heat, hot water and electricity. Similar with PV-ASHP, but not the same, it can produce more capacity of energy and the users consume the lowest energy among three solar

assisted air source heat pump systems, as this system has the highest and maximized solar utilization. But at this step, there are also some problems facing by PV/T-ASHP system. The most complex control system is basic for operation and management. The maintenance is much difficult. All these cause that it has the longest payback time. These characteristics restrict the development of PV/T-ASHP systems [106]. The summary of the main characters of solar assisted air source heat pump systems is given in Table 2- 4.

Table 2- 4 Summary of comparison among solar energy assisted ASHP systems

System	Advantage	Disadvantage
ST-ASHP	High efficiency; Shortest payback time; Low installation requirement; Lowest investment;	Affected by ambient temperature;
PV-ASHP	Saving electricity, even can support other equipment; Highest COP of HP; Lower input power;	More investment; Existing electricity storage problem; Affected by solar irradiation; Installation problem;
PV/T-ASHP	Highest solar energy utilization; Supply heat and electricity as the same time; Most energy production and lowest consumption;	Most investment; Most complex system and control; Most installation and maintenance problem; Longest payback time;

2.5 Limitations and future directions

There are still some limitations which need to be broken through before the solar assisted ASHP system can be applied widespread in market. The main issues are concluded in the following.

Methodologies adopted in existing literatures varies from researcher to researcher. Each one can set up different experiment mode, define boundary conditions and choose different models. Such inconsistence limits the marketization promotion of solar assisted ASHP systems. Another challenge lies in gap between solely simulation or laboratory testing and real application [55].

The most studied system is ST-ASHP type. On the contrary, experiment of (BI)PV/T-ASHP is covered by only few papers, and the rest papers on this system concept are all from simulation points of view. This means that the (BI)PV/T-ASHP has not yet been largely applied or there are still practical problems, such as technic or installation, to be solved before it can get wider application. In addition, optimization of the systems is required, including the structure optimization of some component in the whole system [40], the operation mode optimization as their running mode is adjusted by time which is not accurate and the capacity or volume optimization about different components [54].

There is lack of standardized indictor to evaluate the system performance [107]. Although COP and SPF are adopted in most papers, the process and the evaluation parameters are different from each to the other. Moreover, few papers [98] take into

account of the environmental and economic parameters. Common standards and official certifications can help users to make better choice and comparison among different solar assisted ASHP systems.

While solar assisted ASHP system suffers from existing limitations in single system, combined two or more system may have a prospective development in the future, e.g. combination of the heat recovery system and solar ASHP system, which can avoid the disadvantages in single system and provide more solutions to buildings energy systems.

2.6 Conclusions

Three major solar assisted ASHP systems are reviewed comprehensively from their system concepts, boundary conditions, research methodologies, performance indicators, and main research finding in the recent literatures. Conclusions are generally summarized as below:

It is so important to define the boundary conditions of solar assisted ASHP system from the beginning, according to the IEA SHC Task 44/HPP Annex 38. This can help to evaluate the system performance in a standard way. The experiment is usually conducted in laboratory and simulation is conducted by TRNSYS software. COP is significant to evaluate the performance of the system and adopted in most papers. Weather data in different locations is mostly sensitive to the system performance, which contains temperature and solar radiation etc.

For future work, more studies should be conducted on the PV/T-ASHP system especially the experiment method, as most of researches existed are simulation studies. The structure optimization for PV/T-ASHP system is a popular trend to achieve its performance improvement. Based on this consideration, I conducted this thesis focusing on the performance study on a PV/T-ASHP system with a novel absorber in solar collector.

Chapter 3: Experiment setting of the PV/T-ASHP system

To improve the heat transfer performance and efficiency, in this chapter, a novel construction of the heat exchanger including an ultra-thin superconducting thermal absorber with internal fins shaped bubbling with two different sizes is proposed. This solar thermal absorber has two different sizes of fins, in contrast with the existing similar solar thermal absorber [29, 23], this novel structure solar thermal absorber has lower resistance and the turbulence for the liquid in the absorber is higher. This is because of its design and fins' structure. First, the width for this absorber is only 4 mm, which is much smaller than the original absorbers. The capacity is also reduced, so the resistance becomes lowers. Besides, the fins increase the liquid turbulence compared with the original flat absorber type [29]. The novel absorber is also studied using simulations and the novel absorber model is built for CFD. The performance of the novel absorber is further simulated for different boundary conditions.

Based on the research conducted by our group [29], the performance of this kind of absorber is better than the original types. However, only one structure is considered in that work[29]. In this chapter, seven different fin shapes models of the thermal absorbers are also built to make a comparison with original absorbers. The performance of these thermal absorbers including the temperature and the

efficiency is further analyzed. The absorber with the best performance is then chosen to be further investigated using simulation and experiment methods. This research aims to propose a novel thermal absorber and evaluate its performance for future applications.

First, the construction, the corresponding analytical method, and simulation boundary conditions in the CFD model are introduced. Then the simulation results for different conditions and different constructions are presented and discussed.

3.1 Simulation models of the solar absorber

To compare the impact of the different shapes on thermal performance, different construction absorbers models are built. We consider the following seven models, the original type with big and small bubbling, the flat absorber, deleting small bubbling absorber based on the original type, deleting the big bubbling leaving small absorber based on the original type, changing all the bubbling to big, changing all bubbling into small, and changing the whole width of the absorber from 4mm to 5mm, total seven types. For a fair comparison, the design sizes are kept constant and equal to the original type as shown in Figure 3- 1. The boundary condition is also different from the original three modes. The boundary condition of the absorber surface connected to the PV collector is constant, 30 ˚C, the heat flux for other surfaces is set to 0, changing the inlet water velocity from 0.2 m/s to 1 m/s, per 0.1 m/s variations. The outlet boundary condition is the outflow.

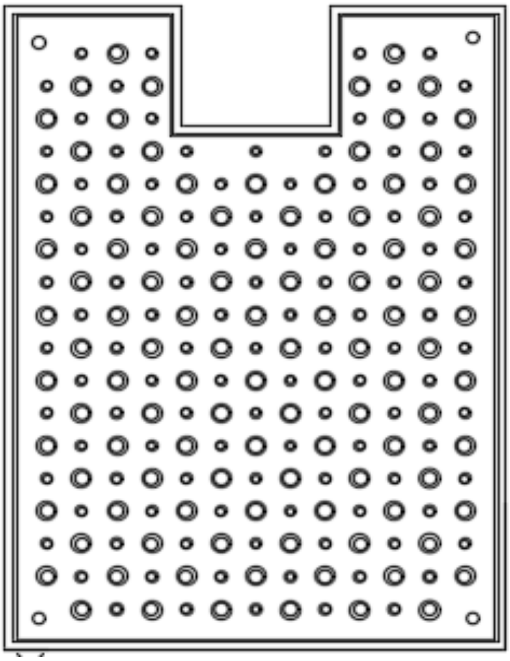

(a) First (4/5mm)

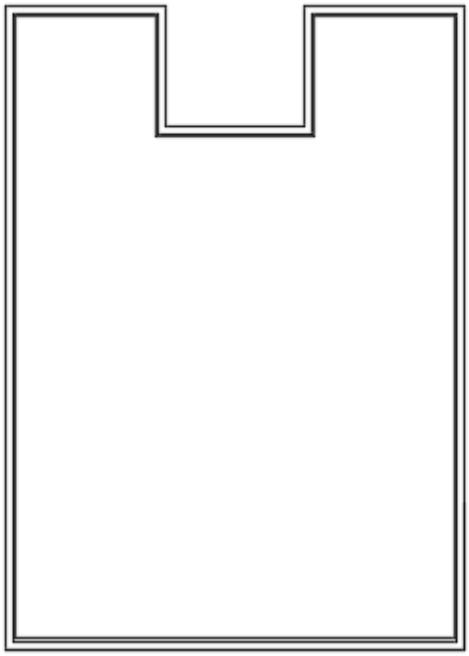

(b) Flat

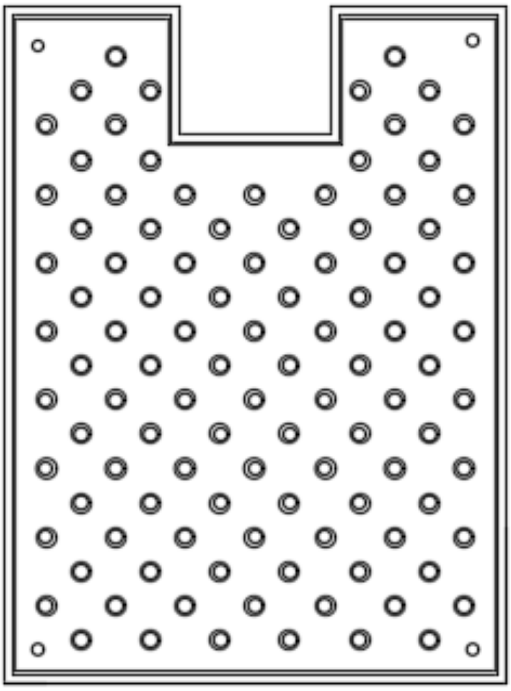

(c) Deleting small

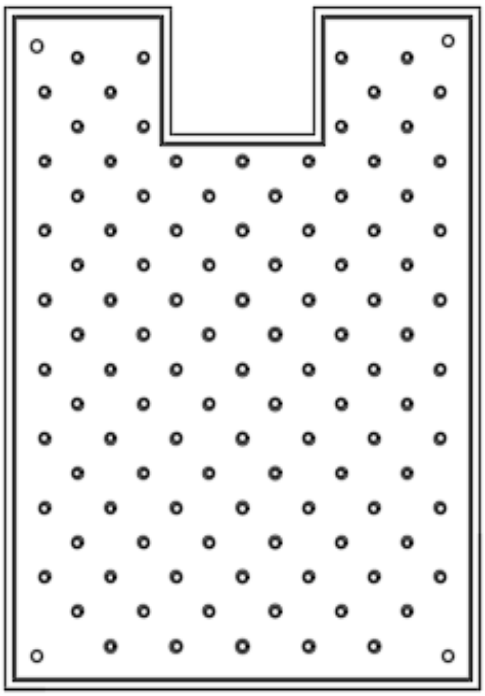

(d) Deleting big

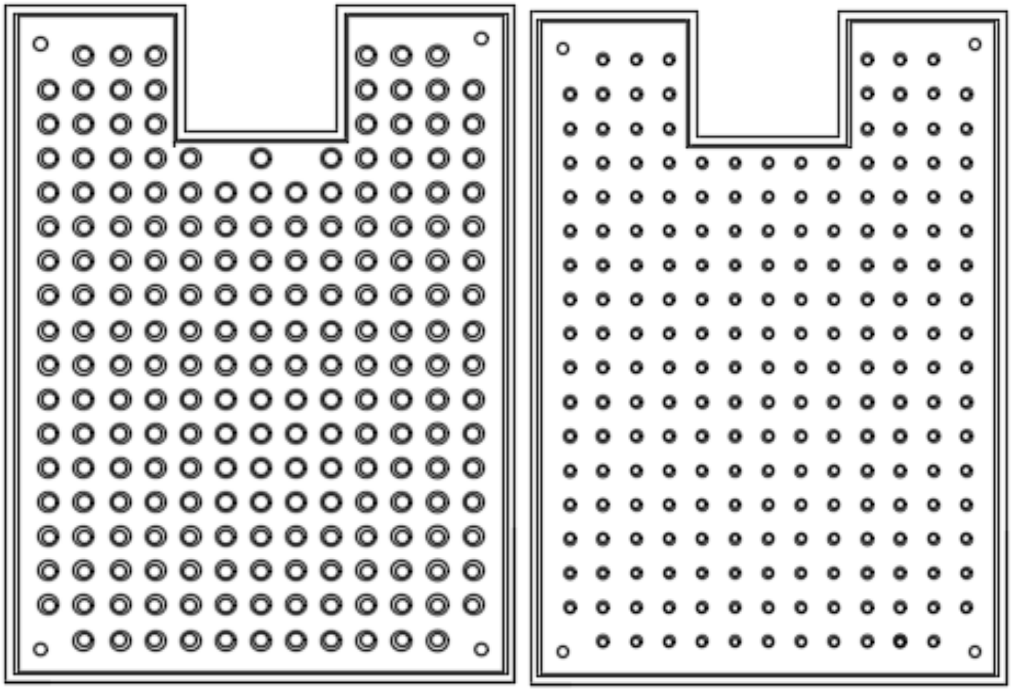

(e) All big (f) All small

Figure 3- 1 Different fin shapes of the thermal absorber

In the CFD model building process, a realizable k-ε turbulence model is chosen to calculate the thermal performance of the novel absorber. The realizable k-ε turbulence model originates from the statistical data, similar to the standard k-ε turbulence model. However, the realizable k-ε model differs from the standard k−ε model in the following two aspects. First, it contains a new formulation for the turbulent viscosity C_μ. Furthermore, in contrast to the standard model, C_μ is variable. The second difference is a new transport equation for the dissipation rate, ε, which is derived from an exact equation for the transport of the mean-square vorticity fluctuation. As a result, the realizable k-ε turbulence model mainly provides improved predictions for the spreading rate of jets and has a superior

ability to capture the mean flow of complex structures and for flows involving rotation, boundary layers under strong adverse pressure gradients, separation, and re-circulation. The equations for the realizable k-ε turbulence model are [108, 109]:

$$\frac{\partial}{\partial t}(\rho k) + \frac{\partial}{\partial x_i}(\rho k u_i) = \frac{\partial}{\partial x_i}\left[\left(\mu + \frac{\mu_t}{\sigma_k}\right)\frac{\partial k}{\partial x_i}\right] + G_k + G_b - \rho\epsilon - Y_M + S_k \tag{3-1}$$

$$\frac{\partial}{\partial t}(\rho\epsilon) + \frac{\partial}{\partial x_j}(\rho\epsilon u_j) = \frac{\partial}{\partial x_j}\left[\left(\mu + \frac{\mu_t}{\sigma_\epsilon}\right)\frac{\partial \epsilon}{\partial x_j}\right] + \rho C_1 S_\epsilon - \rho C_2 \frac{\epsilon^2}{k + \sqrt{v\epsilon}} + C_{1\epsilon}\frac{\epsilon}{k} C_{3\epsilon} G_b + S_\epsilon \tag{3-2}$$

$$C_1 = \max[0.43, \frac{\eta}{\eta + 5}] \tag{3-3}$$

$$\eta = S\frac{k}{\epsilon} \tag{3-4}$$

$$S = \sqrt{2S_{ij}S_{ij}} \tag{3-5}$$

$$\mu_t = \rho C_\mu \frac{k^2}{\epsilon} \tag{3-6}$$

where, u_i represents the velocity component in the corresponding direction; μ_t denotes eddy viscosity; G_k represents the generation of turbulence kinetic energy due to the mean velocity gradients, calculated in the same manner as the standard k-ε turbulence model; G_b is the generation of turbulence kinetic energy due to buoyancy; $C_{1\epsilon} = 1.44$, and $C_2 = 1.9$.

In this study, the realizable k-ε turbulence model in Fluent is selected to build the thermal collector model in standard wall functions with water as the liquid materials. The simulation tool is Fluent 6.3.

Through simulation, the thermal performance of these different types of absorbers is analyzed. The heat collecting and thermal efficiency of these absorbers are calculated by the equations as presented in (3-7) and (3-8)

$$Q_C = m_w \times (T_{OUT} - T_{IN}) \quad (3\text{-}7)$$

where, m_w is the water mass volume, T_{OUT} is the outlet water temperature and T_{IN} is the inlet water temperature of this absorber.

The results of the heat collecting and the efficiency of each type are shown in Figure 3- 2 and Figure 3- 3. For different shapes of the absorbers, the trend of the heat collecting and the efficiency, η, is the same as the variation of the inlet water velocity. The higher the inlet water velocity, the higher the heat collecting, and the lower the efficiency, η. Taking the first absorber type as an example, by increasing the inlet water velocity from 0.2m/s to 1m/s, the heat collecting is changed from 15×10^6 J/h to 49.5×10^6 J/h, however, the efficiency, η, is reduced from 96% to 55%. The performance of the absorbers with bubbling is much higher than that of the flat type both in terms of heat collecting and efficiency aspects.

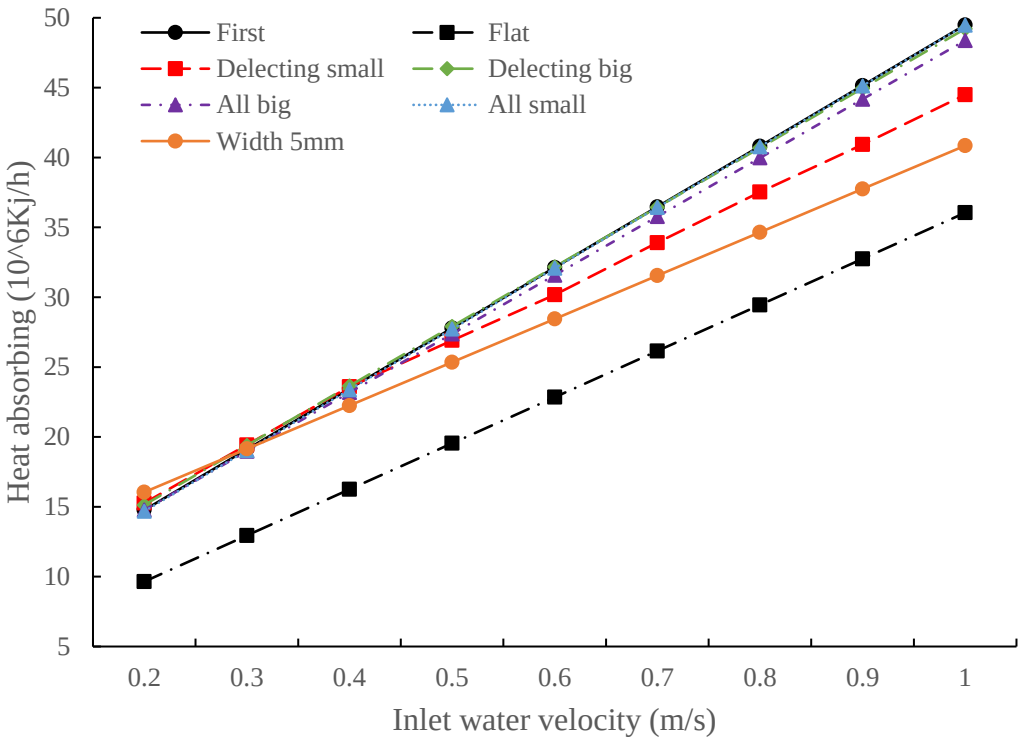

Figure 3- 2 Heat absorbing per hour of different construction collectors (10^6kJ/h)

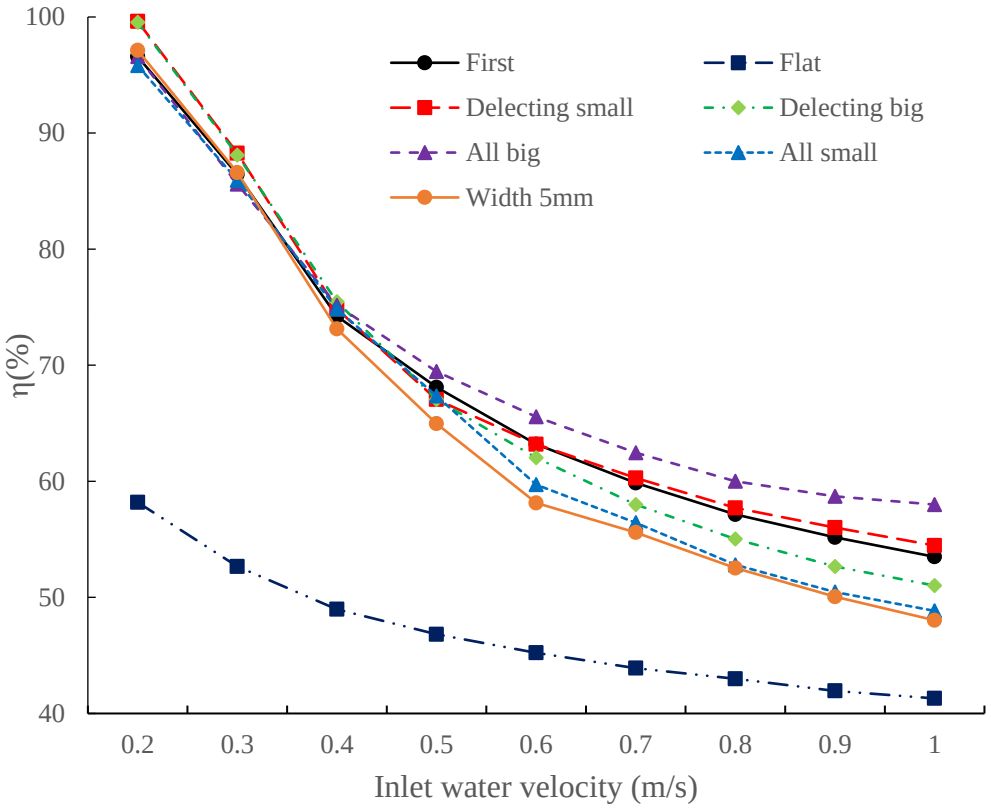

Figure 3- 3 The efficiency of different construction absorbers (%) versus inlet water velocity

For heating collection, increasing the inlet water velocity increases the heating collecting for all seven types of absorbers. For the first absorber type, the values vary from 15×10^6 J/h to 49.5×10^6 J/h. By deleting the small type the values are changed from 15.2×10^6 J/h to 44.5×10^6 J/h, and by deleting the big type the values are increased from 15.1×10^6 J/h to 49.2×10^6 J/h. All big type gains from 14.8×10^6 J/h to 48.4×10^6 J/h, all small type increases from 14.7×10^6 J/h to 49.5×10^6 J/h. Changing the width to 5mm type, the heat collecting increases from 16×10^6 J/h to 40.8×10^6 J/h, while the flat type is the lowest, 9×10^6 J/h to 36×10^6 J/h.

In terms of efficiency, the efficiency of the heat transfer is decreased by increasing the inlet water velocity and its rate of reduction is decreased by the velocity. When the velocity is larger than 0.6 m/s, the rate is much lower than before. The efficiency value for the first type is also reduced from 96 % to 55 %, in the deleting small type, the values reduced from 99.6% to 54.5% and for the deleting big type, it is decreased from 99.5 % to 51 %. While for all big and all small types, the values are reduced from 96.6 % to 58 % and from 95.8 % to 48.8 %, respectively. Changing the width to 5mm, the efficiency varies from 97 % to 48 %, and the lowest is the flat type, where it goes from 58 % to 41 %.

Note that the gradient is reduced by increasing the velocity. By increasing the velocity to larger than 0.6 m/s, the rate becomes much slower than before. When the inlet water velocity is 0.5 m/s, which is suitable considering both heat collecting and efficiency of all these seven types of absorbers, the first type has the second-highest heat collecting capacity (27.8×10^6 J/h) and efficiency (68%) amongst all seven types, while the efficiency for other types is 46.8 %, 67 %, 69 %, 67.3 %, 64.9 %, respectively. Except for the all big type which is 69 %, but the difference is rather small. Moreover, considering that the all big type needs higher power in real application with bigger resistance than the first type, the first novel thermal absorber is a better design compared with the other shapes.

3.2 Simulation models of the designed absorber

3.2.1 The boundary conditions of the simulation

A series of boundary conditions are set to simulate the thermal performance of the ultra-thin superconducting absorber, see Table 3-1. The boundary conditions presented in Table 3-1 include the variations in several aspects such as (1) the heat flux (I) in the range from 400 W/m^2 to 1000 W /m^2; (2) the inlet water temperature from 10 ˚C to 35 ˚C; (3) the velocity of inlet water from 0.2-1 m/s. The base set is under 800 W/m^2, the inlet water temperature is 20 ˚C, and the inlet water velocity is set to 0.5 m/s [23].

The materials of the absorber are steel and aluminum, the value of thermal conductivity for these materials is 16.27 W/m ˚C, and 237 W/m ˚C, respectively. The realizable k-ε turbulence model is used with a turbulent intensity of 5% and the viscosity ratio is 10. Density and other thermal properties are assumed to be constant. All models are meshed by using 1mm triangles, while for comparison, 2mm and 3mm triangles are also meshed to verify the accuracy of the simulation.

Table 3 - 1 List of simulation models for the novel ultra-thin superconducting absorber [23]

Simulation Mode	I (W/m^2)	T_{in} (˚C)	V_{in} (m/s)
1	400 500 600 700 800 900 1000	20	0.5
2	800	10 15 20 25 30 35	0.5
3	800	20	0.2 0.3 0.4 0.5 0.6 0.7 0.8 0.9 1

3.2.2 Simulation Results

Using CFD simulation, the impact of operational parameters (heat flux, the inlet water temperature, and inlet water velocity) on the novel ultra-thin superconducting solar absorber is investigated. We further evaluate the thermal performance of different shapes with the same materials and compare them for different inlet water

velocities. Furthermore, we compare the performance based on the outlet water temperature and the map of the whole plate temperature, the outlet water temperature, and the difference between inlet, and outlet water temperature are calculated. In this study, the heat loss to the surrounding through radiation transfer is ignored for brevity, and the efficiency of the thermal absorber is calculated by equation (3-8).

$$\eta_{th} = \frac{Q_u}{IAt} = \frac{cm\Delta T}{IAt} = \frac{cm(T_{out} - T_{in})}{IAt} \quad (3\text{-}8)$$

We consider three different mesh sizes because it can cover the errors caused by using only one size mesh. Another reason for using different mesh sizes is to compare the result and select the best mesh for the model. As the width of the novel solar thermal absorber is 4mm, using 1mm mesh, the result is more accurate and calculation time is reasonable. The simulation convergence results for all three mesh sizes are accurate and for 1mm mesh size, the convergence result is shown in Figure 3- 4.

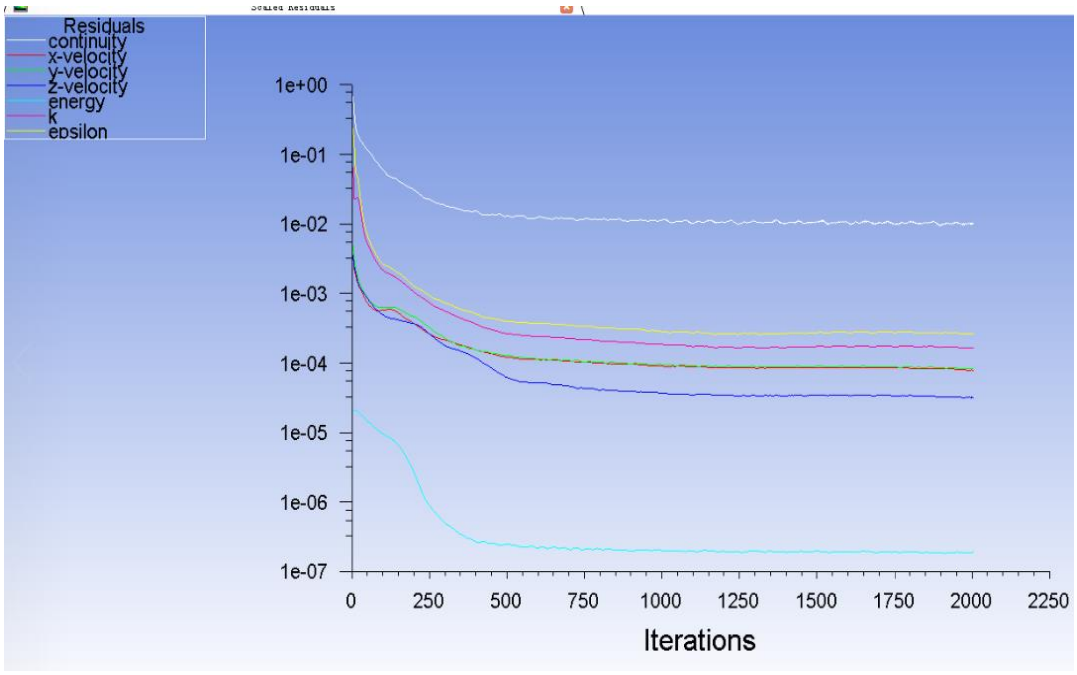
Residuals
continuity
x-velocity
y-velocity
z-velocity
energy
k
epsilon
1e+00
1e-01
1e-02
1e-03
1e-04
1e-05
1e-06
1e-07
0
250
500
750
1000
1250
1500
1750
2000
2250
Iterations

(a) 1mm

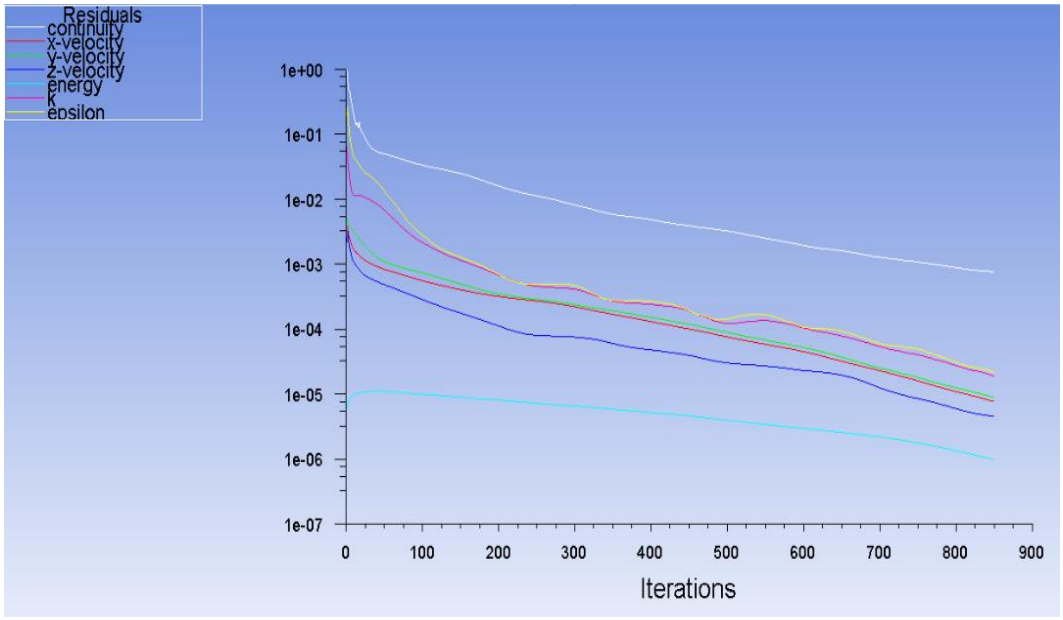
Residuals
continuity
x-velocity
y-velocity
z-velocity
energy
k
epsilon
1e+00
1e-01
1e-02
1e-03
1e-04
1e-05
1e-06
1e-07
0
100
200
300
400
500
600
700
800
900
Iterations

(b) 2mm

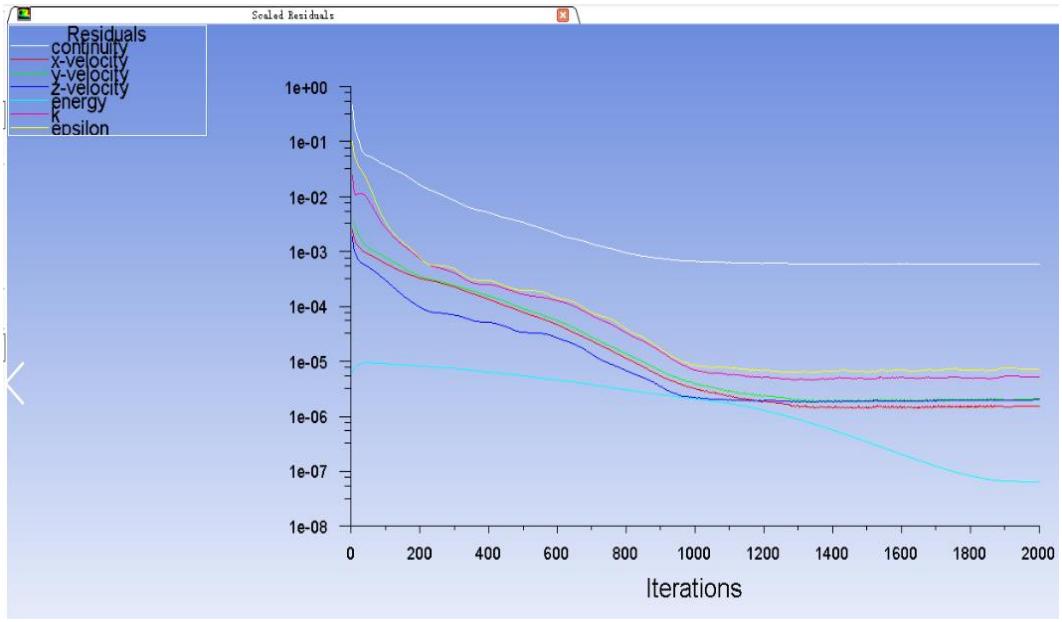

(3) 3mm

Figure 3- 4 Simulation result with different mesh sizes

3.2.2.1 Impact of the heat flux

The simulation results are shown in Figure 3-6, where the heat flux is changed from 400 W/m^2 to 1000 W/m^2, with 100 W/m^2 increase steps while other parameters are kept constant, i.e., inlet water temperature is 20 ˚C and its velocity is 0.5 m/s. The results about the outlet water temperature, the inlet, and outlet water difference, and the efficiency of the absorber are also shown Figure 3- 5, and the temperature and pressure distribution examples under solar irradiation with 800 W/m^2 are shown in Figure 3- 6. It is seen that by increasing the heat flux, the outlet water temperature is increased while the inlet water temperature is constant. It is also seen that the temperature difference (ΔT) between the inlet and outlet water is increased from

0.034 ˚C to 0.41 ˚C. Higher heat flux enhances the solar heat transfer of the absorber, causing a significant improvement of the efficiency, η, from 10.8% to near 60%. As a result, the heat flux has a significant impact on the efficiency, η, of the ultra-thin superconducting absorber. But considering the lower outlet water temperature which is better for the PV collector, the heat flux should be not so high in real applications. Note that the heat flux is directly related to the solar irradiation.

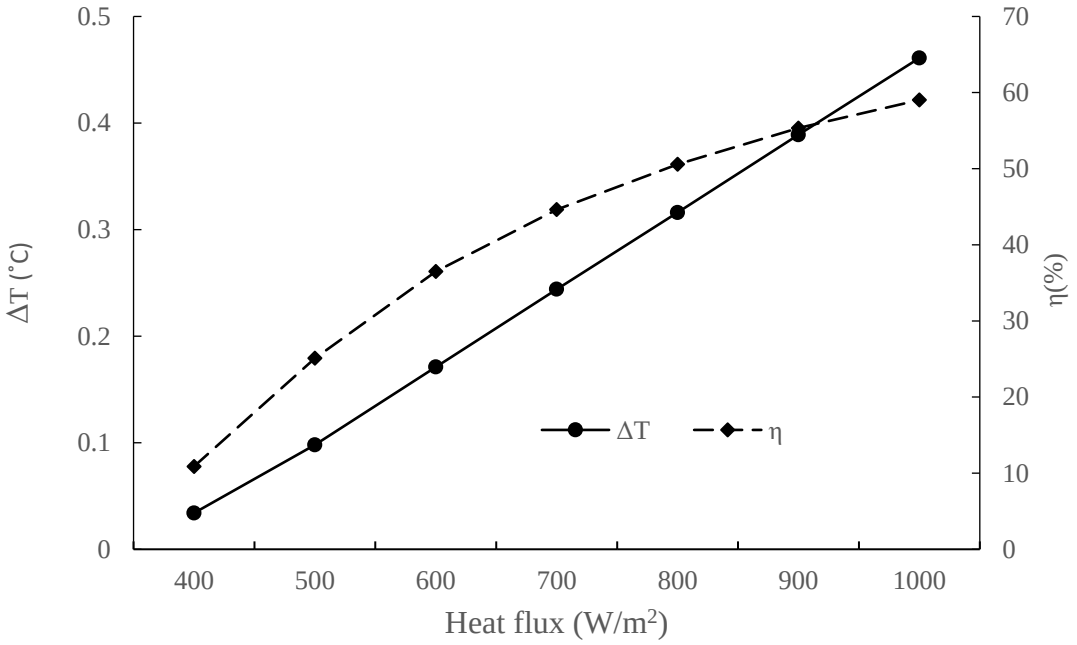

Figure 3- 5 Thermal performance of water temperature difference between the inlet and outlet (ΔT), the efficiency (η) for novel absorber in mode 1

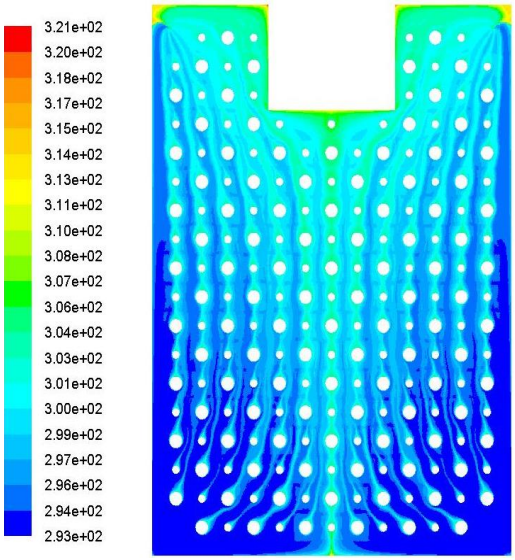

Figure 3- 6 Temperature distribution examples under 800 W/m^2

3.2.2.2 Impact of inlet water temperature

For simulation mode 2 the simulation results are presented in Figure 3-9, where the inlet water temperature is varied from 10 ˚C to 35 ˚C with the increased steps of 5 ˚C, and heat flux 800W/m^2 and inlet water velocity 0.5 m/s. For mode 2, the temperature and the map of the velocity are simulated and the outlet water temperature is recorded in the simulation result. The thermal performance results are shown in Figure 3- 7.

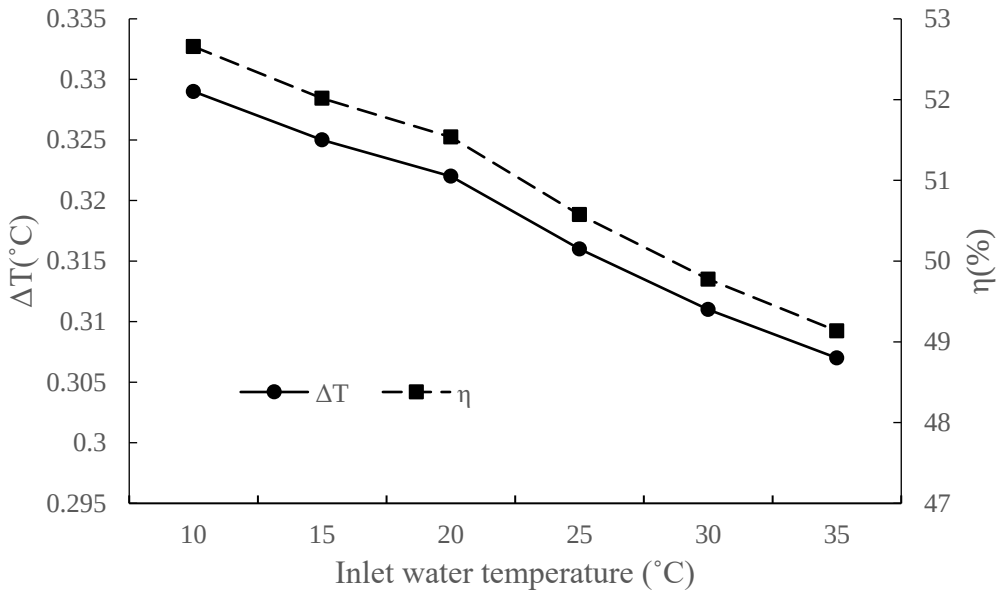

Figure 3- 7 Thermal performance of the water temperature difference between inlet and outlet (ΔT), the efficiency for novel absorber under mode 2, η.

The outlet water temperature is increased by increasing the inlet water temperature. Different from the impact of the heat flux on the thermal performance of the efficiency, by increasing the inlet water temperature, the difference between the inlet and the outlet temperature is decreased. This results in decreasing the efficiency of the ultra-thin superconducting absorber from 52.7 % to 49 %. The trend is opposite with the heat flux impact and the degree is also different. The impact of the inlet water temperature also affects the efficiency (η) of the absorber. Our results also suggest a low impact of the inlet temperature on the performance of the absorber. Nevertheless, improving the temperature of the inlet water is often costly. Therefore, for the real applications, from the absorber point of view, the natural water could be directly used as the inlet water.

3.2.3.3 Impact of the inlet water velocity

For simulation mode 3 which is shown in Figure 3-10, the inlet water velocity is changed from 0.2 m/s to 1.0 m/s, with 0.1 m/s steps. Similar to other simulation modes we also keep other parameters constant, i.e., heat flux is 800W/m2 and inlet water temperature is 20˚C. In this simulation model, the temperature and the map of the velocity are simulated and the outlet water temperature is recorded in the simulation results. The thermal performance results are shown in Figure 3- 8.

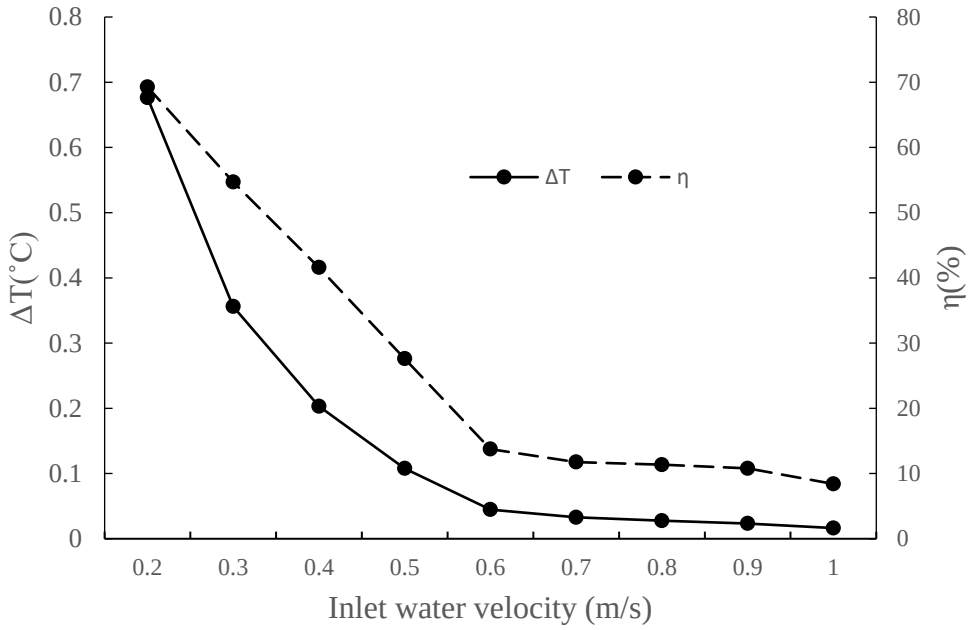

Figure 3- 8 Thermal performance of the novel absorber for mode 3

The inlet water velocity highly affects the efficiency of the novel absorber. With the increase of the inlet water velocity from 0.2 to 1 m/s, the efficiency is reduced from 70% to under 10%. For the inlet water velocity larger than 0.6m/s, the temperature difference between the inlet and outlet water is close to 0. This means

the water in the absorber does not gain enough heat before it is pushed out through the outlet. Moreover, for higher inlet water velocity, the heat transfer distribution is increased. Therefore, the heat transfer resistance is also increased hence the thermal efficiency is decreased. However, if the water velocity is too low, although the efficiency is high enough, the heat transfer capacity is low. In practice, the inlet water velocity 0.5 m/s might be suitable considering the efficiency and the using time for the collector.

3.3 Design of the PV/T-ASHP system

3.3.1 The detailed information about an office room

The experiment considers an office room which is located in Beijing and its size is shown in Figure 3-9. The length is 12.5 m, and the width is 3 m and the height is 2.9 m. This is an office room with four workers which is used for daily works. The main body of the assembly room is a 10 cm polystyrene board with a heat transfer coefficient of 0.04W/(m^2·K). The room has a broken bridge aluminum door with a 330mm *2510 mm window and a heat transfer coefficient of 1.75W/(m^2·K). The size of the sliding door is 1120mm * 1100mm which includes a plastic steel window, hollow glass with anti-theft steel mesh. The size of the steel door is 845mm * 2025 mm. Ignoring the influence of the column, according to the "Code for Design of Heating, Ventilation and Air Conditioning of Civil Buildings" GB50736-2012, the indoor design parameter is 18℃, and the outdoor design parameter is -7.5 ˚C.

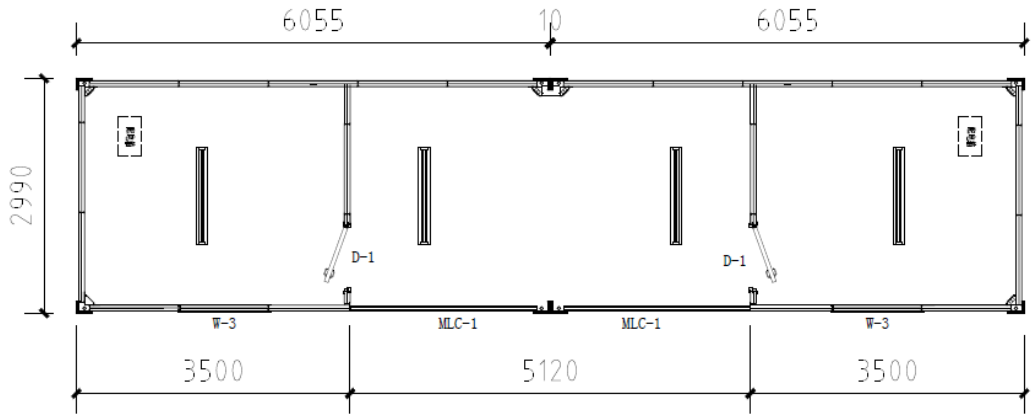

(a) top view

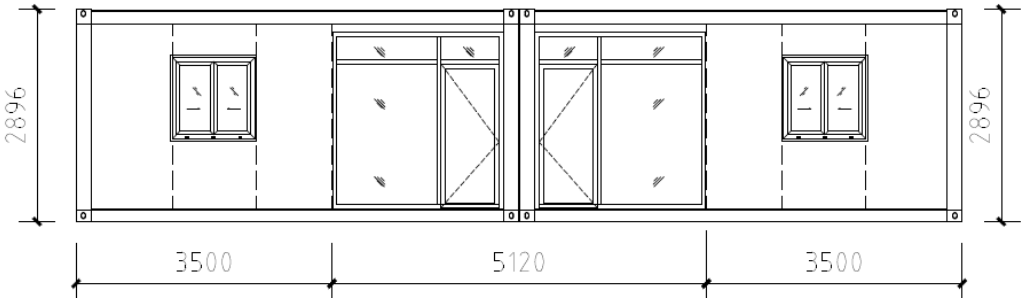

(b) front view

Figure 3- 9 Size of the experiment office room (units: m)

The building has four walls, east, south, west, and north. The height of the ceiling is 2.9m. Therefore,

The area of the east outer wall is: $2.99 \times 2.896 = 8.66\ m^2$

The area of the west outer wall is: $2.99 \times 2.896 = 8.66\ m^2$

The area of the south outer wall is: 12.12×2.896-0.845×2.025×2-1.12×1.1×2=29.2 m^2, the south outer window: 1.12×1.1×2=2.46 m^2, the door: 0.845×2.025×2=3.4 m^2

The area of the north outer wall is: 12.12 × 2.896=35.1 m^2

Roof: 2.99×12.12=36.2 m^2

1) The basic heat consumption of the enclosure structure is:

$$q = KF \times (t_n - t_w)\,\partial$$

$where,\ t_n$ is the design temperature for this office and t_w is the design ambient temperature. K is the heat transfer coefficient and F is the area.

The basic heat consumption of the external wall:

Q_1=0.04×(0.95×8.66×2+0.8×29.2+0.95×35.1)×(18+7.5)=74.6W

Basic heat consumption of exterior windows and doors:

Q_2=1.75×2.46×0.8×(18+7.5)=87.8W

Q_3=1.75×3.4×0.8×(18+7.5)=121.4W

Roof: Q_4=0.04×36.2×(18+7.5)=36.9W

2) Cold air penetration: according to the gap method, the effect of the heat pressure and outdoor wind speed with height is not considered

The building has only south-facing gaps, including:

Window: (1.12×4+1.1×4+1.1×3)×2=24.36m

Door: (0.845×4+2.025×7)×2=35.11m

Air infiltration volume:

$V=\sum(lLn)=24.36\times0.5\times0.15+35.11\times0.5\times2\times0.15=7.1m^3/(h\cdot m)$

$Q_5=0.278\times V\rho\times(tn-tw)c$

$Q5=0.278\times7.1\times(18+7.5)\times353/(375-7.5)=48W$

3) Heat consumption of cold wind intrusion:

$Q_6=NQ_3=1\times121.4=121.4W$

4) Ground division (64 m^2)

$R=R_0+10/0.04=0.47+250(m^2\cdot K)/W$

$K=0.004W/(m^2\cdot K)$

$Q_7=0.004\times64\times(18+7.5)=6.5W$

5) Thermal index:

We calculate the total load of the building based on the above

$Q_{total}=Q_1+Q_2+Q_3+Q_4+Q_5+Q_6+Q_7=74.6+87.8+121.4+36.9+48+121.4+6.5$

$=496.6W$

The building heat index is $Q_f=496.6/36=13.8\ W/m^2$

3.3.2 Design of the system

The final used design description is presented in the following. The configurations of the PV/T collector are shown in Figure 3- 10. The inclined angle of the collector is 47˚, and it faces south. Based on the calculation results for this office room's thermal index, to satisfy the heating load demand for this room, the total surface area for the PV/T collector with two arrays is designed for 2.6 m^2, and that for each one is 1.3 m^2. The structure of the collector is shown in Figure 3- 10 (b). From top to the bottom, the collector is composed of the metal frame, glass, two EVA files, and the film consists of the solar cell, the absorber, and the back insulation.

Figure 3- 11 also shows the geometrical parameters for the collector. The thermal absorber consists of two metal layers and the thickness is 4mm. The front metal is flat, while the back metal has evenly-distributed extruded pin-fins. These fins increase the heat exchange area and further strengthen the fluid disturbance. Stronger flow disturbance enhances the heat transfer coefficient. For further strengthening of the fluid disturbance, we design two types of pin-fins, which have different sizes. The shapes of the two pins are both cylindrical. The diameters of the pins are 3 cm, and 1.5 cm, respectively.

There are two water inlets and water outlets which are located at the bottom and top of the absorber, respectively. The dimension of an absorber is 123 cm × 90 cm. The distance between the two neighbor fins is 12.5 cm. For installation, the distance from the edge to the absorber is 2 cm for the top, and 0.5 cm for the bottom. The distance between the pin and the edge is 5.5 cm. For installation, there is one blank

area of 27 cm × 23 cm at the top, and the installation angle is 47˚, south-facing. As the solar angle is near 50 ˚N at the noon and considering the seasonal changes, especially in the heating season the solar angle is 26.5 ˚N. To gain the most solar energy, the solar angel 47˚ is chosen.

(a)

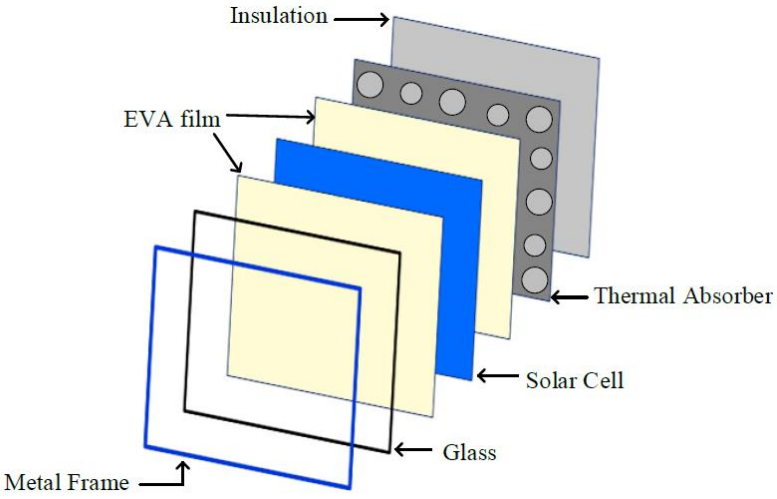

(b)

Figure 3- 10 Configuration of the PV/T collector (a) photo and (b) schematic of the structure

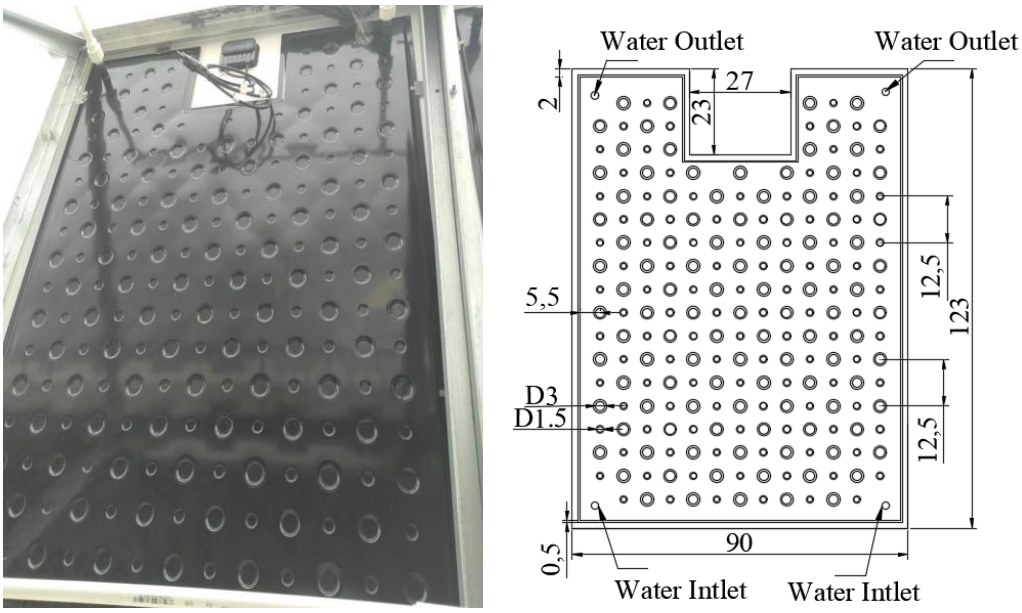

(a) (b)

Figure 3- 11 Configuration of the novel solar ultra-thin superconducting absorber (a) photo and (b) schematic (cm)

The schematic of the experimental setup and the working principle of the PV/T system are shown in Figure 3-12. Figure 3-13 further shows the pictures of the main equipment, i.e., the PV/T collector, the water tank and the evaporator of the ASHP system in the experiment. In this experiment, the PV/T system and the ASHP system are combined in parallel mode. The ASHP system has two functions, including gaining the energy from the outside air and gaining energy through heat exchange with the water tank which stores the heat gained by the PV/T collector.

The PV/T system gains solar energy and transfers it into electricity and heat. The electricity produced by the PV /T collector is stored in the battery and supplied to the users. The electric box, as shown in Figure 3-13, is used to measure the total amount of electrical energy. The heat energy is supplied to the water tank for storage, which is supplied to the ASHP system for room heating and hot water supply.

The design parameters of the main equipment in the PV/T-ASHP system are shown in Table 2- 2. The water tank volume is 100 L, which is used for hot water storage. The refrigerant used in the ASHP system is R 22. The experiment is located in an office room near Beijing (117˚E, 40˚N), a cold region of China. The lab room is 3.5 m × 3 m × 3 m, the door is 2 m × 0.85 m and the window is 1.1 m × 1.1 m, south facing. This system is operated according to the office room working schedule, it is turned on at 8 am and turned off at 5 pm seven days a week.

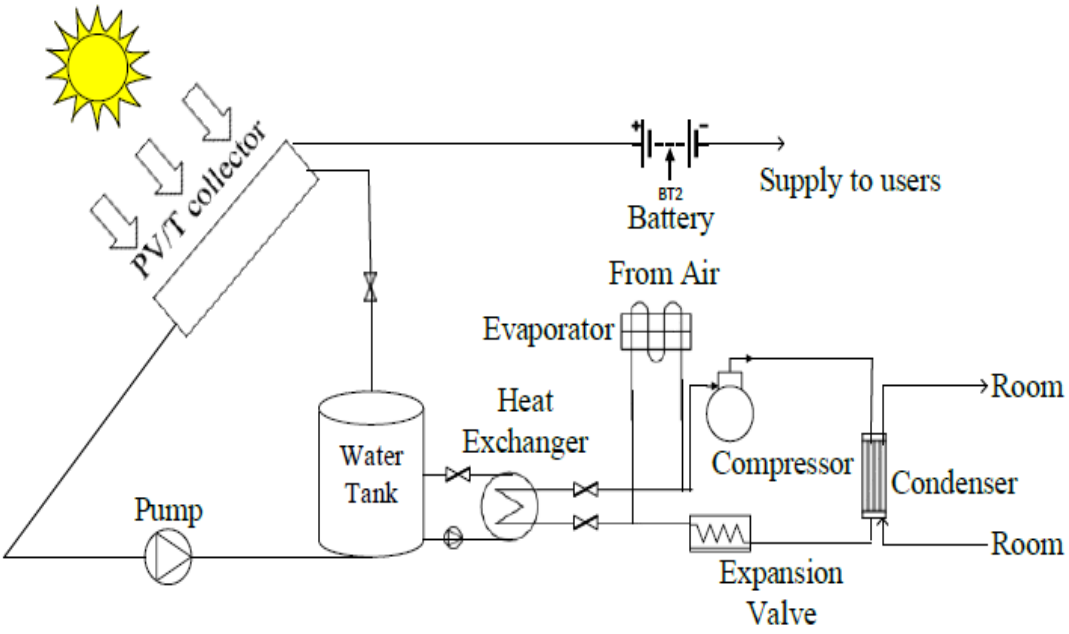

Figure 3- 12 The schematic of the experimental setup of the PV/T-ASHP system

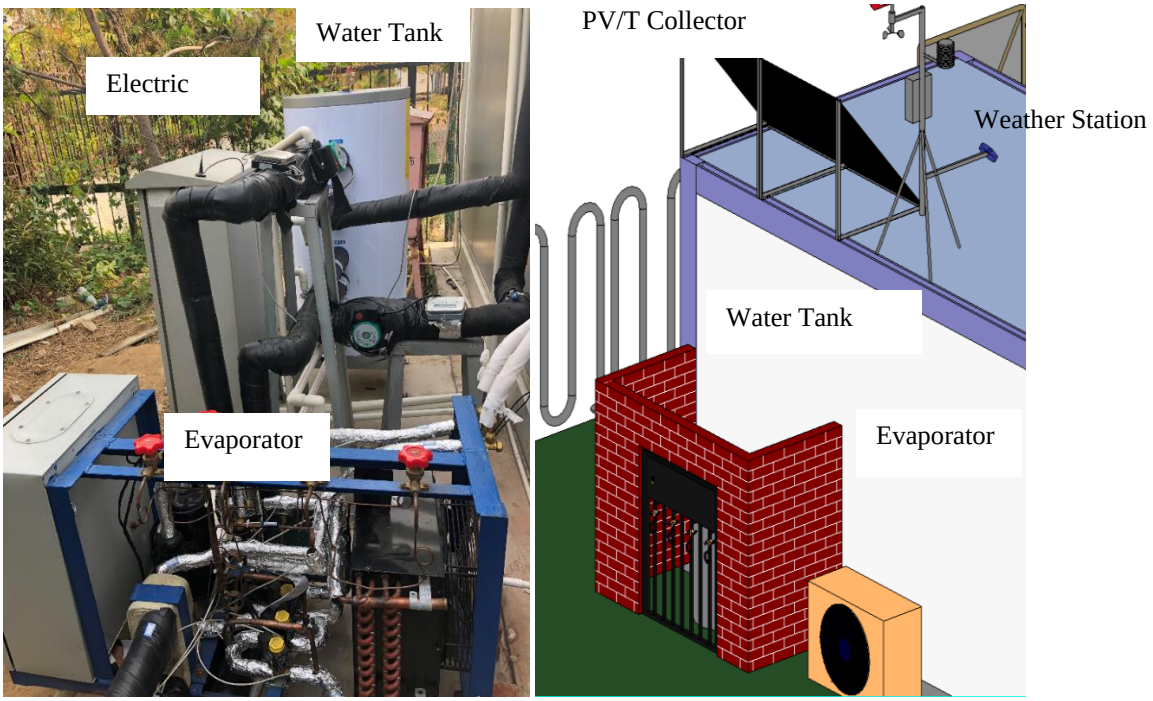

Figure 3- 13 The picture of the part of the PV/T-ASHP system

Table 3 - 2 The parameters of the main equipment

	Number	Size/Capacity
PV/T Collector	2	1.3m*1m
Water Tank	1	100L
Pump	2	50L/min
Condenser	1	3500W
Heat Exchanger	1	3000w
Evaporator	1	2500W
Expansion Valve	1	1.8MPa/0.5 MPa

3.4 Measurement and calculation

The external environment conditions are measured by the weather station installed next to the PV/T collector (Figure 3-12 (a)). The measurements include the external temperature, humidity, wind speed and solar irradiation. For the PV/T-ASHP system, the main measurements include the water temperature at the solar collector inlet, the temperature of the outlet water from the tank and that at the thermal absorber surface temperature. We use the temperature probe with the accuracy of ±0.01℃ for the measurement. The water flow used an ultrasonic heat meter, with the range 0.07-7m3/h and the accuracy of level-2, ±0.14m3/h. Experiments were

operated from 9:00 to 17:00, and the time interval between the measurements was 10 min.

The performance of this PV/T-ASHP system is described separately, for the PV/T collector system and ASHP system, mainly include the COP of ASHP system. The performance indicators are the COP of the ASHP system, the thermal efficiency of the PV/T collector, and the self-sufficiency of electricity and thermal energy for the PV/T-ASHP system. These indicators are defined as follows:

$$COP = \frac{Q_{user}}{P_{ASHP}} \tag{3-8}$$

$$\eta = \frac{Q_{gain}}{S} \tag{3-9}$$

$$R_{ele} = \frac{P_{PV/T}}{P_{sys}} \tag{3-10}$$

$$R_{heating} = \frac{Q_{gain}}{Q_{user}} \tag{3-11}$$

where, COP is the coefficient of the ASHP performance, Q_{user} is the energy capacity supplied to users, P_{ASHP} is the power consumption by the ASHP system. η is the thermal efficiency of PV/T collector, S is the total solar irradiation gained by the PV/T collector, and Q_{gain} is the heat transfer capacity, which is stored in the water tank. Furthermore, R_{ele} represents the self-sufficiency of electricity, $P_{PV/T}$

is the electric power produced by PV/T collector, P_{sys} is the power consumption of the system, and $R_{heating}$ is the self-sufficiency of heat during heating seasons.

3.5 Conclusion

In this chapter, the model of the proposed novel ultra-thin superconducting solar absorber in the PV/T collector was built through CFD software. Then the novel absorber was simulated under different boundary conditions and its performance for different constructions of the absorbers was compared. Finally, the performance under different conditions was analyzed.

Several main conclusion includes: (1) The heat flux has a significant impact on the efficiency (η) of the ultra-thin superconducting absorber. Higher heat flux enhances the solar heat transfer of the absorber hence significantly increases the efficiency (η) from 10.8 % to near 60 %. (2) From the result, the impact of the inlet temperature cannot significantly affect the performance of the absorber and by increasing the inlet water temperature, the difference between the inlet and the outlet temperatures is reduced and the efficiency of the ultra-thin superconducting absorber reduced from 52.7 % to 49 %. (3) With the increase of the inlet water velocity from 0.2 to 1 m/s, the efficiency is reduced from 70 % to under 10 %. For the inlet water velocity larger than 0.6 m/s, the temperature difference between the inlet and outlet water temperatures is near 0. (4) For the inlet water velocity of 0.5 m/s, the first type has the highest heat collecting (27.8×10^6 J/h) and efficiency

(68 %) amongst all types, except the all big type with efficiency (69 %) but the difference is small. Moreover, the all big type needs more power in practice due to the larger resistance compared with the first type. The experiment performance of the novel ultra-thin superconducting absorber needs further study in the future.

Chapter 4: Experiment of testing of the solar collector in the PV/T-ASHP system and model validation using Matlab

One of the most common methods to improve the thermal performance of the collector is by optimizing its design. The common designs include a sheet-and-tube structure, rectangular tunnel with or without fins/grooves, flat plate tube, micro-channel heat pipe array/ heat mat, extruded heat exchanger, roll-bond heat exchanger, and cotton wick structure [110]. Several studies on the thermal absorber were conducted in the past few decades. A sheet-and-tube absorber requires a relatively low investment as the corresponding industry is rather mature and it also provides satisfactory performance [111]. Nevertheless, its structure is complex. The application of sheet-and-tube absorber is limited because of its large weight [112].

Amongst the existing structures, the absorber of a rectangular tunnel with or without fins/grooves has the lowest weight and incurs the lowest investment [113, 114]. However, its heat transfer efficiency is the lowest [115, 116]. Although the contact between the PV cells and absorber of a flat plate tube is simple, the thermal resistance of its structure is high [117, 118]. An absorber with a micro-channel heat pipe also called a heat mat, improves thermal performance. However, the thermal resistance is also increased [119, 120, 121]. The applications of the roll-bond

absorber and cotton wick structure absorbers are also limited [122] mainly because of their high construction and maintenance cost. The extruded absorber demonstrates high potential compared to the above absorbers, particularly, the super-thin extruded pin-fins absorber. It generally achieves higher efficiency than other designs of the absorber plates. This is because its special design enhances the heat transfer and its weight and the investment required are significantly lower than the extruder absorber [123] [124]. The main results were as follows: the hybrid PV/T panel enhances the electrical return of PV panels by nearly 3.5% and increases the overall energy output by nearly 324.3% under certain circumstances. Their results demonstrated that the PV/T panel achieves an electrical efficiency of approximately 16.8% (5% improvement compared with the stand-alone PV panel), and yields an additional amount of heat with a thermal efficiency of nearly 65%.

However, there are two issues. One is that the existing studies are either solely based on simulations, or conducted in laboratory conditions [124, 123]. Hence, the feasibility of its actual marketable applications has not been verified. In this study, our objective is to investigate the application performance of a novel construction extruded absorber. The effect of its application on the thermal performance of an entire PV/T-assisted ASHP system is studied and analyzed for an office room during the heating season.

Moreover, the effects of several uncertain factors such as the dynamic weather conditions on this system have not been studied [110]. In this chapter, the variation in the thermal efficiency of the solar collector under different environmental

conditions is also analyzed using both mathematical and experimental methods. This study addresses the research gap in the related literature and is essential for future market release.

4.1 Working principle of the solar collector

The PV/T collector absorbs solar energy and produces electricity which is stored in a battery. It also produces heat, which is transferred to the absorber. The absorber supplies the heat to other equipment such as the water tank, for further use. The PV cell absorbs part of the solar energy and transforms it into electricity. The remaining solar energy is transformed into heat which is absorbed by a thermal absorber.

The collector can be divided into multiple layers, as shown in Figure 4 - 1. Three hypotheses are considered to simplify the model. First, the temperature at each layer is assumed to be uniformly distributed. Second, the glass absorbs the solar radiation. , where the solar energy is partly absorbed and the remaining is reflected. Third, considering that the EVA film is very thin and R_{PV} is marginal, in our modeling, we ignore the heat loss that happens through the PV cell to the surrounding environment.

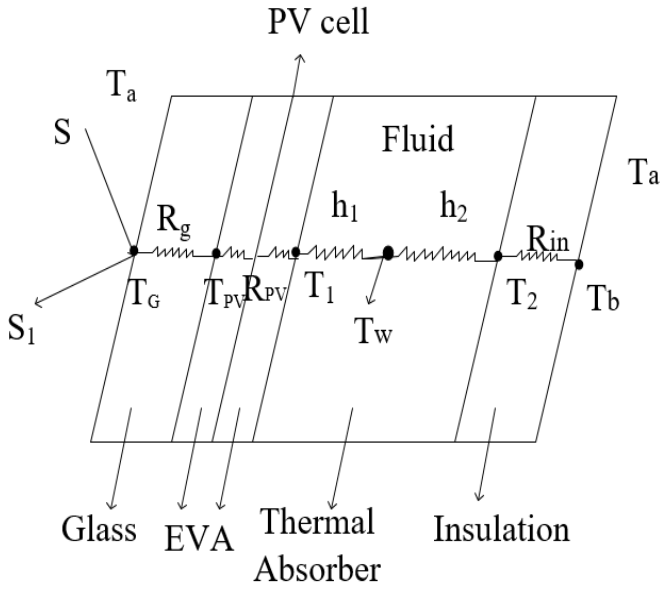

Figure 4 - 1Thermal resistance network of PV/T collector

For the glass surface, part of the solar radiation (S) on the surface/glass of the collector is reflected in the atmosphere, and the remaining part is absorbed and transferred to the PV-cell layer. Equation (4-1) is developed to show the mathematical relationship among different parts of energy.

$$S - S_1 + h_G(T_G - T_a) = (T_{PV} - T_G)/R_g \qquad (4\text{-}1)$$

where S represents the solar radiation that reaches the collector glass surface, S1 is the solar radiation that reflects to the atmosphere from the glass surface, h_G is the glass radiative heat transfer coefficient (J/h·m^2·K), T_a is the ambient temperature (K), T_G is the glass surface temperature (K), T_{PV} is the PV cell surface temperature (K), and R_g is the thermal resistance of the glass layer (h·m^2·K/J).

Part of the solar energy that is absorbed by the PV cell is then transformed into electricity and stored in the battery. The remaining energy is transferred to the thermal absorber. The heat transfer is calculated using the following Equation (4-2).

$$\frac{(T_{PV} - T_G)}{R_g} = \frac{(T_1 - T_{PV})}{R_{PV}} \tag{4-2}$$

where T_1 is the thermal absorber surface temperature (K) and R_{PV} is the thermal resistance of the PV cell (h·m^2·K/kJ).

In the thermal absorber, the water absorbs heat and then supplies the energy to the users. The energy balance is as the following:

$$q_u = h_1(T_1 - T_w) - h_2(T_w - T_2) \tag{4-3}$$

where q_u is the heat absorbed by the water (J/h·m^2), T_w is the mean water temperature in the thermal absorber (K), T_2 is the back surface temperature of the thermal absorber (K), h_1 is the heat transfer coefficient to the channel at the front, and h_2 is the heat transfer coefficient to the channel at the back (J/h·m^2·K).

The heat is then transferred to the back-insulation material according to the following equation:

$$\frac{T_2 - T_{\mathrm{b}}}{R_{\mathrm{in}}} = h_b(T_{\mathrm{b}} - T_a) + Q_{loss} \tag{4-4}$$

where T_{b} is the back surface temperature of the insulation (K), R_{in} is the thermal resistance of the insulation (h·m^2·K/J), h_b is the insulation radiative heat transfer coefficient (kJ/h·m^2·K), and Q_{loss} is the heat loss to the surrounding environment through insulation (kJ/h·m^2). The convection coefficient is $h_{loss-c} = \frac{8.6V^{0.6}}{L^{0.4}}$,where V is the ambient wind speed. Radiation heat transfer coefficient is $h_{loss-r} = \varepsilon\sigma(T_G + T_S)(T_G^2 + T_s^2)$, where the sky temperature is $T_S = 0.055T_a^{1.5}$ [125].

The absorber thermal efficiency is essential for evaluating the performance of the PV/T collector. In this experiment, the solar collector thermal efficiency is calculated using Equation (4-5):

$$\eta_{th} = \frac{Q_u}{IAt} * 100 \tag{4-5}$$

where, η_{th} is the thermal absorber heat efficiency (%), Q_u is the heat of the water absorbed through thermal absorber (kJ), I is the solar irradiation absorbed by the collector, W/m^2, and A is the collector area (m^2).

The heat transfer efficiency is evaluated via both experimental measurement and mathematical model calculation. According to Emmanouil et al. [126], the error in the heat loss calculation includes, the measuring set-up error (1.5%), imperfections of the energy model (2.6 %), and variation in the meteorological conditions (3.5 %). The total combined uncertainty is 9% for a confidence level of 95% and a coverage coefficient (k) of 2.

The external environmental conditions are measured by the weather station installed next to the PV/T collector. The measurements include the external temperature, humidity, wind speed, and solar radiation. The main measurements for the PV/T-ASHP system include the water temperature at the solar collector's inlet, temperature of the outlet water from the tank, and temperature of the thermal absorber's surface. We use a temperature probe with an accuracy of ±0.01 °C for our measurement. The water flow is measured using an ultrasonic heat meter with a range of 0.07–7 m^3/h and level-2 accuracy (±0.14 m^3/h). Experiments were conducted during 9:00–17:00. And the time interval between the measurements was 10 min.

4.2 Matlab model of the solar collector

In this section, the mathematical model of the solar collector for calculating its thermal performance is presented. To simplify the model, we make the following assumptions: a) There is no heat loss through the back-insulation material and the collector edge. b) The heat transfer coefficient is constant and uniform for the pin-fins. c) There is no heat loss during the process of the heat transfer among the different layers in the solar collector. d) The temperature gradient across the solar collector thickness is omitted as in [124]. Furthermore, the detailed calculation for the solar collector is as the following.

4.2.1 Heat transfer for the novel thermal absorber with frustum pin-fin banks

Based on the above hypotheses, the heat transfer coefficient is constant and uniform throughout the fin surface. The transfer process is a one-dimensional steady-state heat conduction problem with variable cross-section. Because the diameter and the distance are linear, the length of the frustum H $(4\ \mathrm{mm}) < \mathrm{D}$. D is the diameter of the frustum. The frustum pin-fin is shown in Figure 4 - 2. We further assume that the heat transfer coefficient is constant and uniform over the whole fin surface.

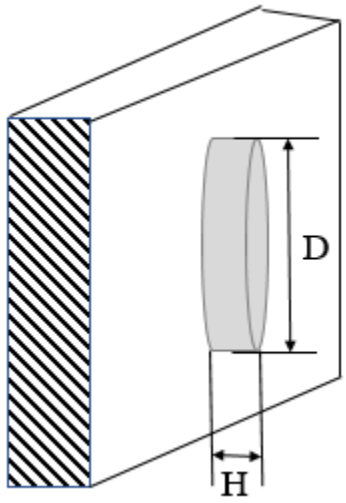

Figure 4 - 2 The schematic of the simplified frustum pin-fin

Considering the big pin-fin as an example, the fin efficiency is:

$$\eta_f = \frac{th(mH')}{mH'} \tag{4-6}$$

where the variable m is:

$$\mathrm{m} = \sqrt{\frac{4h}{\lambda d}} \tag{4-7}$$

and H' is: $H' = \mathrm{H} + \frac{D_{big}}{4}$

and the small pin-fin is the same as the big pin-fin, except for its diameter.

Under steady conditions, the useful heat gain Q_u is equal to the heat conduction through both pin-fin and un-finned surfaces, which is calculated as:

$$Q_u = \int A q_u \, dA = h_{conv,fT}(\eta_f A_{fin} + A_{unfin})(T_1 - T_f) \tag{4-8}$$

$$T_f = (T_{in} + T_{out})/2 \tag{4-9}$$

$where, A_{fin}$ is the total surface of all the fins include big fin and small fin, the A_{unfin} is the area of the un-finned of the plate surface,

$$A_{fin} = \frac{n}{2}\pi(D_{big} + D_{small})H \tag{4-10}$$

$$A_{unfin} = A_P - \frac{n}{2}\pi\frac{D_{big}^2 + D_{small}^2}{4} \tag{4-11}$$

And n is the total number of pin-fins.

For the fully developed turbulent flow in the channel, the Nusselt number is calculated by Gnielinski equation [127]:

$$Nu_f = \frac{(f/8)(Re - 1000)Pr_f}{1 + 12.7\sqrt{f/8}\,(Pr_f^{2/3} - 1)}[1 + (\frac{d}{l})^{2/3}]c_t \quad (4\text{-}12)$$

Where l is the length of channel and f is the Darcy coefficient of the turbulent flow, $f = (1.82lgRe - 1.64)^{-2}$ [127].

4.2.2 Heat convection across the line pin-fin banks

The aligned arrangement pin-fin banks are shown in Figure 4 - 3. For this novel thermal absorber, the distance between fins L_1 is equal to L_2. Considering the difference of the diameter between the big and small fins, we take the mean value as the diameter of the fin.

$$D_{mean} = \frac{D_{big} + D_{small}}{4} \quad (4\text{-}13)$$

In this experiment, the number of rows of the aligned pin-fin banks is 18, over 16, the Nusselt numbers are calculated by Zhukauskas equations, shown in Table 4 - 1.

Then the useful heat gain by the flow convection Q_c

$$Q_c = m_w C_p(T_{out} - T_{in}) = \mathrm{hA}(T_{out} - T_{in}) \quad (4\text{-}14)$$

$$\mathrm{h} = \lambda N_u / D_{mean} \quad (4\text{-}15)$$

The mass flow rate of water m_w is a design parameter in the experiment.

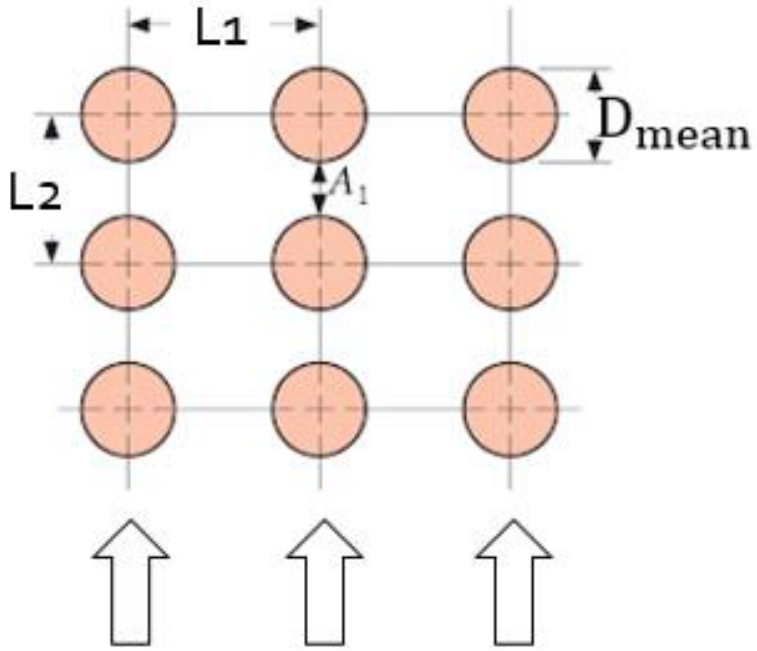

Figure 4 - 3 Arrangement of the aligned pin-fin banks

Table 4 - 1 Calculation equations for determining the average surface heat transfer coefficient of the fluid across the aligned pin-fin banks [127]

Equation	Re
$Nu_f = 0.9Re_f^{0.4}Pr_f^{0.36}(Pr_f/Pr_w)^{0.25}$	1-10^2
$Nu_f = 0.52Re_f^{0.5}Pr_f^{0.36}(Pr_f/Pr_w)^{0.25}$	10^2-10^3
$Nu_f = 0.27Re_f^{0.63}Pr_f^{0.36}(Pr_f/Pr_w)^{0.25}$	10^3-2×10^5
$Nu_f = 0.033Re_f^{0.8}Pr_f^{0.36}(Pr_f/Pr_w)^{0.25}$	2×10^5-2×10^6

4.2.3 The simulation steps

Based on Equations (1)-(14), a computation program is developed for simulation and its flowchart is shown in Figure 4 - 4. The initial operation condition is as the following. The base setting is under 800 W/m^2, wind speed is 1 m/s, and the outside temperature is 25 ˚C, the inlet water temperature is 20 ˚C, and the inlet water velocity is 0.5 m/s.

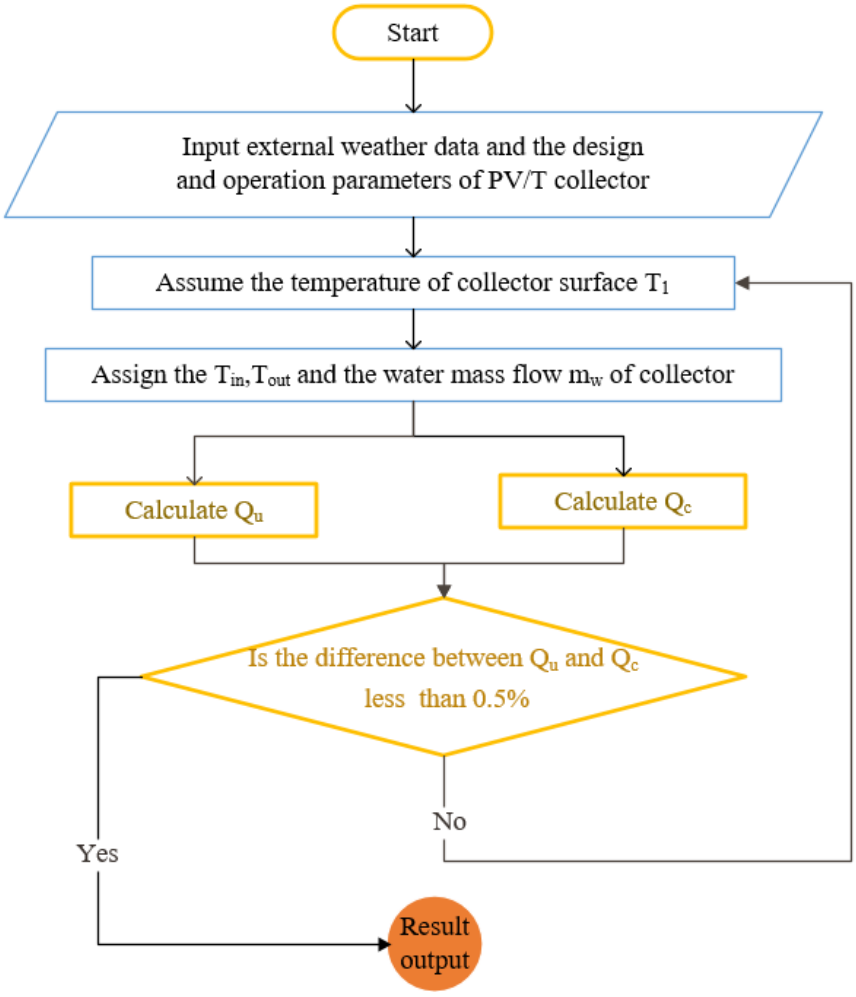

Figure 4 - 4 The flowchart of the simulation process

As illustrated in Figure 4 - 4, the computation steps are as the following: 1) Input the external weather conditions and the design parameters. 2) Set the operating conditions. Assume the absorber surface temperatures T_1 . 3) Assign the experimental operation parameters concerning water. These include the water mass flow m_w, and the inlet temperature T_{in} and outlet temperature of the absorber T_{out}. 4) Calculate the heat gain through heat conduction. 5) Calculate the heat gain from the water convection part. 6) Compute the difference between Q_u and Q_c. If $|(Q_u - Q_c)/Q_c| \leq 0.5\%$, then calculate the thermal efficiency of the absorber and then output. Otherwise, reset the absorber surface temperatures T_1 and T_2, and repeat the previous steps.

4.3 Validation of the Matlab model

To verify the accuracy of the mathematic model, the model results are compared with the corresponding experimental results for different external environmental conditions. The comparison results are shown in Table 4-2. As it is seen that the largest error is 9.6 % and the average error is 1.5 %. These results confirm the model's accuracy and validity.

Considering the uncertainty of during the measurement, these errors are reasonable for engineering research. Note that a few assumptions are made in constructing the simulation model, e.g., the heat loss through the frame to the surrounding is ignored. Errors arise during the measurement and the environmental conditions are varying

over time, which results in inaccuracy. For example, although the wind speed is close to 1 m/s, it cannot be maintained at 1 m/s. Therefore, the largest error of 9.55 % between the simulation and the experiment is reasonable [123].

Table 4 - 2 Comparison of simulations and experiments

S (W/m^2)	Ta (^oC)	Va (m/s)	η (%)		Error (%)
			Sim	Exp	
586	-5	3	12	12.9	6.98
612	0	1.5	23	22.5	2.31
602	5	2	23	23.7	3.10
606	10	3	24	23.7	1.07
598	15	1.5	31	32.4	4.39
590	20	0.5	40.2	41.1	2.19
696	25	1	39.8	39.8	0.06
601	30	1.5	40.1	40.0	0.25
323	10	0.5	20.5	22.4	8.48
410	10	0.5	28.2	29.2	3.42
495	10	0.5	31.2	32.2	3.11
656	10	3	24.1	22.0	9.55
679	10	0.5	36.2	34.6	4.62
789	10	1.5	30.2	31.0	2.58
924	10	2	32.1	31.8	0.94

4.4 Parametric study of the solar collector

The experimental results on the performance of the solar collector are presented and analyzed. Moreover, the application results and simulation results are analyzed and compared in this section. This is to investigate the variations in the thermal efficiency of the novel solar collector under different environmental conditions.

Compared with the extensive variations in solar radiation and ambient temperature, the variation in the wind speed is generally smooth. We selected sunny days during the experimental period. The thermal efficiency is shown in Figure 4 - 5. This figure shows the thermal efficiency of the solar collector versus the solar irradiance and outdoor temperature. The efficiency of the solar collector varies from 5% to nearly 60% during the period of experiment. Meanwhile, the average efficiency is approximately 30.7%. Figure 4 - 5 shows that the thermal efficiency of the solar collector is increased by increasing solar radiation. Most of the values vary from 20% to 42.5%. For the ambient temperature of approximately 26 °C, the solar radiation is approximately 600 W/m^2, the wind speed varies from 1.5 m/s to 2 m/s, and the thermal efficiency is at its highest (65%). Figure 4-5 also indicates that the change for the thermal efficiency along with the environmental conditions is rather complex. As shown in the right corner in Figure 4-5, the thermal efficiency is high because the wind speed for this figure is not stable. This may be caused by multi-environment factors including solar irradiation, ambient temperature, and wind speed.

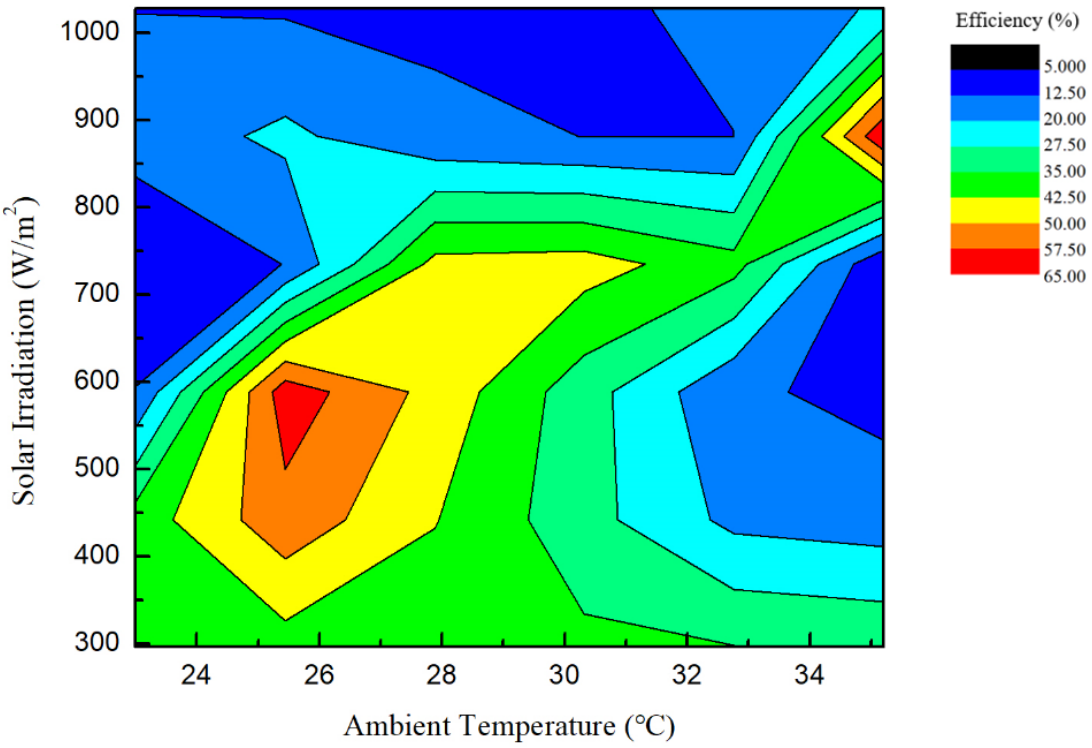

Figure 4 - 5 Thermal efficiency of the PV/T solar collector (where the wind speed < 3 m/s)

Figure 4 - 5 suggests that the thermal efficiency of the solar collector is affected by a few factors. We further consider a certain day, October 3, 2018, as an example. The reason for choosing this day is that it was a sunny day which was common during 2018. Moreover, the variation of the environmental conditions was more stable than the rainy days. Figure 4 - 6 (a) and (b) show that the variations in solar radiation and ambient temperature follow particular trends, whereas the thermal efficiency and wind speed fluctuate without following an apparent trend. We set the model to clarify the influence of each factor (including the environment and the

collector operation) on the thermal efficiency. The results are presented in the following section.

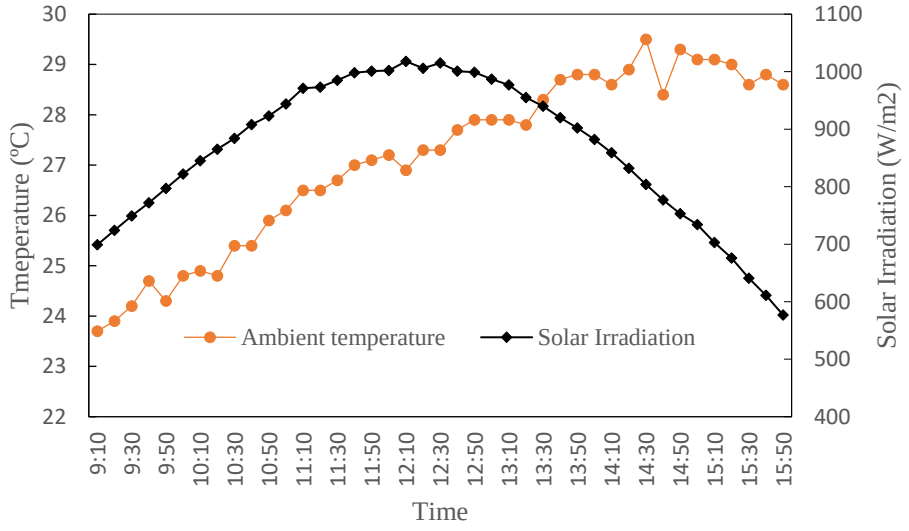

(a) Ambient temperature and solar irradiation

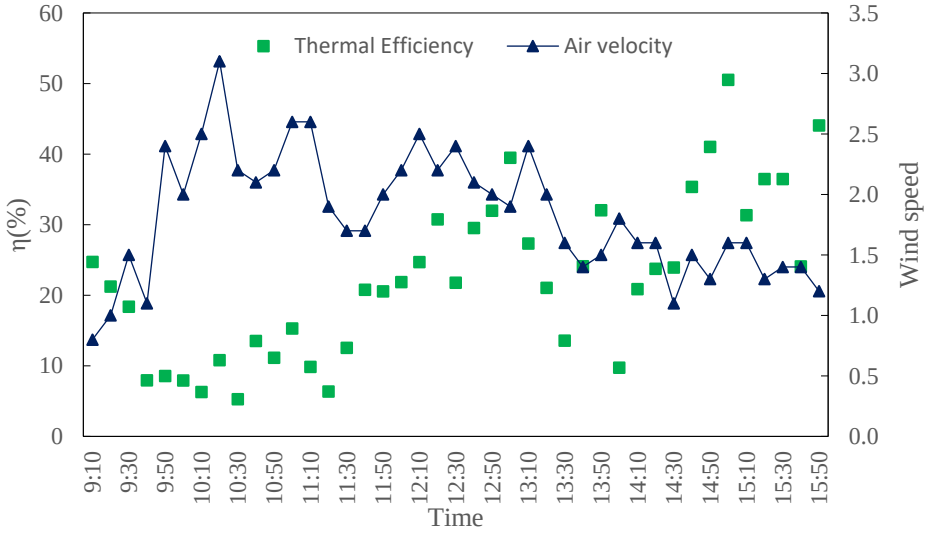

(b) Wind speed and thermal efficiency

Figure 4 - 6 The results of a typical date

4.5 Comparison of the experiment and the Matlab model

Using the mathematical model, we calculate the thermal efficiency of the solar collector under different external environmental and operational conditions. To identify the effect of these factors on the thermal efficiency, we set benchmarks for the external environmental conditions, i.e., solar radiation of 600 W/m^2, ambient the air temperature of 10 °C, outdoor wind speed of 1 m/s, inlet water temperature of 10 °C, and inlet water velocity of 0.3 m/s [23]. The operating conditions of the system are also constants, i.e., the installation angle of the solar collector (47 °). The results on the thermal efficiency of the solar collector are discussed in the following.

To identify the impact of solar radiation and wind speed on the thermal efficiency, the solar radiation is varied from 300 W/m^2 to 1000 W/m^2 at intervals of 100 W/m^2, and the wind speed varies from 0.5 m/s to 3 m/s, while other environmental conditions remain unchanged. It can be seen from Figure 4 - 7 that the thermal efficiency (η) increases by increasing the solar radiation. Higher solar radiation enhances heat transfer by increasing solar energy gain. The thermal efficiency of the solar collector is increased from approximately 18 % to nearly 40 %. Moreover, Figure 4-7 shows that thermal efficiency is increased by increasing solar radiation, whereas it is decreased by increasing the wind speed. Comparison of the simulations and experimental results shows that the values are highly similar and the average error is 4.67 %.

It is further seen that the thermal efficiency is increased by increasing the ambient temperature, whereas it is decreased by increasing the wind speed as in Figure 4 - 8. The thermal efficiency increases by increasing the ambient temperature because a higher ambient temperature improves the solar gain of the collector. Besides, as the temperature difference between the solar collector and the environment is reduced, the heat loss to the surrounding environment is also reduced. The experimental results illustrate that the thermal efficiency increases from 24 % to 46 % when the outside air temperature varies from -5 °C to 30 °C. The average error between the experimental and simulation results is 2.54%. The largest error is observed to be 6.98% when the ambient temperature is -5 °C and wind speed is 3 m/s.

In general, the wind speed varies more than the solar radiation level and ambient temperature. To obtain more accurate results, the influence of the wind speed on the thermal efficiency of the PV/T solar collector is analyzed via simulation. The simulation results are shown in Figure 4 - 7. It displays the variation trend upon the outside wind speed variations from 0 to 5 m/s while other parameters are constant, i.e., solar radiation of 600 W/m^2 and the ambient temperature of 10 °C. Figure 4 - 8 shows that thermal efficiency is decreased by increasing the outside wind speed. This is because the higher the wind speed, the higher the heat transfer coefficient between the environment and the solar collector. Therefore, the heat loss to the environment from the solar collector is increased. Based on these results, the thermal efficiency is decreased from 37.5 % to nearly 22 % by increasing the

outside wind speed. The thermal efficiency is generally decreased for the wind speed lower than 1 m/s. Meanwhile, the thermal efficiency is reduced more rapidly where the wind speed varies from 1 m/s to 3 m/s. For the outside wind speed higher than 3 m/s, which is an extreme condition, the thermal efficiency varies less.

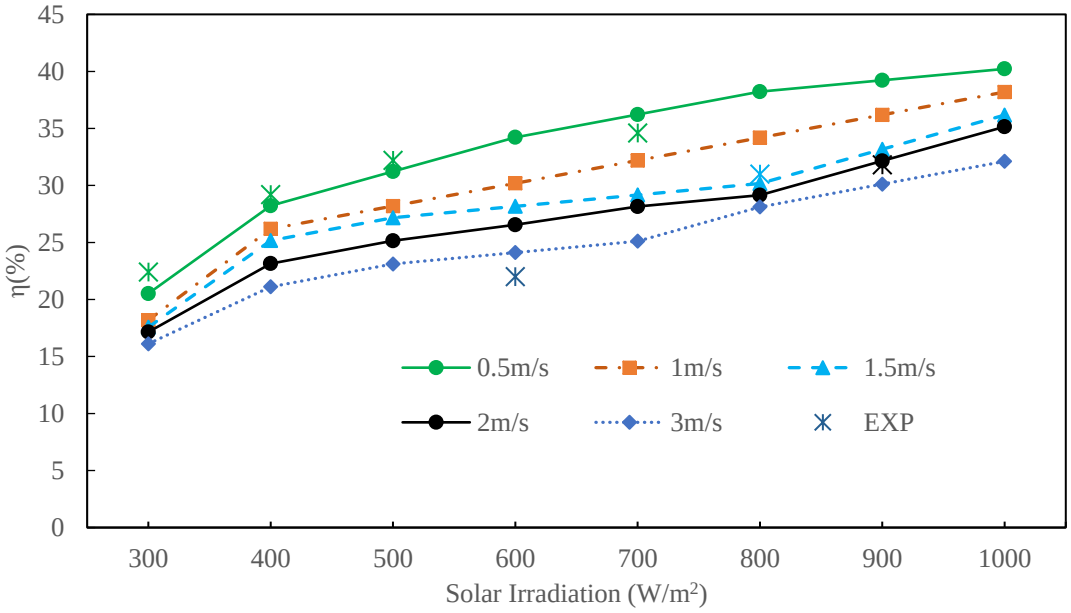

Figure 4 - 7 Thermal efficiency under different solar irradiation and wind speed where the ambient temperature is 10 ˚C

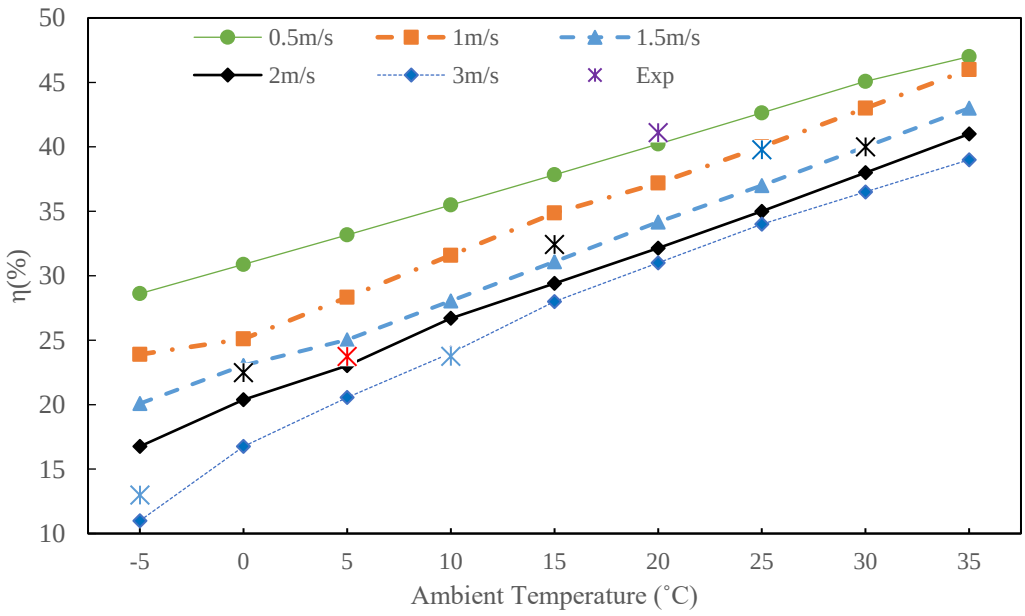

Figure 4 - 8 Thermal efficiency under different ambient temperatures and wind speeds, where the solar radiation is 600 W/m^2.

4.6 Conclusions

An experimental setup of the PV/T-ASHP system for an office room is constructed in this section to verify the actual application performance of the proposed ultra-thin superconducting solar collector with pin-fins. The heating season performance of this system is also analyzed. Moreover, the thermal performance of the solar collector of the PV/T with pin-fins under different environmental conditions is investigated through both simulations and experimental methods to clarify the variation in the thermal efficiency of the solar collector in different environmental conditions. Three environmental factors are analyzed: solar radiation, ambient

temperature, and wind speed. The absorber thermal efficiency is calculated and compared between the simulation and experiment. The main conclusions are as follows:

A parametric study of the thermal efficiency of the solar collector under different environmental and operating conditions reveals a good agreement between the simulation and experimental results. The average error between the simulation and experiment is 1.52% which is acceptable because there are influencing factors both in the simulation and experiment. The higher the solar radiation and ambient temperature, the higher the thermal efficiency. Meanwhile, the higher the wind speed, inlet water temperature, and inlet water velocity, the lower the thermal efficiency. The highest efficiency of this solar collector is nearly 65% during the experiment.

The results presented in this section are anticipated to be useful for further design of the PV/T system. Further work is needed to optimize the design and operation for enhancing the system's performance. Further research should be also conducted on this system to achieve more benefits in terms of environment-friendliness and energy efficiency.

Chapter 5: Performance study of the PV/T-ASHP system

Most of the researches related to PV/T-HP system were focused on their performance. However, almost all of them were conducted using simulation or in laboratory experiments, where the experimental conditions and duration were limited. Hence, there is a lack of experimental investigation throughout the year, which is essential for marketing. Besides, the economic and environmental analyses in the existing researches are very limited. In this thesis, we presented a PV/T assisted ASHP system that supplies heating and domestic hot water for users. We then implemented our design in Beijing, China. A series of experiments were also conducted throughout 2018 to investigate the performance of this system. The results of the COP of the ASHP system, the thermal and electrical efficiency of the PV/T collector, the self-sufficiency rate of thermal energy, and the self-sufficiency rate of electricity of this system in each month, were identified and presented in this Section. Moreover, the analysis of economic and environmental impacts, such as the payback time and pollution emission are presented in this section.

5.1 Description of the experimental device

The schematic of the experimental setup and the working principle of the PV/T system are shown in Figure 5-1. The main equipment is also shown in Figure 5 - 2. The design parameters of the main equipment in the PV/T-ASHP system are shown in Table 5 - 1. The water tank volume is 100L, which is used for hot water storage. The refrigerant used in the ASHP system is R22. The experiment is located in an office room in Beijing (117˚E, 40˚N), which is in the cold region of China. The office room is 3.5 m ×3 m ×3 m, the door is 2 m × 0.85 m and the window is 1.1 m × 1.1 m, south facing, a top layer office room. Stronger flow disturbance enhances the heat transfer coefficient for the PV/T collector [128]. I To further strengthen the fluid disturbance, we design two types of pin-fins of different sizes. The shape of both of these pins is cylindrical and the diameters of the pins are 3 cm and 1.5 cm respectively.

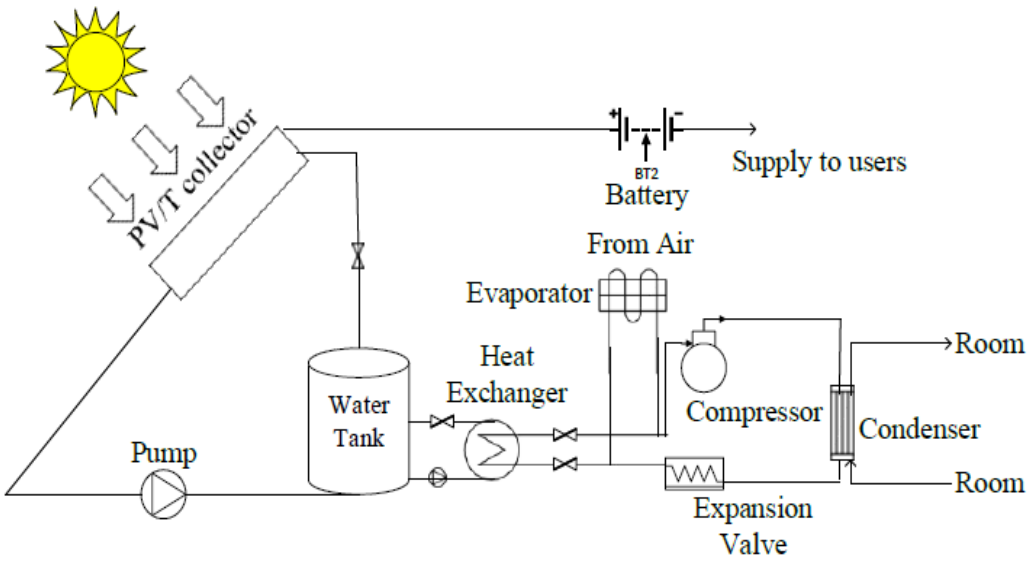

Figure 5 - 1 The schematic of the experimental setup of the PV/T-ASHP system

Figure 5 - 2 The picture of the part of the PV/T-ASHP system

Figure 5 - 3 Configuration of the novel solar absorber

Table 5 - 1 The parameters of the main equipment

	Number	Size/Capacity
PV/T Collector	2	1.3m*1m
Water Tank	1	100L
Circulation Pump	2	50L/min
Condenser	1	3500W
Heat Exchanger	1	3000w
Evaporator	1	2500W
Expansion Valve	1	1.8MPa/0.5 MPa

The external environment conditions are measured by the weather station installed next to the PV/T collector (Figure 3-12(b)), and the weather data is recorded at every 10 minutes. The measurements include the external temperature, humidity, wind speed and solar irradiation. For the PV/T-ASHP system, the main measurements include the water temperature at the PV/T collector inlet, outlet, temperature of water in the tank, and the thermal absorber surface temperature. We use a temperature probe with an accuracy of ± 0.01 ℃ for the measurement. The water flow used an ultrasonic heat meter, with the range 0.07-7 m^3/h and the accuracy of level-2, ± 0.14 m^3/h. Experiments were operated throughout the day, and all the measurements were conducted every 2 minutes.

5.2 Working principle of this PV/T-ASHP system

For the energy transfer process, in this experiment, the PV/T and the ASHP systems are combined in parallel mode. The ASHP system can either absorb heat from the air outside or from the water tank which stores heat gained by the PV/T collector. The PV/T system gains solar energy and transfers it into electricity and heat. The electricity produced by the PV /T collector is then stored in the battery and supplied to the users. The electric box, as shown in Figure 3 - 2, is used to measure the total amount of electrical energy. The heat energy is supplied to the water tank for storage which is then supplied to the ASHP system for room heating and hot water supply.

During the experiment period, at part of spring and autumn, winter (heating season), the PV/T-ASHP system supplies electricity, hot water, and heating to the users from 9:00 to 17:00. The ASHP system firstly absorbs heat from the water tank. If the energy is not sufficient to satisfy the demand, the ASHP changes to absorb heat directly from the outside air. While for part of the spring and summer season (cooling season), the PV/T-ASHP system supplies electricity, cooling, and hot water to the users, the ASHP is used for cooling and PV/T is used for supplying electricity and hot water.

5.3 Calculation of the PV/T-ASHP system performance

Based on the experimental data collected in 2018, the monthly performances, i.e., COP of ASHP system, the thermal efficiency of PV/T collector and the self-sufficiency of electricity and thermal energy for whole PV/T-ASHP system, of the PV/T collector system and ASHP system are separately calculated, as defined by using following equations. , .

$$COP = \frac{Q_{user}}{P_{ASHP}} \tag{5-1}$$

$$\eta = \frac{Q_{gain}}{S} \tag{5-2}$$

$$R_{ele} = \frac{P_{PV/T}}{P_{sys}} \tag{5-3}$$

$$R_{heating} = \frac{Q_{gain}}{Q_{user}} \tag{5-4}$$

where COP is the coefficient of the ASHP performance, Q_{user} is the energy capacity supplied to users, P_{ASHP} is the power consumption by ASHP system. η is the thermal efficiency of PV/T collector, S is the total solar irradiation gained by the PV/T collector, and Q_{gain} is the heat transfer capacity, which is stored in the water tank. Furthermore, R_{ele} represents the self-sufficiency of electricity, $P_{PV/T}$ is the electric power produced by PV/T collector, P_{sys} is the power consumption of

the system. $R_{heating}$ is the self-sufficiency of thermal energy during the heating season.

5.4 Analysis of the result

The results of each month are listed in Table 5 - 2. Results of indoor temperature show that this PV/T-ASHP system satisfies the user demand for indoor thermal comfort, as the temperature is warmer than the design value (18 ˚C) in the heating seasons. Similarly, during the cooling seasons, the indoor temperature is lower than the design temperature (28˚C).

Table 2 shows the 24-hour average value of the solar irradiation in each month. The lowest irradiation level is in January, and May has the highest irradiation level. This is because, during the summer, the solar irradiation is stronger, whereas it is often more wind and rain during the winter. Therefore, the amount of electricity production from the PV/T collector in May is the highest including the total electricity and the useful electricity. The average ambient temperature is the highest, 28.4 ˚C, in July and lowest, -3.4 ˚C, in December. The PV/T collector absorbed the largest amount of heat in April, 6264 kW. For the PV/T collector, the thermal efficiency varied from 8.82% (in December, when the solar irradiation and ambient temperature were both low) to 41.70 %, and the average was 28.9 %. The total amount of the produced electricity is 9330 kWh for the whole year, while the useful amount of electricity is 6819.5 kWh throughout the year. The heat transferred by

the solar collector was also 46354 kW during the year. For the ASHP part, the average COP was ranged from 2.3 to 4.6, the average was 3.425 which was bigger than reported in [101]. The heating and cooling supplied to the office were equivalent to 36115.5 W and the electricity consumption by ASHP was 10432 kWh throughout the year.

Note that in January, the system only worked for the first two weeks. Therefore, the average ambient temperature was a little higher than the average value over the month. Moreover, the office was not in use during January so the indoor temperature was 18 ˚C, while the system was still on to avoid frozen. Therefore, the heating self-sufficiency rate for January was much higher than in December.

Table 5 - 2 Experimental data obtained in 2018 for each month

				PV/T				ASHP					
	Average Solar Irradiation (W/m2 ·h)	Average Ambient Temperature (˚C)	Average Humidity (%)	Total electricity (kWh)	Useful electricity (kWh)	Heat transfer (kW)	Thermal Efficiency (η)	Heating/ cooling (kWh)	Electricity Consumption (kWh)	COP	Average Indoor Temperature (˚C)	Self-sufficiency rate of electricity	Self-sufficiency rate of thermal energy
Jan (two weeks)	189	-1	28.3	734	525	2554	21.66%	3557.22	889	4	18	59.06%	71.80%
Feb	200.7	-0.6	30.3	684	460	3269	26.11%	3790.94	876	4.3	25	52.51%	68.23%
Mar	240.7	9.9	33	869	647	6264	41.70%	3794.78	823	4.6	20	78.61%	-
Apr	189.2	14.5	47.5	830	617	4754.4	40.31%	2745.25	798	3.4	21.8	77.32%	-
May	248.5	23.3	37.9	875	652.5	4404.48	28.40%	2027.9	835	2.4	25.7	78.14%	-
Jun	219.8	26.9	52.4	866	624	4356.96	31.77%	2196.45	856	2.6	30.2	72.90%	-
Jul	203.3	28.4	67.8	821	596	4595.52	36.22%	2121.77	800	2.7	27.8	74.50%	-
Aug	207.6	26.8	62.4	755	585	4352.64	33.59%	2262.92	986	2.3	27.4	59.33%	-
Sep	217.6	24.5	59.2	794	575	4813.44	35.45%	2774.78	942	2.9	26.4	61.04%	-
Oct	217.2	13.5	57.3	717	518	2981.28	22.00%	3371.62	899	3.8	22.5	57.62%	88.42%
Nov	217.2	5.6	32	702	512	2812.3	20.75%	3580.02	912	3.9	20.3	56.14%	78.56%
Dec	217.4	-3.4	19.1	683	508	1196	8.82%	3891.83	916	4.2	18.5	62.25%	30.73%
Total				9330	6819.5	46354.0		36115.5	10432				

For the PV/T-ASHP system, the electricity self-sufficiency reaches the highest 78.61 %, and during heating seasons, the thermal self-sufficiency reaches up to 88.42 %. Even during December, it could cover the heat demand of 30.73 % by the solar collector. While in cooling seasons, the heat absorbed by the PV/T collector is only used for hot water. This suggests that this system can offer over half of the total energy consumption.

To analyze the real-time performance of this PV/T-ASHP system, we use a set of experimental data under typical climate conditions in different seasons (April 1, 2018, June 30, 2018, October 30, 2018, December 31, 2018). We consider these four days because they represent different climates from different seasons. Using this data we can draw general conclusions for similar days throughout the year, see the results in Figures 5-4 to 5-8.

For the windy day of April 1, 2018, the results of this system are presented in Figure 5 - 4. This system supplied heating, electricity and hot water. The average indoor temperature was 20 ˚C. As seen in Figure 5 - 4 (a), the temperature is decreased from 11 ˚C to 4 ˚C during the daytime. The solar irradiation during the daytime was increased from 9:00 to 11:00, then it fluctuated slightly from 11:00 to 15:50, and then quickly reduced. The values varied from the lowest, 150 W/m^2 in the morning at 9:00, to the highest, 900W/m^2, at 15:40. For the PV/T collector, Figure 5 - 4 (b) shows that at the beginning, its absorber surface temperature is the same as the outlet water temperature, 16 ˚C. Then as the collector absorbed heat from the solar, its surface temperature was increased up to near 40 ˚C. The thermal efficiency of

the collector varied from the lowest 10 % to the highest 60 %. This is because it is affected by the external environment conditions including the ambient temperature and solar irradiation. The thermal efficiency was also varied a lot from 9:00 to 11:20, where the ambient temperature and solar irradiation varied frequently. In Figure 5 - 4 (c), the photoelectric efficiency is shown to reduce from 11.8 % to 2.5%, with an average of 4 % on April 1, 2018. The COP of ASHP is increased from 2, at 9:00, to its largest, 3.6, at noon. It is then reduced to 2.5 in 17:00.

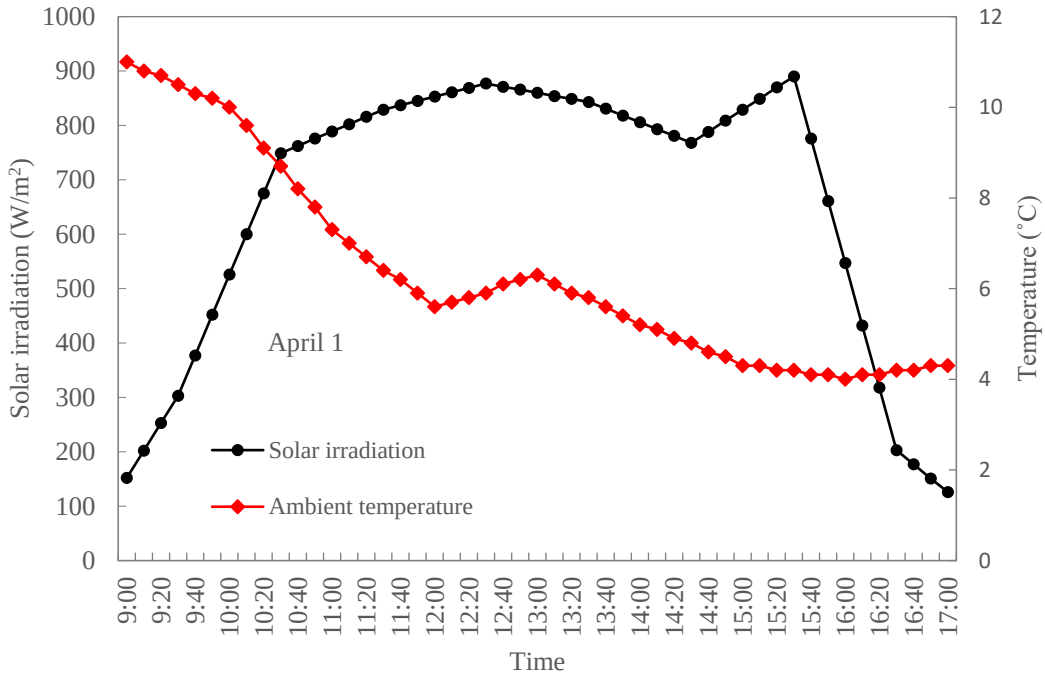

(a) The environmental conditions

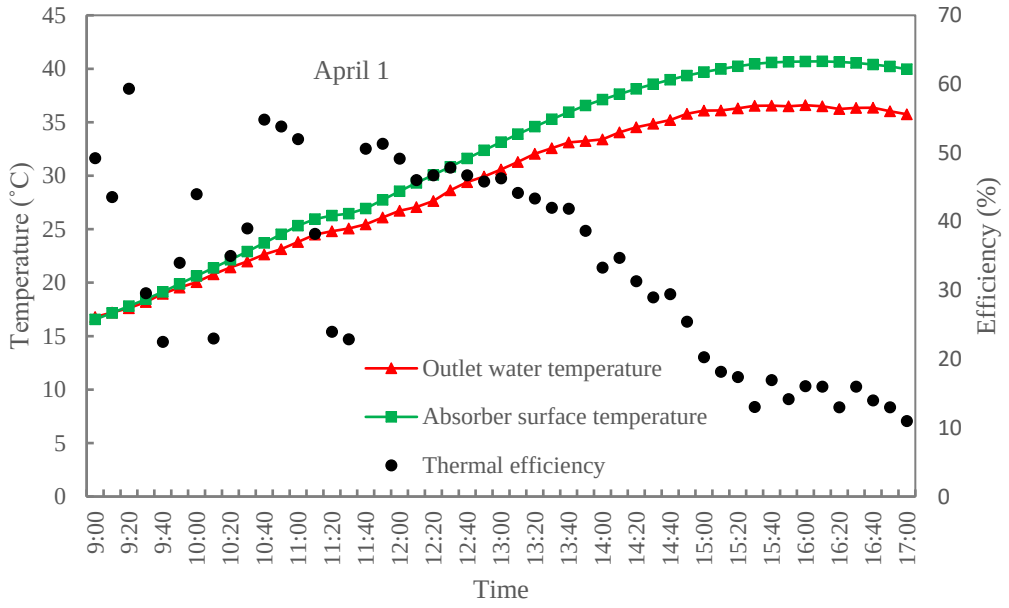

(b) The performance of the PV/T collector

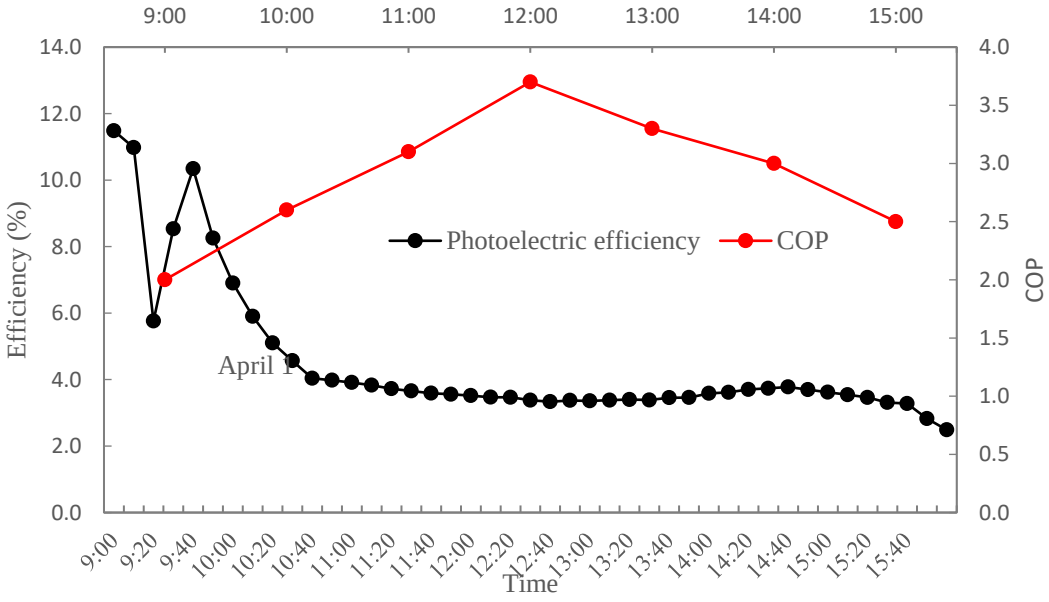

(c) The performance of the collector and ASHP

Figure 5 - 4 The results of a typical day (April 1)

For an overcast day on June 30, 2019, the system produced both cooling and electricity. The performance results are shown in Figure 5 - 5. The average indoor temperature is 28.6 ˚C. Figure 5 - 5 (a) shows the variation of the solar irradiation, especially during 12:00 to 15:00, with the lowest value around 200 W/m^2 at this period. The ambient temperature had a slight increase from 28 ˚C to 33 ˚C. Figure 5 - 5 (b) shows that the absorber surface temperature and the outlet water temperature of the collector were increased to around 10 ˚C during this day. The thermal efficiency of the collector also varied a lot from 12:00 to 15:00, from 18 % to 50%, and the average thermal efficiency was around 30 %. The variation trend of thermal efficiency was caused by the significant influence of solar irradiation. In Figure 5 - 5 (c), the photoelectric efficiency also varied a lot from 12:00 to 15:00, due to the significant impact of the solar irradiation and the average photoelectric efficiency was about 3.8 %. For the ASHP, the COP had an upward trend, from 2.3 at the beginning, i.e., 9:00, to the highest value, 3.5, at 14:00.

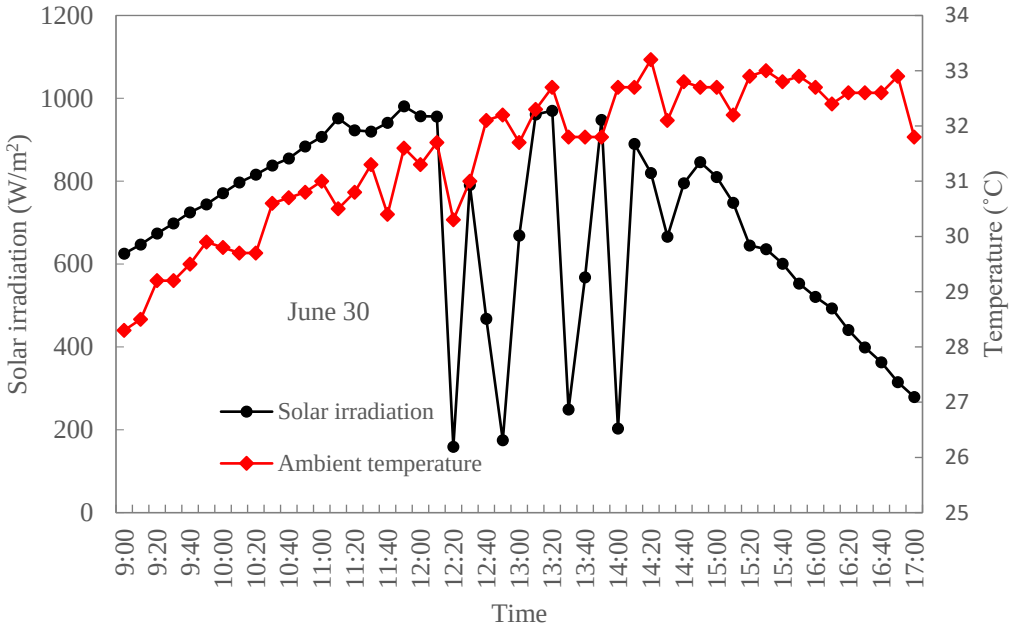

(a) The environmental conditions

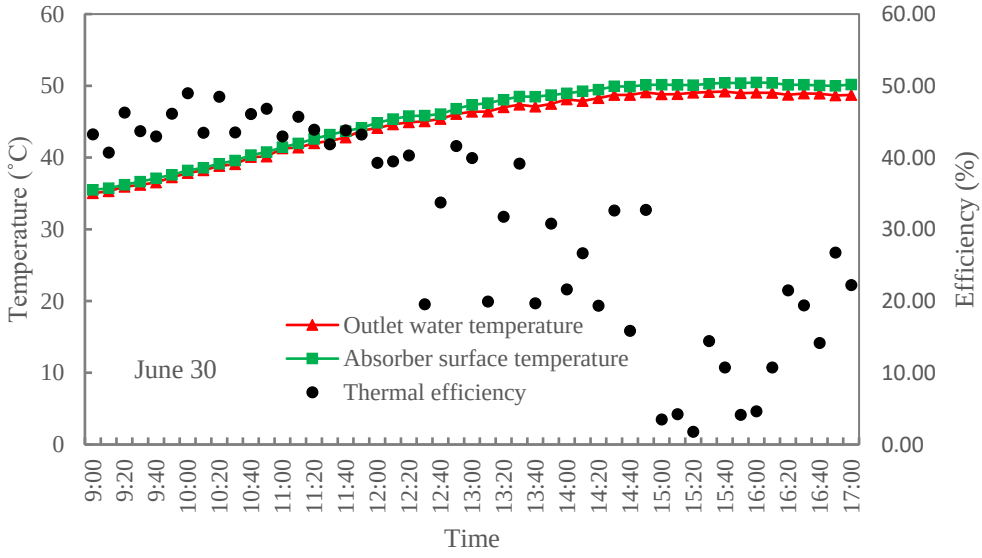

(b) The performance of the PV/T collector

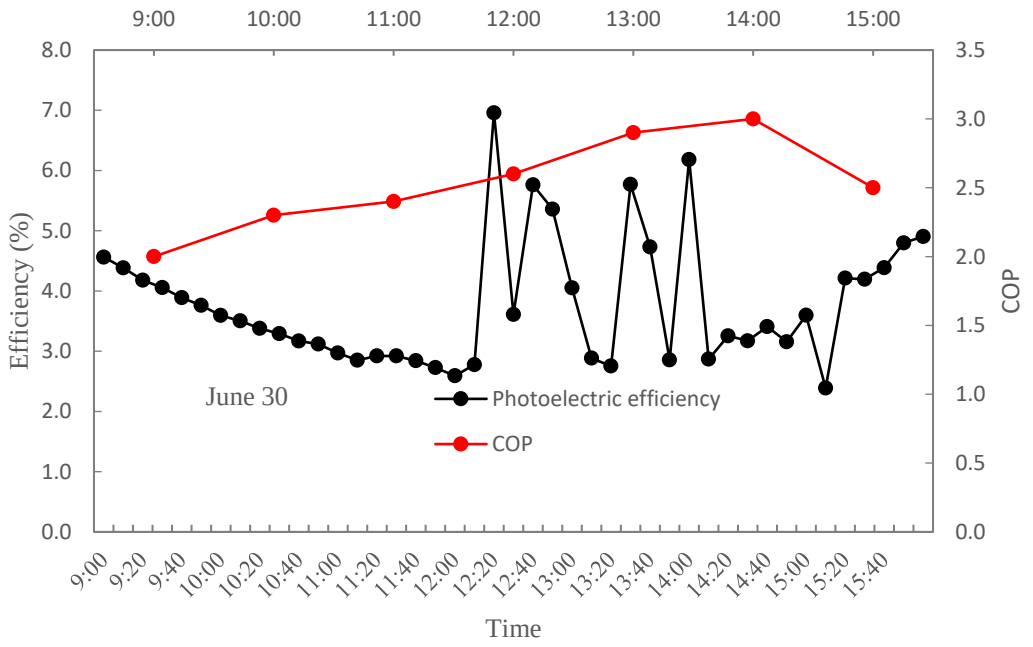

(c) The performance of the collector and ASHP

Figure 5 - 5 The results of a typical day (June 30)

The system performance results on a sunny day (October 30, 2018 in the heating season) are showed in Figure 5 - 6. On this day, heating, electricity and hot water were supplied. The average office room temperature was 19 ˚C. As shown in Figure 5 - 6 (a), on October 30th, the ambient temperature had an upward trend from 14 ˚C to the highest 23 ˚C at 14:30, then had a slight decrease to near 20 ˚C around 17:00. Solar irradiation was a typical trend in this day, and it initially increases then decreases. The highest irradiation value was 1100 W/m^2 at noon. From Figure 5 - 6 (b), it is seen that the absorber surface temperature and the outlet water temperature have a similar upward trend versus the ambient temperature change.

Firstly, the absorber surface temperature increases from 15 ˚C to 36 ˚C from 9:00 to 15:20, and then it slightly declines to 35 ˚C. The outlet water varies from 16 ˚C to the highest 33 ˚C, and finally down to 32 ˚C. The thermal efficiency is decreased with a small fluctuation from 65 % to 10 %, where the average is 35 %. The reason for the decreasing thermal efficiency is that afternoon, the solar irradiation was significantly decreased and the absorbed heat also decreased. Therefore, the efficiency was reduced. The photoelectric efficiency and COP of ASHP change are presented in Figure 5 - 6 (c). As it is seen, the photoelectric efficiency varies with solar irradiation. The average photoelectric efficiency is 4% and the COP of ASHP is over 3, with an average of 3.3.

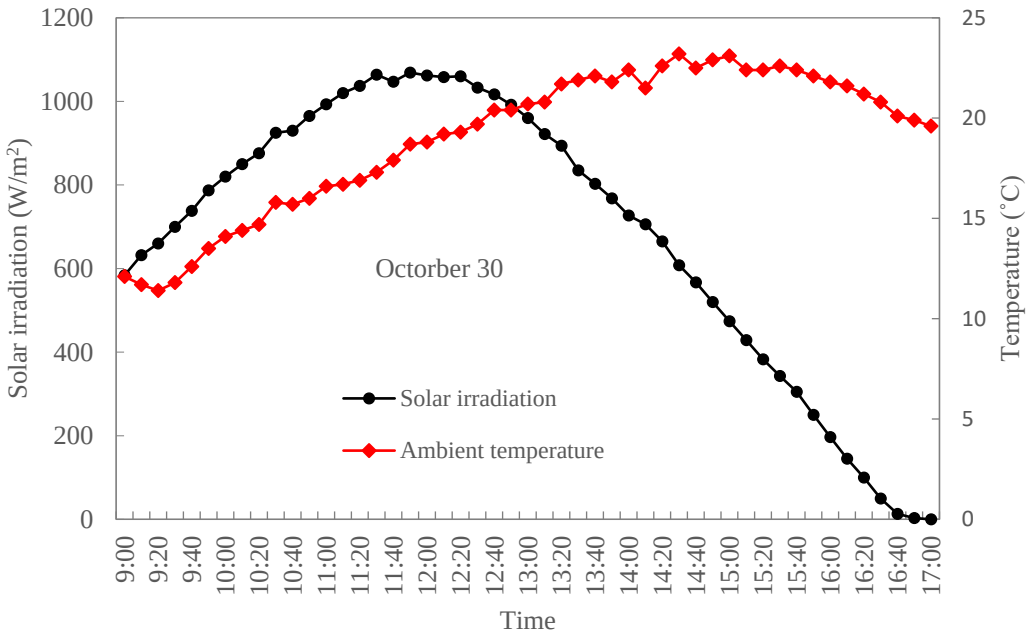

(a) The environmental conditions

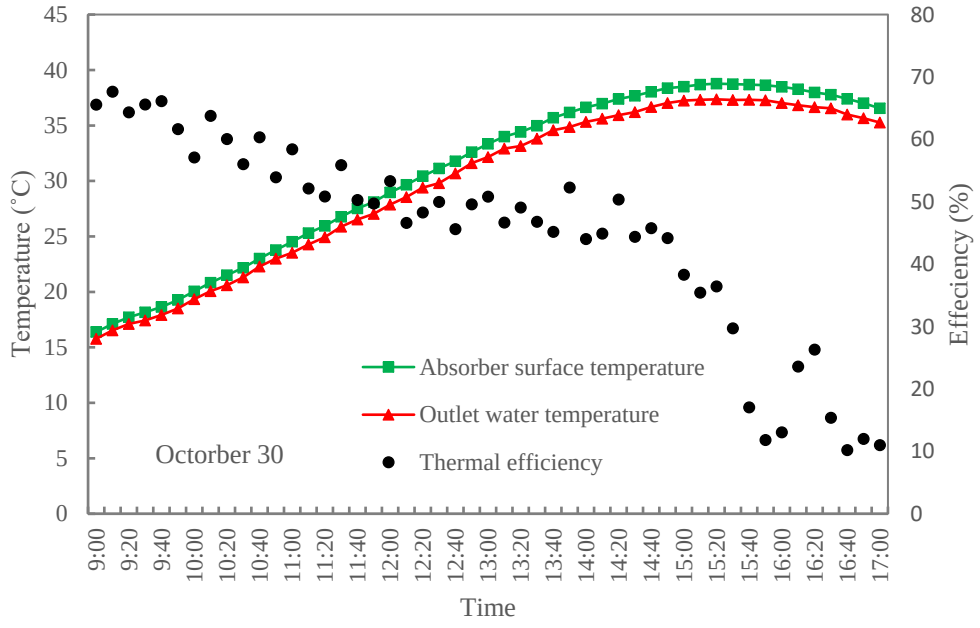

(b) The performance of the PV/T collector

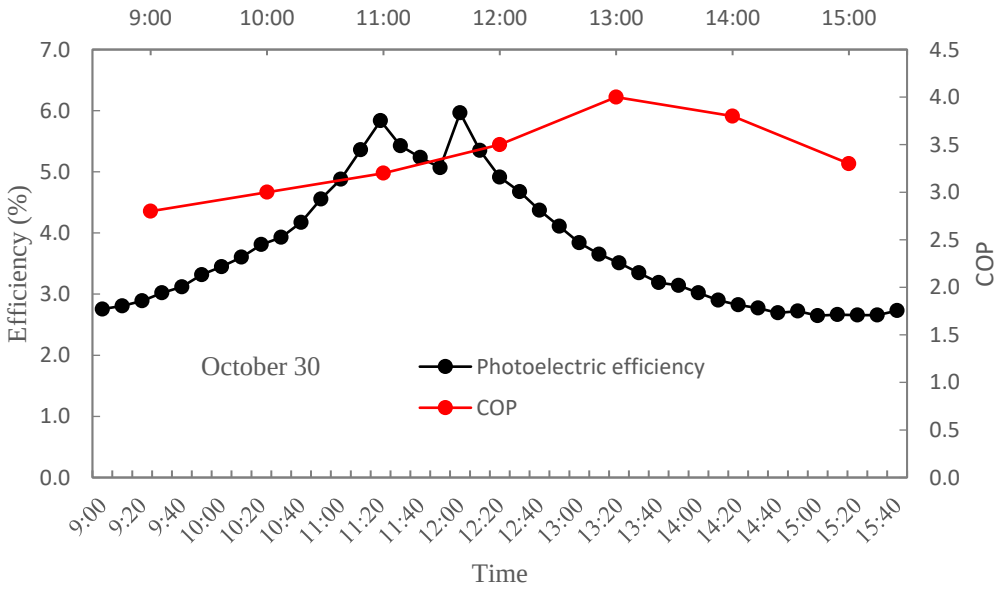

(c) The performance of the collector and ASHP

Figure 5 - 6 The results of a typical day (October 30)

For the extreme conditions, we also analyze the results on December 31, 2018, where both heating and electricity were supplied. The average value of the office room temperature was 18 ˚C. The external environmental conditions are presented Figure 5 - 7 (a), and the ambient temperature is increased from -8 to 0 ˚C, and the average value of the ambient temperature is -4.5 ˚C. As it is seen the solar irradiation presents a similar trend to a normal day, it is increased first and then decreased. The peak value of solar irradiation is 900 W/m^2 at noon. Figure 5 - 7 (b) shows that the thermal efficiency fluctuated around 30%. There is a bigger temperature difference between the absorber surface and the outlet water temperature during this day compared with other days discussed above. Although the trends are the same, the values are lower than the abovementioned days, as the absorber surface temperature is from 13.5 ˚C to 25 ˚C and the outlet water temperature is 10 ˚C to 17 ˚C. The temperature difference between the ambient temperature and the outlet water temperature is also higher. Therefore, the COP of ASHP is on average 3.7 and higher than before (in Figure 5 - 7 (c)). Meanwhile, the photoelectric efficiency is also higher than other days, on average 8% on December 31, 2018.

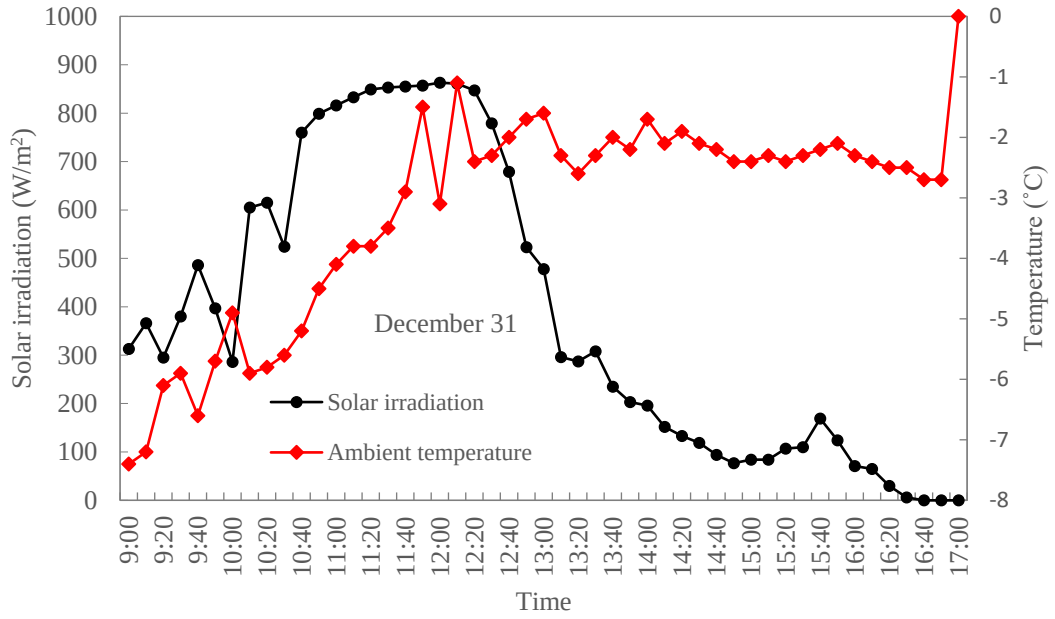

(a) The environmental conditions

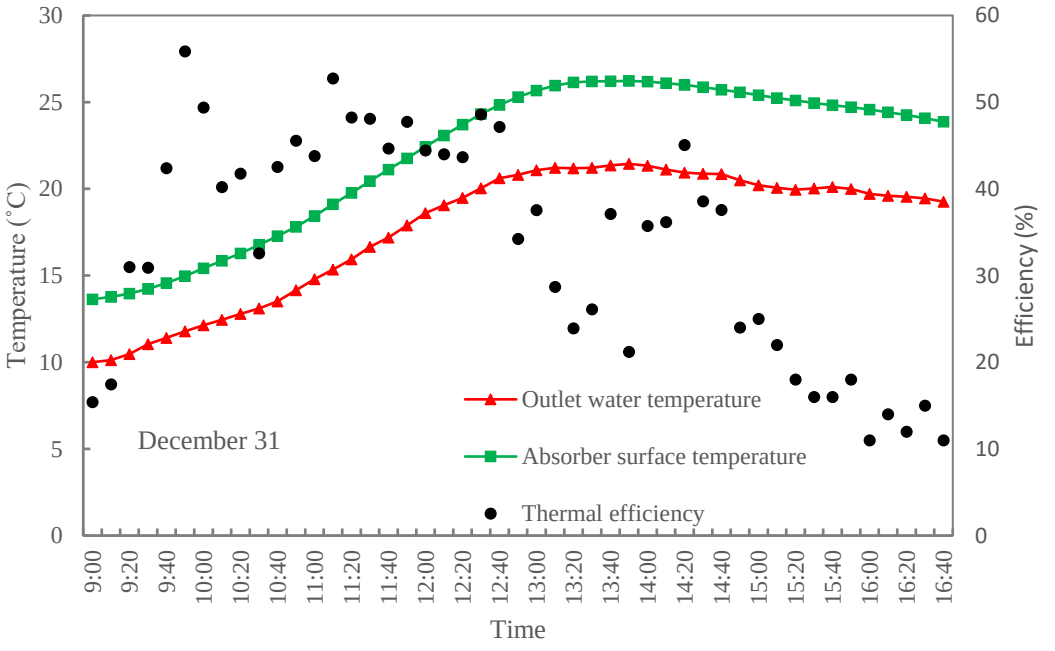

(b) The performance of PV/T collector

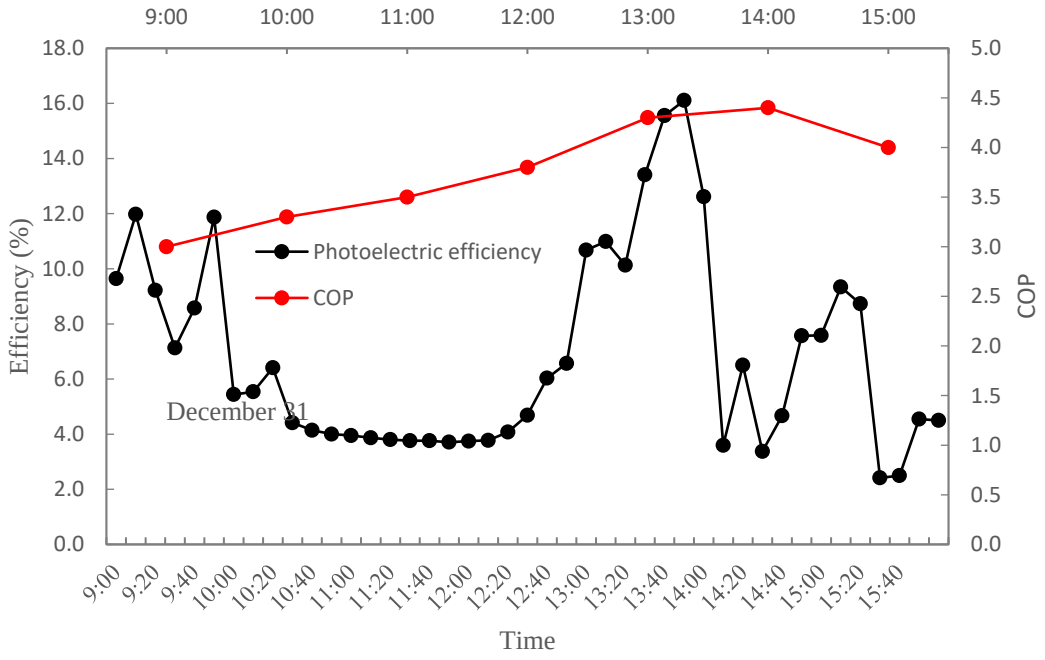

(c) The collector performance and ASHP

Figure 5 - 7 The results of a typical day (December 31)

From the above results, we can see that the performance of the solar collector and the whole system including the COP, thermal efficiency, photoelectric efficiency, and so on in different environmental conditions varies significantly. Ambient temperature and solar irradiation changes cause a big influence on the performance of the whole system. The larger the difference between the ambient temperature and the outlet water temperature of the solar collector, the higher the COP of ASHP and electric production efficiency. The results here are also consistent with those presented in Chapter 4.

5.5 Economic analysis

The designed PV/T-ASHP system supplies heating, cooling, and hot water. For the office buildings, an air conditioner is generally used. This PV/T-ASHP system can be used both in new or renovated buildings. The total cost of the whole system installation was 8000 RMB, and the PV/T system electricity part cost 17625 RMB including the measurement equipment and weather station 2600 RMB, and the heating part cost 10000RMB. The cost of the ASHP system was 3750 RMB.

In this case, an office room with a dimension of 37.5 m^2 is considered and the initial investment for the whole system is 850 CNY/m^2, while the installation cost (including equipment maintenance and labor fees) accounted for 10%. For renovated buildings, the initial investment except the ASHP system is 750 CNY/m^2 which includes the installation and maintenance cost.

To calculate the reduced running costs, electric price is considered. The total useful electricity is 6819.5 kWh. In Beijing, the electric price is 0.4883 RMB/kWh for normal residential buildings. Therefore, for one whole year, the reduced electricity cost is 3330 RMB (without considering the interest rate growth), and because the area for this room is 37.5 m^2, so the reduced running cost is 89 CNY/m^2. Note that the hot water supply to the office room is only used for washing hands, hence it is not concluded in the energy-saving part.

Based on the values of initial investment and reduced running costs for the whole year, the static payback time of this case is 9.5 years. Adding the ASHP system, for renovation, the payback time becomes 8.5 years.

5.6 Environmental analysis

According to statistical analysis, in 2018, China's thermal power generation accounted for 73.32% of the total power generation, followed by hydropower generation, 16.24%, nuclear power generation, 4.33%, and wind power generation, 1.32%. Coal is the main energy source for thermal power generation. In this paper, we analyze the system's environmental benefits based on the standard coal, and each kilowatt hour of electricity is equivalent to 0.4 kg standard coal saving.

The coefficient of energy consumption and pollution emissions is shown in Table 5-3. It is shown that each kilowatt-hour of electricity saving leads to 0.997 kg of carbon dioxide (CO_2) deduction, 0.03 kg of sulfur dioxide (SO_2) deduction, and 0.0015 kg of nitrogen oxides (NO_X) deduction. Note that 1 kg standard coal saving is equivalent to reducing 2.493 kg of carbon dioxide (CO_2) emission, 0.075 kg of sulfur dioxide (SO_2) emission, and 0.0375 kg of nitrogen oxides (NO_X) emission. In 2018, the PV/T-ASHP system produced useful electricity 6819.5 kWh in total. According to calculation, it can save 2.73 t of standard coal. As a result, it can lead to 6.8 t of carbon dioxide (CO_2) deduction, 204.59 kg of sulfur dioxide (SO_2)

deduction, and 102.29 kg of nitrogen oxides (NO_X) deduction throughout the year. Therefore, this system could effectively reduce environmental pollution.

Table 5 - 3 The coefficient of energy consumption and pollution emissions

Energy source	Carbon dioxide (CO_2)	Sulfur dioxide (SO_2)	Nitrogen oxides (NO_X)
1 kWh	0.997	0.03	0.015
1 kg standard coal	2.493	0.075	0.0375

5.7 Comparison of the proposed system with the previous research results

As shown in the relative published references, Alejandro et al. [129] conducted both simulations in TRNSYS and experimental studies for industrial use in Spain. The TRNSYS simulation results claimed that the system could achieve around 40 % of electricity self-sufficiency. Compared to Alejandro et al. [129], this PV/T-ASHP system achieves higher (over 50%) electricity self-sufficiency. For the same system and in similar use, Wang et al. [101] and Raghed et al. [68] conducted the study on the PV/T-ASHP system both in a cold region, Beijing and Toronto, respectively. In the heating seasons, the average COP of the ASHP system was 3.03 in Wang et al. [101] . Raghed et al. [68] also found the COP varied from 2.47 to 3.45. In this study, for the only heating season, the average COP of this system from October to February is up to 4, much higher than the abovementioned researches. The reason was mainly due to the design of the absorber, as the absorber in this paper was with

pin-fins, which enhances the heat transfer of the absorber causing performance improvement. In general, this system performed well with additional characteristics, e.g., energy-saving, and environment friendly.

5.8 Conclusion

In this chapter, a PV/T-assisted ASHP system, which supplied heating and domestic hot water for an office building was designed and built. A series of experiments were conducted throughout the year in 2018. The COP of the ASHP system, the thermal transfer efficiency of the PV/T collector, the self-sufficiency rate of thermal energy, and the self-sufficiency rate of electricity of this whole system in each month were also investigated. The following conclusions have been drawn based on the research presented in this chapter:

- For the PV/T-ASHP system, the electricity self-sufficiency can reach the highest at 78.61 %, and in the heating seasons, the thermal self-sufficiency reaches up to 88.42 %. Even during December, it could supply the heat demand of 30.73 % by a solar collector. The average COP in the heating seasons reaches 4.
- In general, the ambient temperature and solar irradiation change significantly affect the system. The larger the difference between the ambient temperature and the outlet water temperature of the solar collector, the higher the COP of ASHP and electric production efficiency.

- In terms of the economic impact, the payback time is 9.5 years, and for renovated buildings, the payback time is 8.5 years. In terms of the impact on the environment aspect, the system we designed to prevent the emission of 6.8 t of carbon dioxide (CO_2), 204.59 kg of sulfur dioxide (SO_2), and 102.29 kg of nitrogen oxides (NO_X) throughout the year.

Chapter 6: Energy estimating of the PV/T system using Artificial Neural Network (ANN)

Photovoltaic/thermal (PV/T) system plays an important role in solar system development and application on reducing pollution and meeting the rapidly increasing energy demand. Modeling the system performance is required for the optimization and design of such a system. Its performance is affected by many factors, and therefore difficult to be estimated using the normal regression method. Through the studies in Chapters 3, 4, and 5, we can see that the requirement cost for investigating the performance of such systems is very high both in terms of time and monetary investments. Nevertheless, the comparisons among different systems with the same conditions are necessary for users and system performance prediction is therefore required. Artificial neural network (ANN) as an intelligent method is presented and conducted in this chapter. Environment factors including solar radiation, humidity, ambient temperature, wind speed, and wind direction and operation parameters of inlet/outlet water temperature, the collector surface temperature, and water volume are considered as the inputs for an office building in Beijing based on the one year's experiment data in Chapter 5. The electric and

thermal efficiency of PV/T systems are as the outputs. The different numbers of factors and different ANN network constructions are conducted and compared.

6.1 Background

Along the rapid population growth, the energy demand is growing worldwide [130]. To deal with both of the large energy demand and environment problems, renewable energy resources have gained significant attentions in recent years, with the sustainable and non-pollution advantages [131]. Among all renewable energy resources, solar energy have attracted the greatest attention, as it is abundant and essentially inexhaustible [132, 133, 134]. There have been many different devices using solar energy, such as solar collectors, solar assisted heat pumps, PV/T system and so on. Among them, PV/T system, which absorb the solar energy and produce both thermal energy and electricity, leads to better system performance [135]. PV/T system has been studied by using experimental and theoretical methods to figure out how the different parameters affect the performance of PV/T [136, 137, 138, 12, 139]. However, there are many limitations for experiments, such as its high cost and the general short experimental time , and the results are only suitable for limited similar system. Theoretical results are generally simplified models with some assumptions [132]. Facing this problem, various modeling approaches are proposed to predict the performance of PV/T system.

Multiple regression has been used in predicting the performance of the PV/T collector. For linear regression analysis, there are many researches focused on the influence of external environment changing or system design and operation on the performance of PV/T collector [140, 141, 29]. Helmers and Kramer [142] applied multi-linear regression model was used and validated by measurement data. The input measured variables were the relevant ambient conditions, including the direct normal irradiation, local wind speed and ambient temperature. The outputs were the electrical and thermal power of PV/T collector. As a result, the normalized root mean square errors (NRMSE) were 1.9% and 2.9% for electric and thermal power, respectively.

Artificial neural network (ANN), as an intelligent based behavior of human brain technique, has been verified to be a useful tool to model the PV/T system especially solving the high nonlinear partial problem. Ability to find the relationship between inputs/outputs and also to have high speed simulations are the known benefits of these networks [143, 144, 132]. There have been many researches using ANN to model the PV/T both of electrical and thermal performance even under dynamic behavior. Kalani et al. [145] introduced a new method to model a photovoltaic thermal nanofluid based collector system (PVT/N) located at Ferdowsi university of Mashhad, Iran by using three different methods, namely, radial-basis function artificial neural network (RBFANN), multi-layer perception artificial neural network (MLPANN) and adaptive neuro fuzzy inference system (ANFIS) model. They identified the relationships between input and output parameters, including

solar irradiation and ambient temperature for input parameters and fluid outlet temperature of the collector and electrical efficiency of PV for output parameters. RBFANN yielded significantly lower RMSE compared to that of the ANFIS ($p < 0.0003$). ANFIS was found to result in a higher performance than the MLPANN ($p < 0.002$) and RBFANN ($p < 0.001$) in predicting fluid outlet temperature. Ghaini et al. [146] used an ANN to approximate the photovoltaic yield. The input parameters were the arrays of aspects ratio and mass flow rate. The output parameters were the approximate PV yield under four fluid flow configurations. Graditi et al. [147] compared two approaches: a physical modelization and ANN. A new hybrid method, Hybrid Physical Artificial Neural Network (HPANN) was proposed and compared with Multi-Layer Perceptron ANN (MLPANN). The inputs were ambient temperature, solar irradiation and clear shy solar irradiation model and outputs was the power production. The values of RMSE was less 10%. Gunasekar et al. [148] developed an ANN to predict the energy performance of a PV/T evaporator in solar assisted heat pump system. The input variables were solar intensity, ambient temperature, relative humidity and wind velocity, each of them has three values. The output variables were evaporator heat gain, solar energy input ratio, panel efficiency and panel temperature. The prediction from the ANN illustrated that photovoltaic panel temperature yields maximum R2 value of 0.9999, minimum RMS value of 0.014 ˚C and minimum COV value of 0.0545. Kamthania and Tiwari [149] used ANN to analyze the performance of a semi transparent hybrid PV/T double pass air collector under four weather conditions at New Delhi.

The ambient air temperature, global solar radiation, diffuse radiation and number of clear days as the input parameters. Electrical energy, thermal energy, overall thermal energy and exergy were the estimated parameters. The RMSE varies from 0.10–2.23%. Ravaee et al. [150] used ANN to develop both thermal and electrical modeling of PV/T collector. The inputs were ambient temperature of collector, cell temperature, fluid temperature at duct inlet, fluid velocity in duct, solar identity and time. The output were the thermal efficiency and electrical efficiency. R2 was 0.9976, with RMSE and COV values of 0.3974 and 0.0526. Ammar et al. [151] used the ANN based control to optimum the thermal and electric power of a PV/T panel for a given solar radiation and ambient temperature. Input parameters included the glazing temperature, solar cell, absorber plate and water circulation. The outputs were electric power and thermal profit. The normal mean bias error (NMBE) was -13.05%. Khatib et al. [152] used two different ANNs generalized regression artificial neural network and cascaded forward neural network to predict current-voltage (I-V) curve, while Karatepe et al [153], Celik [154] and Bonanno et al. [155] also used the ANN to conduct the I-V curve extracting of PV solar cells. The input variables were solar radiation, ambient temperature and open circuit voltage and short circuit current. As a result, the average mean absolute percentage error, mean bias error and root mean square error were 1.09%, 0.0229 A and 0.0336 A respectively.

Aside from above mentioned methods, genetic algorithm (GA) was proposed by Singh et al. [156, 157] to improve the efficiency of PV/T system in India. The

influencing parameters were length and depth of the channel, velocity of air fluid flowing into the channel, thickness of the tedlar and glass, temperature of inlet fluid. The objective functions were the overall exergy efficiency and overall thermal efficiency. The data was obtained for whole one year, while the used data were the average parameters obtained at 11:00 AM for each month. The overall thermal efficiency and overall exergy efficiency improvements were 13.14% and 4.6 %, respectively. Singh et al. [158] also compared the GA and GA-FS (generic algorithm-fuzzy system), It has been observed that the GA–FS approach is a better approach as compared to GA approach because it converges faster as compare to GA because the use of the fuzzy knowledge base with GA and take less time for identification of optimized system parameters. Kim et al. [159] applied back-propagation network (BPN) model incorporating genetic algorithms (GAs) to cost estimation. Sobhnamayan et al. [160] used GA to optimize the exergy efficiency of PV/T water collector.

Evolutionary Algorithm (EA) was also used to optimize the single channel glazed PV/T array by Singh et al. [161]. The objective function was the overall exergy gain. Seven design parameters were the influence factors including length of the channel, mass flow rate of flowing fluid, velocity of flowing fluid, convective heat transfer coefficient through the tedlar, overall heat transfer coefficient between solar cell to ambient through glass cover, overall back loss heat transfer coefficient from flowing fluid to ambient and convective heat transfer coefficient of tedlar.

A summary of the main results of aforementioned is presented in Table 6 - 1. After reviewing the previous papers, a few key points are identified as below:

- Most of the employed methods used to optimize or predict the performance of PV/T were ANN and MLR. Although there are many researches on the analysis of the PV/T system [12], the researches used the different algorithm based on ANN, but it still requires further exploration [144]. As we can see that there are insufficient datasets in previous researches, even the datasets in some researches are only few days measurement [148, 156, 132]. So the application of ANN still need further investigation based on large data.
- Different algorithm methods and indicators have been adopted by researchers, but most of them are only be applied or validated by one model construction. However, the number of influence factors were stable for each research. There are no researches focusing on the comparison between the effects of different influence factors combination on the results.
- There have been many researches of ANN on solar system [132, 162]. However, the researches on the performances of PV/T systems is still inadequate in China.

This chapter aims to study the performance of PV/T collector using an ANN algorithm with a back propagation (BP) algorithm based on a PV/T system with whole year experimental measurement in Beijing. Moreover, the results are compared with different number factors' combination to find the most accurate model.

Table 6 - 1 overviewed of main results of previous researches of PV/T collector models

Ref.	Model	Location	Data	Input parameters	Output parameters	Accuracy
Helmers and Kramer	MLR	Germany, Fraunhofer	15294	direct normal irradiation, local wind speed and ambient temperature	electrical and thermal power	NRMSE=1.9% (electric), 2.9% (thermal power)
Singh et al.	GA	New Delhi, India	one day	length and depth of the channel, velocity of air fluid flowing into the channel, thickness of the tedlar and glass, temperature of inlet fluid	overall exergy efficiency and overall thermal efficiency	overall thermal efficiency and overall exergy efficiency improvements were 13.14% and 4.6 %
Kim et al.	BPN-GA	Seoul,Korea.	530 buildings	building size, location, number of storeys	construction costs	MAER=3.16
Singh et al.	EA	New Delhi, India		seven design variables	overall exergy gain	
Kalani et al.	RBFANN; MLPANN;ANFIS	Iran	10 days with each days 13 points	Solar irradiation, ambient temperature	fluid outlet temperature; electrical efficiency	R2>0.98; RMSE <0.4%
Ghaini et al.	ANN		288 simulation data	arrays of aspects ratio, mass flow rate	approximate PV yield under four fluid floe configurations	r=0.984
Graditi et al.	a physical modelization and HPANN	ENEA Portici Research Center	500 epochs	ambient temperature, solar irradiation and clear shy solar irradiation model and	power production	RMSE <10%

Gunasekar et al.	ANN	Coimbatore city in India	1 day	solar intensity, ambient temperature, relative humidity and wind velocity	evaporator heat gain, solar energy input ratio, panel efficiency and panel temperature	max R2 0.9999, min RMS=0.014 ˚C and COV=0.0545
Kamthania and Tiwari	ANN	New Delhi	2000	ambient air temperature, global solar radiation, diffuse radiation and number of clear days	electrical energy, thermal energy, overall thermal energy and exergy	RMSE 0.10–2.23%.
Ravaee et al.	ANN	Zahedan		ambient temperature of collector, cell temperature, fluid temperature at duct inlet, fluid velocity in duct, solar identity and time	thermal efficiency and electrical efficiency	R2= 0.9976, RMSE =0.3974 COV= 0.0526
Ammar et al.	ANN	Tunisia	100	glazing temperature, solar cell, absorber plate and water circulation	electric power and thermal profit	NMBE=-13.05%
Khatib et al.	generalized regression ANN and cascaded forward NN	Nablus, Palestine	12100	solar radiation, ambient temperature and open circuit voltage and short circuit current	I-V curve	MAPE= 1.09%, MBE=0.0229 A ,RMSE=0.0336 A

6.2 Data colleting

A PV/T system was mainly consisted of PV/T collector, water tank and water circulation heat pump system is measured for whole year 2019. The schematic of the system is shown in Figure 6 - 1. The inclined angle of the collector is 47˚, facing south. The total surface area for the PV/T collector with two arrays is 2.6m^2, and that for each one is 1.3m^2. The water tank volume is 100L, which is used for hot water storage. The refrigerant used in the ASHP system is R22. The experiment is located in an office room in near Beijing (117˚E, 40˚N), a cold region of China.

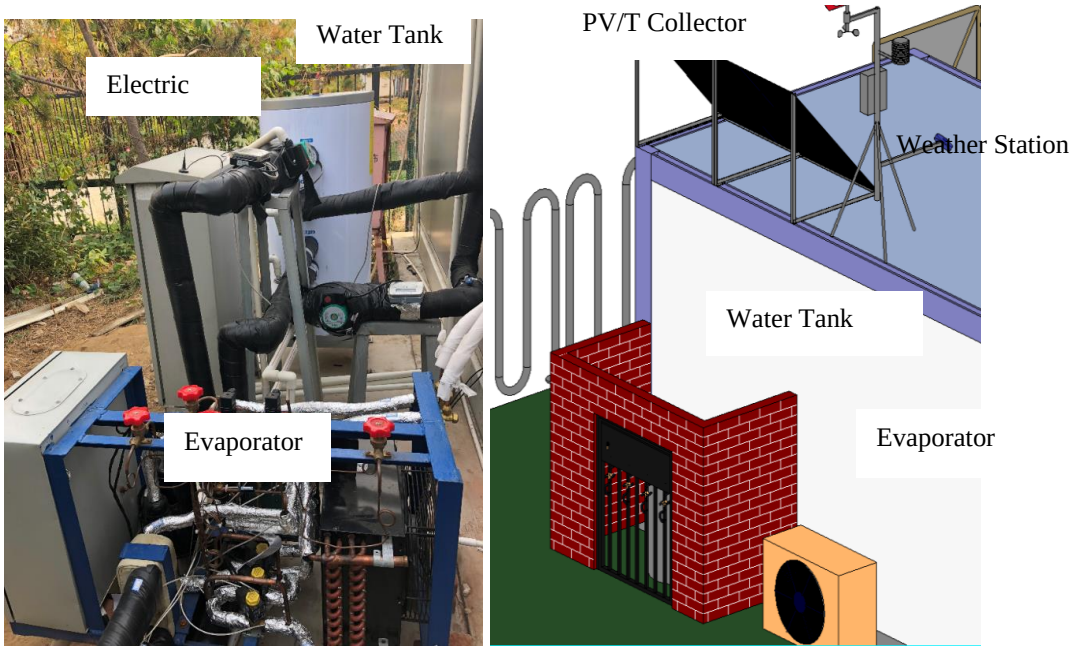

Figure 6 - 1 The picture of the part of the PV/T-ASHP system

The external environment conditions are measured by the weather station installed nearby the PV/T collector (Figure 6 - 1). The measurements include solar radiation (W/m^2), external humidity (%), ambient temperature (˚C), the

wind speed (m/s) and wind direction (˚) for environment parameters and plate surface temperature (˚C), the inlet water volumetric flow (kg/h) and inlet/outlet water temperature (˚C) of solar collector. We use temperature probe with the accuracy of ± 0.01℃ for the measurement. The water flow used ultrasonic heat meter, with the range 0.07-7 m^3/h and the accuracy of level-2, ±0.14 m^3/h. Experiments were operated during 9:00 to 17:00 in the whole 2018 year, and time interval of all measurements was 10 min.

6.3 Methodology

6.3.1 Artificial neural network (ANN)

Artificial neural network (ANN) is a processor which is widely parallel distributed and is composed of simple processing units (called neurons) [163]. It is popularly used to solve complex functions in various applications such as high-speed information proceeding, mapping capabilities, forecasting, optimization and so on to reduce the cost and time [164]. There are many different ANN types, including multilayer perceptron ANN (MLPANN), wavelet neural network (WNN), radial basic function ANN (RBFANN), and Elman neural network (ENN) and so [132]. The common used types are MLP and RBF, and MLP has been used successfully to solar energy system [145, 165, 132, 146, 166]. BP neural network is widely used with ANN, with two process: the forward signal transmission and reverse estimated error transmission. The

structure of ANN with BP algorithm consists input layer, one or more hidden layers and output layer, as shown in Figure 6 - 2.

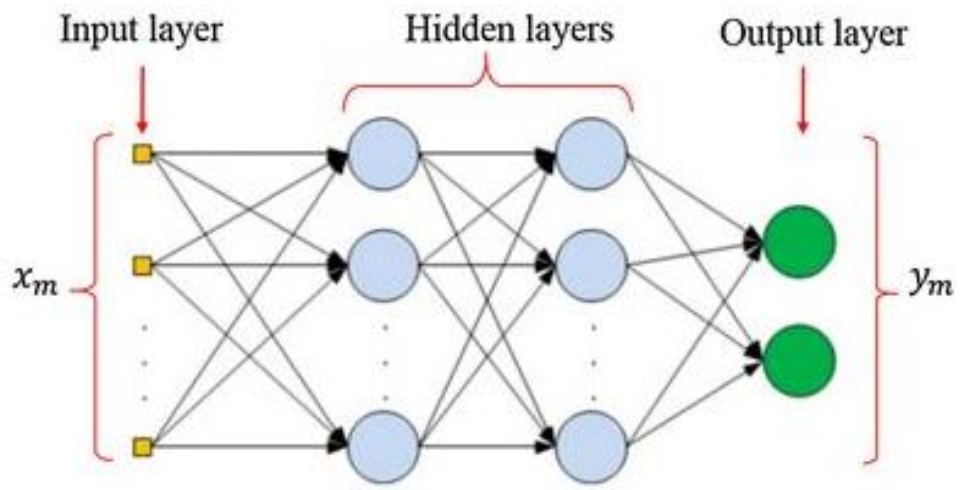

Figure 6 - 2 Graph of multi-layer artificial neural network based on large data [167]

To predict the performance of PV/T collector, the collected data is split into three subset: training, validation and testing with the ratio 3:1:1. And the total data size is 14400, total 300 days in 2018. Majority of data are used for training to test the network, validation data is used to mitigate overtraining of the network to gain acceptable validation error. Then the testing data is used in trained network. The prediction output value is compared with the collected data. to find the best and most suitable ANN network, different structure of ANN with one hidden layer and two hidden layers, which are common used types in existing researches [132], are set and the accuracy are compared.

In this study, the measurement data consists of environment factors and operation parameters. Environmental factors are solar radiation (θ_{sr}), outdoor

humidity (θ_{eh}), ambient temperature (θ_{at}), wind direction (θ_{wd}) and wind speed (θ_{ws}), and operation system parameters contains water volumetric flow (θ_{wf}), outlet water temperature (θ_{wt}), the plate surface temperature (θ_{pt}), and inlet water temperature (θ_{it}). To verify the effect of the environmental and operational factors on efficiency, we divided these factors into three groups. The first contains all factors (total nine), second is only the operation factors (five factors) and only environmental factors (four factors).

6.3.2 Evaluation criteria

The estimation indicator on how well the equation fits the data is expressed by the coefficient of determination, $R^{2,}$ as shown in Equation (6-1). It varies from 0 to 1, higher the value (more near 1), better the fits. And the difference between the observed and fitted values known as the root mean squared error (MSE) is calculated to determine the accuracy of the prediction, the equations are below Eq. (6-2):

$$R^2 = \frac{(\sum_1^{n_{sample}}(y_{observed} - \overline{y_{observed}})(y_{prediction} - \overline{y_{prediction}}))^2}{\sum_1^{n_{sample}}(y_{observed} - \overline{y_{observed}})^2 \times \sum_1^{n_{sample}}(y_{prediction} - \overline{y_{prediction}})^2} \quad (6\text{-}1)$$

$$\text{RMSE} = \sqrt{\frac{1}{n_{sample}} \sum_1^{n_{sample}} (y_{observed} - y_{prediction})^2} \quad (6\text{-}2)$$

Where, n_{sample} is the number of samples, $y_{observed}$ is the true observed/collected data of samples and $\overline{y_{observed}}$ is the average value of true data, $y_{prediction}$is the predicted/estimated value and $\overline{y_{prediction}}$ is the average value of prediction.

Besides the R2 and MSE, the root mean absolute error (MAE) is also calculated for ANN with BP algorithm, as shown in Equation (6-3).

$$\mathrm{RMAE} = \sqrt{\frac{1}{n_{sample}} \sum_{1}^{n_{sample}} \left| y_{observed} - y_{prediction} \right|} \tag{6-3}$$

6.4 Data observation

In order to analyze the real-time performance of this PV/T-ASHP system, a set of experimental data under typical climate conditions in September 30, 2019 were selected. The results are shown in below figures 6-3.

During the heating seasons, the results on Sunday (September 30, 2019) are shown in Figure 6 - 3. As shown in Figure 6 - 3 (a), in September 30, 2019, ambient temperature had an upward trend from 10 ˚C to the highest 20 ˚C at 16:00, then had a slight decrease to around 18 ˚C at the end time 17:00. Solar irradiation first increases then decreases. The highest was 1100 W/m^2 at 12:00. From Figure 6 - 3 (b), we can see that the surface temperature of the absorber and the outlet water temperature had a similar variation profile as the ambient temperature change. Outlet water temperature firstly increased from 15 ˚C to 33

˚C during 9:00 to 15:20, then it slightly downs to 32 ˚C. The absorber surface temperature varied from 32 ˚C to the highest 74 ˚C then to 72 ˚C. The thermal efficiency decreased with a small fluctuation from 65 % to 10 %, average was 45 %. The reason for decrease of thermal efficiency is that after 12:00, the solar irradiation decreased dramatically. It caused a decrease of absorbed heat, and hence the efficiency reduce. And other measurement data including humidity, wind speed and wind direction and so on is shown in Table 6 - 2.

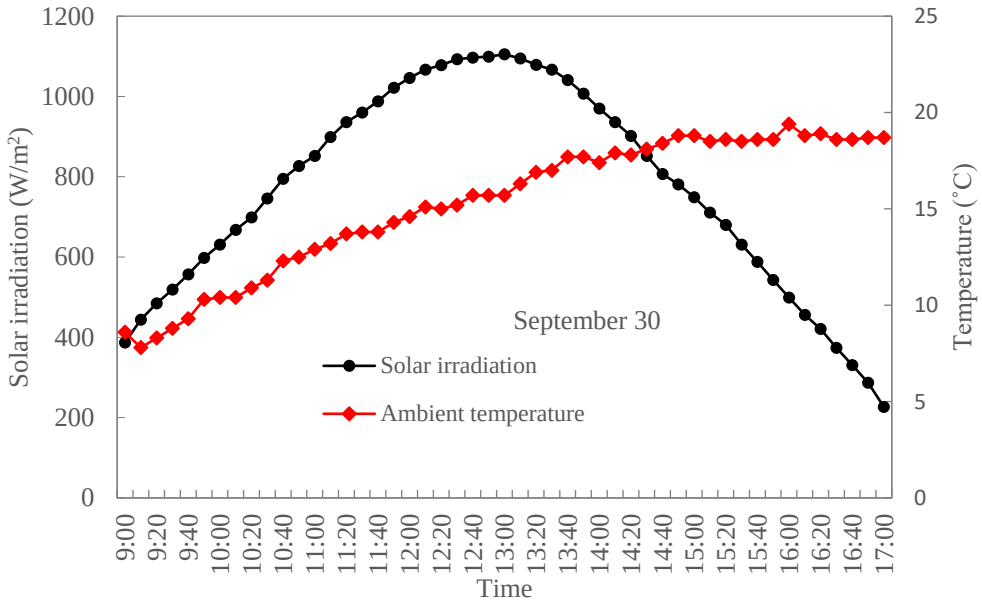

(a) the environment conditions

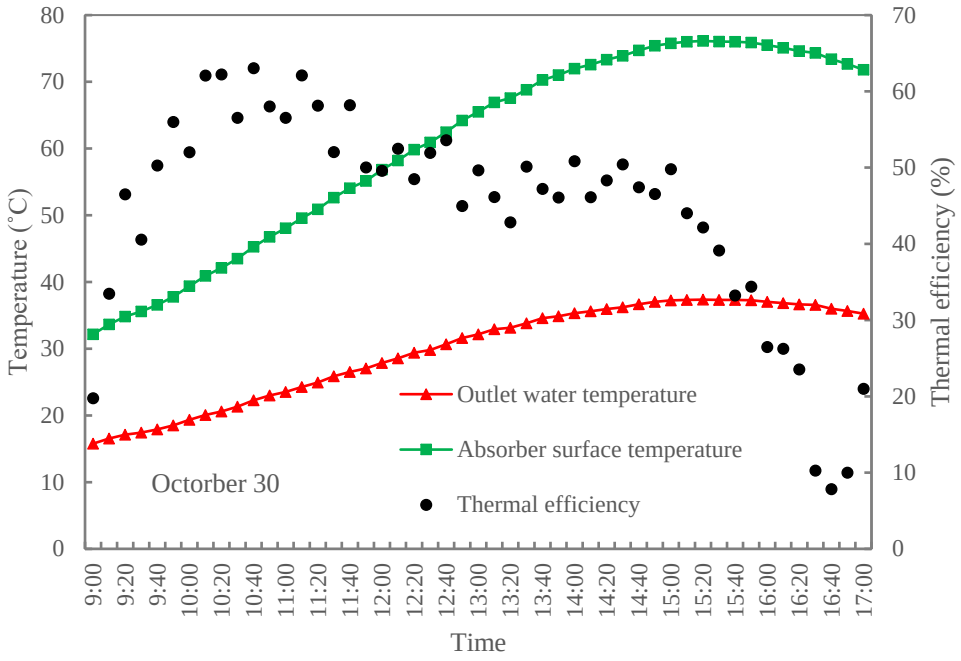

(b) the performance of PV/T collector

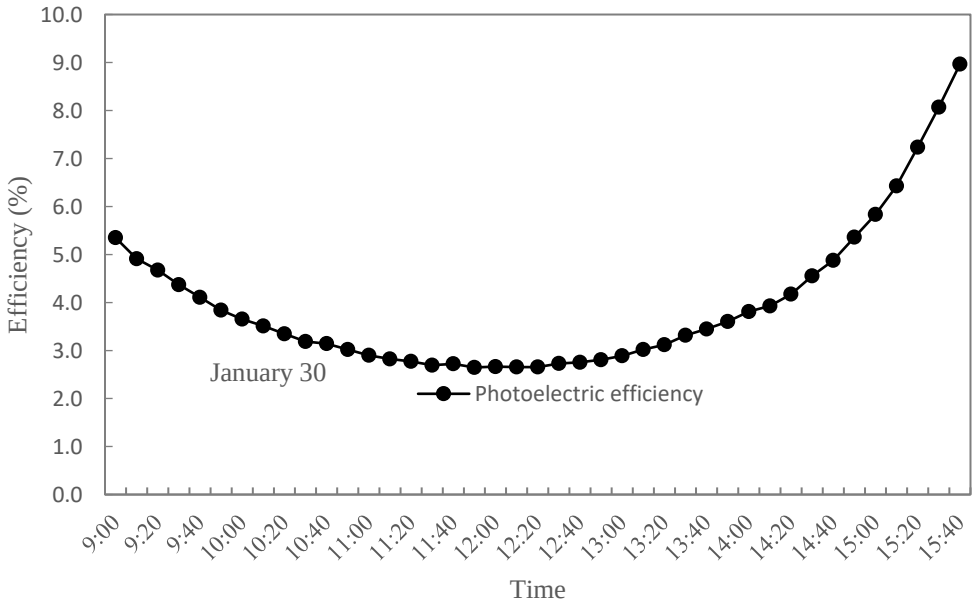

(c) the performance of collector

Figure 6 - 3 The results in one typical day

Table 6 - 2 the typical day measurement results

Time (min)	Inlet water temperature (˚C)	Volumetric flow (kg/h)	Humidity (%)	Wind speed (m/s)	Wind direction (˚)
9:00:00	15.94	1509	51.6	0	164
9:10:00	16.58	1483	55.9	0.5	196
9:20:00	17.15	1511	57.1	0.5	330
9:30:00	17.63	1473	53	0.3	263
9:40:00	18.05	1489	43.5	0.2	148
9:50:00	18.64	1490	45.6	0.1	145
10:00:00	19.36	1493	42.7	0.2	154
10:10:00	20.04	1490	42.6	0.1	12
10:20:00	20.74	1477	37.6	0.4	159
10:30:00	21.32	1498	30.8	0.2	349
10:40:00	22.07	1521	32.4	0.3	320
10:50:00	22.94	1496	32	0.3	349
11:00:00	23.72	1494	27.9	0.6	176
11:10:00	24.4	1497	30.7	0.4	143
11:20:00	25.12	1508	30.3	0.4	151
11:30:00	25.82	1471	29.6	0.4	347
11:40:00	26.6	1480	29.5	0.3	344
11:50:00	27.22	1507	26.9	0.4	164
12:00:00	28.04	1510	27.2	0.4	28
12:10:00	28.79	1518	26.9	0.3	110
12:20:00	29.53	1504	27.3	0.5	32
12:30:00	30.27	1507	26.8	0.4	157
12:40:00	30.86	1482	24.4	0.2	340
12:50:00	31.61	1534	25	0.4	89
13:00:00	32.35	1522	25	0.5	83
13:10:00	32.92	1491	25	0.4	138
13:20:00	33.53	1507	21.7	0.3	139
13:30:00	34.07	1518	23.2	0.5	15

13:40:00	34.68	1520	22.5	0.1	160
13:50:00	35.28	1525	21.7	0.5	13
14:00:00	35.77	1499	21.7	0.1	6
14:10:00	36.03	1529	22.3	0.1	163
14:20:00	36.46	1515	19.2	0.3	174
14:30:00	36.77	1517	19.7	0.1	148
14:40:00	37.28	1515	19.3	0.4	147
14:50:00	37.61	1508	21.6	0.1	158
15:00:00	37.79	1500	19.9	0.2	143
15:10:00	38.05	1523	20.7	0.3	164
15:20:00	38.14	1524	21.3	0.3	136
15:30:00	38.07	1517	21.6	0.2	141

6.5 ANN

The ANN models developed in this Chapter can be divided into three groups, which have different number of input layers. The number of input layer factors are 4 (water volumetric flow (θ_{wf}), outlet water temperature (θ_{wt}), the plate surface temperature (θ_{pt}), inlet water temperature (θ_{it}).), 5 (solar radiation (θ_{sr}), outdoor humidity (θ_{eh}), ambient temperature (θ_{at}), wind direction (θ_{wd}), wind speed (θ_{ws}))and 9 (all factors including environment and operation).

In this study, the number of the input layer neurons was different, whereas the output was two neurons, thermal efficiency and electric efficiency. Different hidden layer and neurons of each hidden layer can lead to different results, as it affects the speed of the convergence and generalization of BP network. In this paper, the BP neural network was designed to have one hidden layer N-X-1 or two hidden layers N-X-Y-1. That is, the input layer has N nodes, the one hidden

layer has X nodes, if there is second hidden layers, the second layers has Y nodes, and the output layers has 1 node. To gain the best accurate results, different BP network with one hidden layer for different input layers and two hidden layers with eight input layers was trained and validated. The number nodes of hidden layers are chose as 5, 10, 15, 20 and 25, respectively.

6.5.1 ANN model with one hidden layer

The results in one hidden layer with different nodes are shown in Table 6 - 3 and

Table 6 - 4 for electric and thermal efficiency respectively. For accuracy, we took the average value from training, testing and validation process. It is clear that the nodes number almost has no influence for electric efficiency and thermal efficiency. But with the same nodes, the results varies a lot and the variation trend for both electric and thermal efficiency are different. The reason is that the influence of environment and operation parameters differs in the results of electrical and thermal efficiency. While the electric efficiency is significantly affected by environment factors, and thermal efficiency is more affected by operation factors than environment factors, through comparing the results between the group 4 and 5 in both Table 6 - 3 and

Table 6 - 4.

Table 6 - 3 R2, RMSE and RMAE with one hidden layer for electric efficiency

Groups	R2	RMSE (%)	RMAE

Nodes	9	4	5	9	4	5	9	4	5
5	0.9747	0.9753	0.7121	0.9781	0.9577	2.5032	0.6022	0.5588	1.2982
10	0.9841	0.9692	0.7355	0.9363	0.9615	2.4376	0.5697	0.5762	1.2880
15	0.9716	0.9798	0.7259	0.9248	0.9514	2.4098	0.5416	0.5628	1.2639
20	0.9772	0.9818	0.7291	0.8981	0.9391	2.4603	0.5488	0.5747	1.2891
25	0.9716	0.9685	0.7362	0.9689	0.9332	2.3951	0.5821	0.5688	1.2695

Table 6 - 4 R2, RMSE and RMAE with one hidden layer for Thermal efficiency

Groups / Nodes	R^2			RMSE (%)			RMAE		
	9	4	5	9	4	5	9	4	5
5	0.7743	0.4810	0.7467	9.8135	13.3691	10.6664	2.5182	3.1148	2.6701
10	0.7971	0.4505	0.7272	9.8139	13.8220	10.6001	2.5557	3.1518	2.6617
15	0.7992	0.4933	0.7288	9.4591	13.3579	10.6149	2.4957	3.1134	2.6745
20	0.8037	0.5019	0.7346	9.3773	13.3439	10.7131	2.4901	3.0961	2.6950
25	0.8025	0.5073	0.7279	9.2248	13.3485	10.7014	2.4932	3.1015	2.6824

Figure 6 - 4 and Figure 6 - 5 show comparison between the results of R^2, RMSE and RMAE. Figure 6 - 4 shows that, the variation of the node's number of one hidden layer caused slight influence on the prediction models, as the R2, RMSE and RMAE only experience small variations in each group for electric efficiency. The best ANN model is the one with the 9 input factors, then is the four environment factors, the last five operation factors. As the average RMSE values are less 1.0% for input Group 9 and 4, while it is near 2.5% for group 5.

And the RMAE for group 9 and 4 are near 0.55, while for group 5 is near 1.3. From these results, we can also see that the difference between group 9 and 4 is small, leading to that the electric efficiency is greatly affected by environment factors.

It is clear that, in Figure 6 - 5, the performance for different groups is group 9 > group 5 > group 4. From Figure 6 - 5, we can also see that the thermal efficiency is affected stronger by operation factor than environment factors. Comparing with electric efficiency results, the accuracy for thermal efficiency is lower. The highest R2 for thermal efficiency is near 0.8, the lowest RMSE percentage is near 8.6 and lower RMAE is near 2.5 with input group 9.

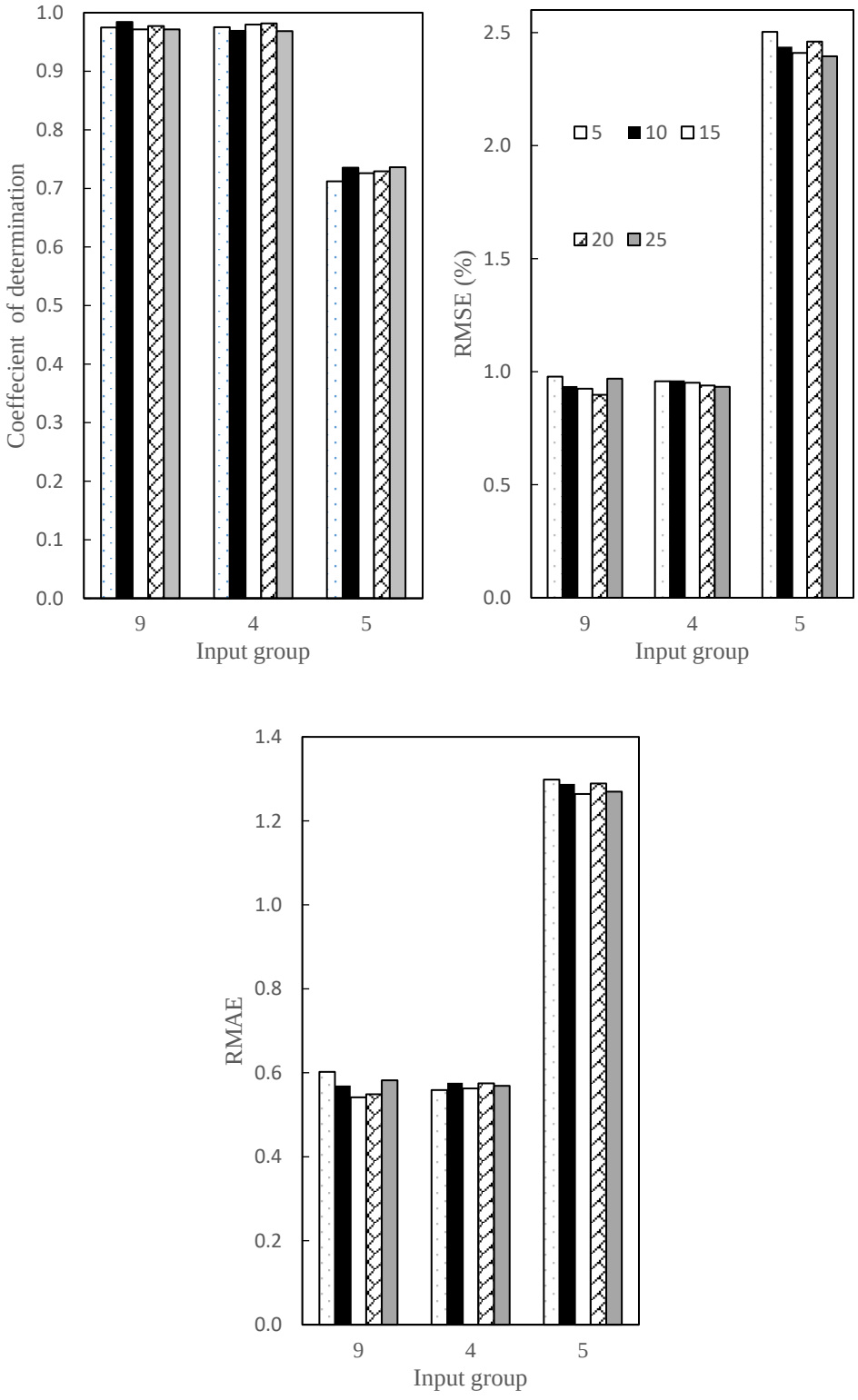

Figure 6 - 4 R2, RMSE and RMAE for electric efficiency with one hidden layer

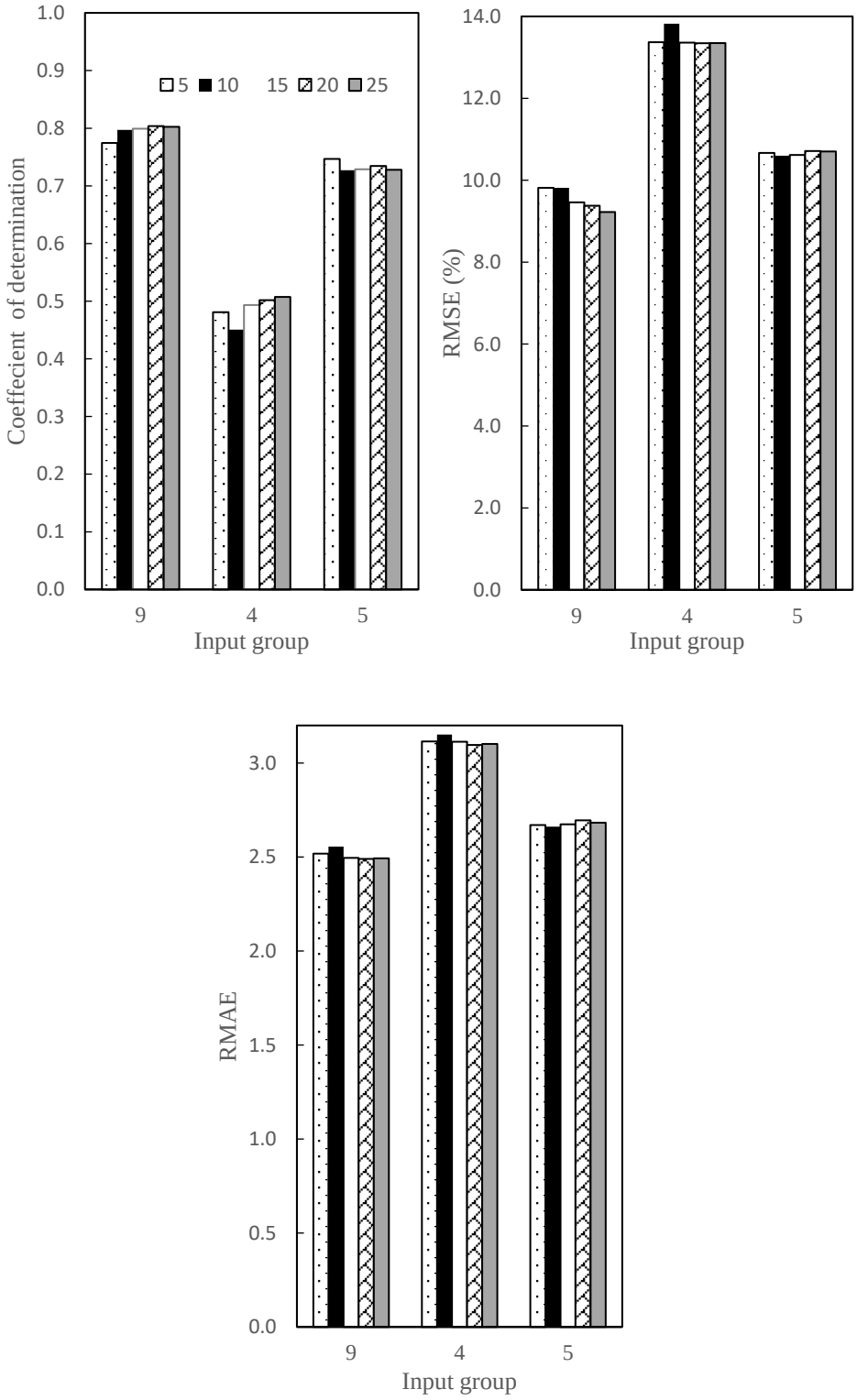

Figure 6 - 5 R2, RMSE and RMAE for thermal efficiency with one hidden layer

6.5.2 ANN model with two hidden layers

Based on the results of R2, RMSE and RMAE in Section 6.5.1, the more factors generate better performance, although the R2, RMSE and RMAE difference between group 9 and group 4 is small for electric efficiency. Combination of two output parameters show the difference is large especially for thermal efficiency. For prediction models of ANN with BP algorithm with two hidden layers, we take the input in group 9 to find the best network as example.

Most of network construction of 9-X-Y-1 with the X/Y varied from 5 to 25, but some of networks did not work well for prediction of the performance of electric and thermal efficiency in this PV/T system. The results can be seen from Table 6 - 5. This also shows that, not all networks are suitable for one system, it is necessary to optimize of the ANN network firstly before using for special system. And from Table 6 - 5, it is easily to find that the R2 difference is minor for different nodes of hidden layers.

Table 6 - 5 R2 for network with two hidden layers

	Electric efficiency					Thermal efficiency				
	X=5	X=10	X=15	X=20	X=25	X=5	X=10	X=15	X=20	X=25
Y=5	0.9669	0.9674	0.9624	0.9652	--	0.9628	0.9642	0.9689	--	--
Y=10	0.9656	0.9695	0.9704	0.0000	0.9754	--	0.9734	0.9646	0.9660	0.9665
Y=15	0.9749	0.9618	0.9649	0.9661	0.9627	0.9592	0.9670	0.9665	0.9686	0.9607
Y=20	0.9740	0.9624	0.9669	0.9697	0.9610	0.9704	0.9709	0.9746	0.9596	0.9647
Y=25	0.9736	--	0.9670	0.9652	0.9678	0.9702	0.9595	0.9648	0.9667	0.9652

The results of RMSE and RMAE with different hidden layer nodes are shown in graphic representation, identifying the output difference. The results of RMSE and RMAE for electric and thermal efficiency, respectively, are shown in Figure 6 - 6 and Figure 6 - 7. For electric efficiency (as shown in Figure 6 - 6), RMSE varies from 0.75% to 0.96%, lower than 1%, and the RMAE varies from 0.5 to 0.68, lower than 0.7 for all networks. The results show that the reality and prediction has a good agreement by using ANN network with two hidden layers. And the best network construction is the 9-25-25-1, as it has the lowest RMSE (0.76%). For thermal efficiency, the RMSE changes from 0.8% to 1.0%, and RMAE changes from 0.5 to 0.68. The beast network construction is 9-10-10-1, with the lowest value of RMSE (0.805%). And compared with electric efficiency prediction, the fluctuations of RMSE and RMAE are little larger for thermal efficiency.

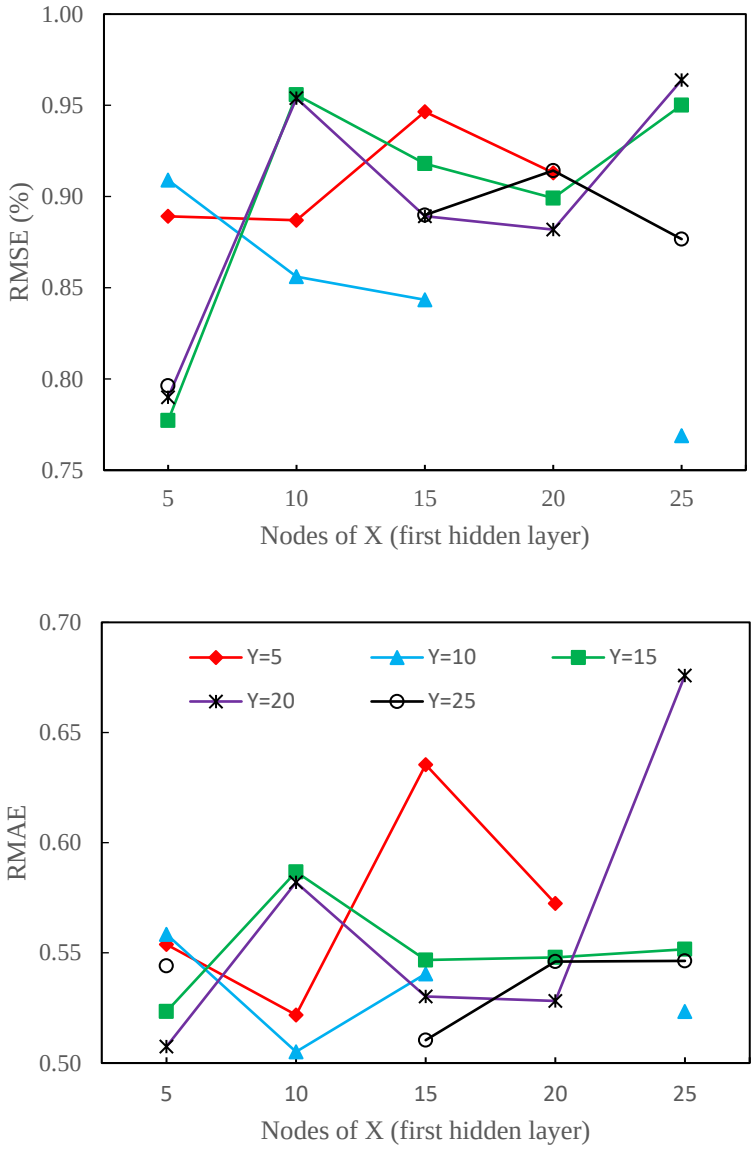

Figure 6 - 6 RMSE and RMAE of electric efficiency with two hidden layers

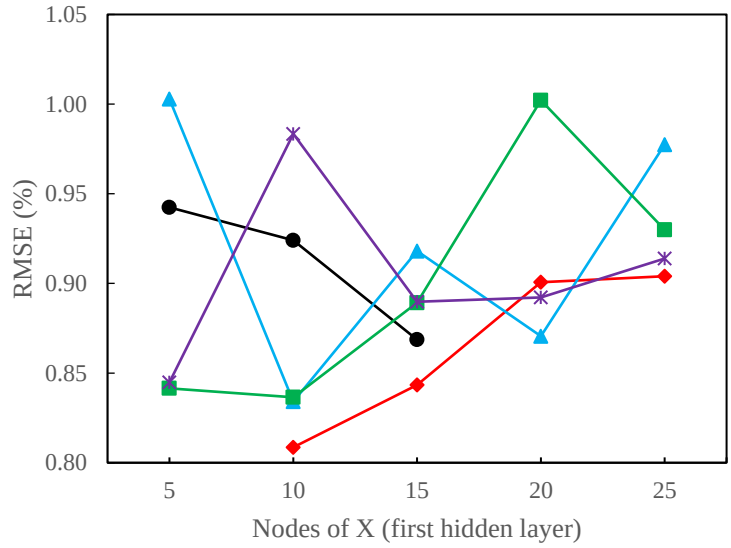

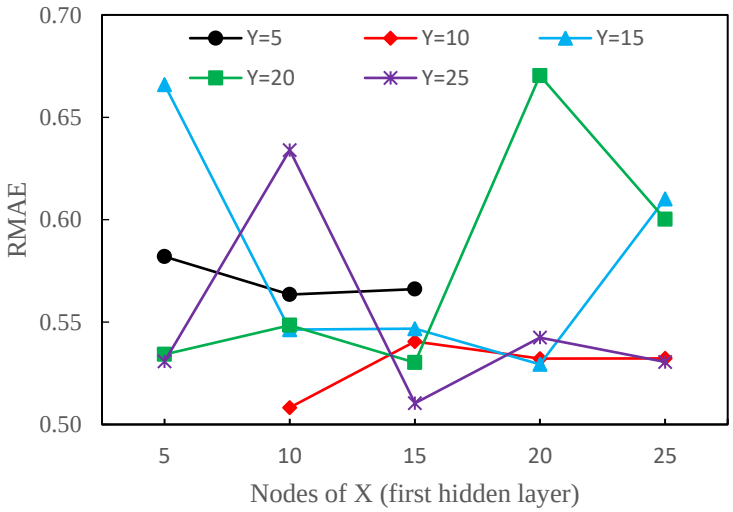

Figure 6 - 7 RMSE and RMAE of thermal efficiency with two hidden layers

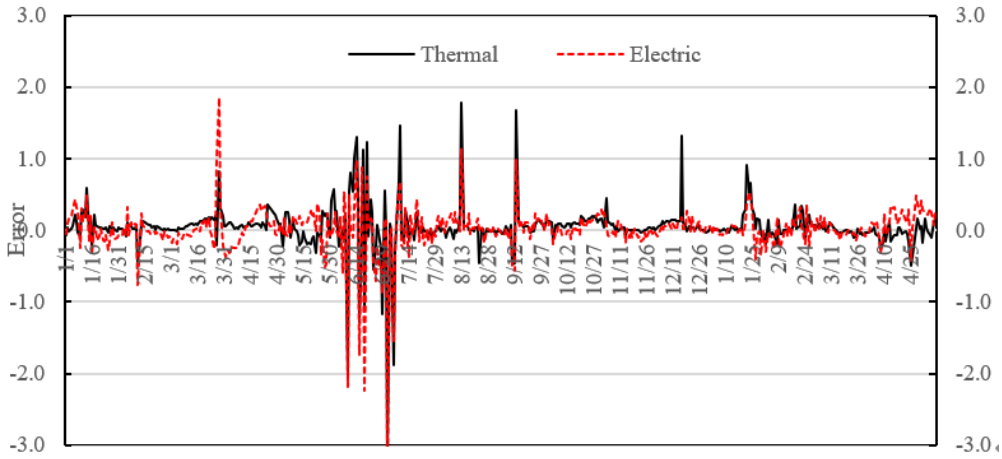

Figure 6-8 The error value of thermal and electric efficiency with 9-15-15-1 network

Figure 6-8 shows the error between prediction and measurement values (only 500 chosen in this figure) with 9-15-15-1 BP network in chosen days in 2018. The error between reality and prediction of electric and thermal efficiency varies from - 3 to 2, average - 0.87, which also means there is a good agreement between the reality and prediction.

6.5.3 Results comparison

Compared the results with nine input layers, it can be seen that the ANN network with two hidden layers performs better than one hidden layer, especially for thermal efficiency.

The best ANN construction for electric efficiency with one hidden layer is 9-20-1, with the lowest RMSE 0.898%. The 9-X-1 network for electric efficiency shows that R2 fluctuates around 0.97, and RMSE is lower 0.98% and the RMAE is lower 0.6. But for 9-X-Y-1 type, the results for electric shows that the average

R2 is about 0.97, but the RMSE is lower than 9-X-1 type, as the average value of RMSE is lower than 0.95%, most of them are only around 0.9%. And the RMAE is also lower, as most of them are about 0.55.

For thermal efficiency, the best ANN network with one hidden layer is 9-25-1, with the lower RMSE 9.225%. For 9-X-1 type for thermal efficiency, there is a trend that the more nodes of X, the better performance of the model. The R2 is around 0.8, RMSE varies from 9.2% to 9.8%, and RMAE is around 2.5 for thermal efficiency of all 9-X-1 types. However, the R2 for 9-X-Y-1 type are all over 0.9, most of them are around 0.97, and the RMSE are lower 1.0%. RMAE are also much lower, as they are all smaller than 0.70 and most of them are near 0.55.

Compared with previous researches that the outputs are the similar, the results in this paper are better than previous researches [142, 132, 149, 147]. The NRMSE are 1.9% for electric and 2.9% for thermal power [142]. The RMSE is lower 10% for power production [147] and 0.10-2.23% for overall thermal energy and exergy [149]. The NMBE is -13.05% for [132]. There maybe caused by few reasons. First, this maybe caused by the number of inputs, as inputs in this paper contains both environment and operation parameters, some of them [142, 132, 149, 147] only considered one or the number is smaller than this paper. This conclusion also dedicates that the more factors considered, the better performance of the prediction model. Second, for previous researches, they only chose one model type without comparing the different constructions of ANN network. So there maybe exist improvement for their ANN model construction.

This suggests that the researches need to find the best suitable ANN network before conducting, though the error maybe not big.

6.6 Conclusions

In this study, we conducted the different ANN network types to predict the performance of PV/T system including electric and thermal efficiency. The case study is based on the data measured in one PV/T system used for an office building in Beijing, China. The whole 2018 year performance data are used. Total nine factors consists of five environmental factors, i.e., solar radiation (θ_{sr}), outdoor humidity (θ_{eh}), ambient temperature (θ_{at}), wind direction (θ_{wd}) and wind speed (θ_{ws}), and four operation system parameters contains water volumetric flow (θ_{wf}), outlet water temperature (θ_{wt}), the plate surface temperature (θ_{pt}), and inlet water temperature (θ_{it}) are considered. The main conclusions are bellow:

- Environment factors have more significant influence on electric efficiency than operation parameters. For thermal efficiency, operation parameters have more significant influence. But the performance with all nine factors are the best for both electric and thermal efficiency.
- ANN network with two hidden layers generally performs better than one hidden layer for both electric and thermal efficiency. The best ANN network construction for electric efficiency is 9-25-25-1, with lowest RMSE (0.76%). For thermal efficiency, it is 9-10-10-1, with the lowest value of RMSE (0.805%).

Combination of this work and previous researches, it is easily concluded that the more factors considered, the better performance of the prediction model. And the comparison results suggest that the researches need to find the best suitable ANN network before directly conducting one construction.

Chapter 7: Conclusions

This chapter presents the conclusions including the experiments and simulations and proposed future work directions on this topic.

7.1 Conclusion of the work

To improve the heat transfer performance and efficiency, in this thesis we propose a novel construction extruded heat exchanger, the ultra-thin superconducting thermal absorber with internal fins shaped bubbling with two different sizes. Furthermore, a PV/T-ASHP system using this kind of absorbers in the solar collector is deployed for an office room real application. Based on this case study, the performance of this system is analyzed through measurements and simulations. The main results of this research are as the following:

For the whole PV/T-ASHP system, our experimental results showed that the electricity self-sufficiency reaches its highest value 78.61%, and in the heating seasons, the thermal self-sufficiency reaches 88.42%, even during December where it can supply 30.73% of the heat demand by the solar collector. The average COP during the heating seasons reaches 4. In general, the ambient temperature and solar irradiation change significantly affect system performance. The larger the difference between the ambient temperature and

the outlet water temperature of the solar collector, the higher the COP of the ASHP and its electric production efficiency.

Regarding the economic impact, the payback time for this system is 5.6 years, and for renovated buildings, the payback time is 5 years. We further investigated the environmental impact and showed that using this system prevents the emission of .8 t of carbon dioxide (CO_2), 204.59 kg of sulfur dioxide (SO_2), and 102.29 kg of nitrogen oxides (NO_X) emissions for the whole year.

It was seen that the environmental factors have a more significant effect on the electric efficiency than that of the operation parameters whereas for the thermal efficiency it is the other way around. Nevertheless, the performance prediction based on all nine factors is required for both electric and thermal efficiency. For this prediction, we showed that the ANN with two hidden layers generally performs better than that of one hidden layer for predicting both electric and thermal efficiency. The best ANN network construction for electric efficiency is 9-25-25-1, with the lowest RMSE (0.76%). For thermal efficiency, it is 9-10-10-1, with the lowest value of RMSE (0.805%). Our comparisons suggest that the researchers need to find the best suitable ANN network before directly conducting one construction.

7.2 Future work

There are still some limitations that need to be addressed before the versatile development of solar-assisted ASHP systems to the wider market. The main issues are concluded in the following:

The gaps between a simulation or laboratory testing and real applications need to be further investigated [55]. In the future, we need to: (1) develop a common simulation tool; and (2) measure the system performance under standard testing conditions. For the experimental issues, more experiments should be conducted in different conditions. To make it more popular even for the community using in the future, the life cycle performance should be also analyzed.

The main focus of this thesis is on the collector design. Further research on the design and construction of the solar collector is required.

For performance prediction, multiple regression and ANN are used and compared to predict the performance of the PV/T in this study. Several factors are considered in our study and future works, more methodologies should be analyzed and compared such as GA, and more factors should be considered for system optimization, e.g., the installation angle of the solar collector and different climate regions.

References

[1] Ellabba, Omar, Haitham Abu-Rub, Frede Blaabjerg. 2014. "Renewable enrgy resources: Current status, future prospects and thier enabling technology." Renewable and Sustainable Energy Reviews 39: 748-764.

[2] "Renewable 2018 global status report," 2018.

[3] Shahsavar, A. A. 2010. Experimental investigation and modeling of a direct coupled PV/T air collector. Solar Energy, 84, 1938-1958.

[4] S.S.S. Baljit, H.-Y. C. 2016. Review of building integrated application of photovoltaic and solar thermal systems. Journal of Cleaner Production, 137 (20), 677-689.

[5] "Technology roadmap-solar photovoltaic energy, International Energy Agency," 2010.

[6] Jinshun Wu, Xingxing Zhang, Jingchun Shen, Yupeng Wu, Karen Connelly, Tong Yang, Llewellyn Tang, Manxuan Xiao, Yixuan Wei, Ke Jiang, Chao Chen, Peng Xu, Hong Wang. 2017. "A review of thermal absorbers and thier integration methods for thr combined solar photovoltaic/thermal (PV/T) modules." Renewable and Sustainable Energy Reviews 75: 839-854.

[7] He Wei, Zhang Yang, Ji Jie. 2011. "Comparative experiment study on photovoltaic and thermal solar system under natural circulation of water." Applied Thermal Engineering 16 (31): 3369-79.

[8] Charalambous PG, Maidment GG, Kalogirou SA, Yiakoumetti K. 2007. "Photovoltaic thermal (PV/T) collectors: a review." Applied Thermal Engineering 27: 275-86.

[9] Buker Mahmut Sami, Mempouo Blaise, Riffat Saffa B. 2014. "Performance evaluation and techno-economic analysis of a novel building integrated PV/T roof collector: an experimental validation." Energy Building 76: 164-75.

[10] "PV/T water collector," www.newformenergy.com, 2016.

[11] Hassani Samir, Taylor Robert A, Saad Mekhilef C, Saidur R. 2016. "A caseade nanofluid-based PV/T system with optimized optical and thermal properties." Energy 112: 963-75.

[12] Zhang X, Zhao X, Smith S, et al. 2012. " Review of R & D Progress and practical application of the solar photovoltaic/thermal (PV/T) technologies." Renewable Sustainable Energy Reviews 16 (01): 599-617.

[13] Zondag HA, et al. 2003. "The yield of different combined PV-thermal collector designs." Solar Energy 74: 253-69.

[14] Ibrahim Adnan, Othman Mohd Yusof, Ruslan Mohd Hafidz, Mat Sohif, Sopian Kamaruzzaman. 2011. "Recent advances in flat plate photovoltaic/thermal (PV/T) solar collectors." Renewable Sustainbal Energy Reivews 15: 352-65.

[15] Kroiß A, Präbst A, Hamberger S, Spinnler M, Tripanagnostopoulos Y, Sattelmayer T. 2014. "Development of a seawater-proof hybrid photovoltaic/thermal (PV/T) solar collector ." Energy Procedia 52: 93-103.

[16] Chow TT, He W, Ji J. 2006 . " Hybrid photovoltaic-thermosyphon water heating system for residential application." Solar Energy 80: 298-306.

[17] Farshchimonfared M, Bilbao JI, Sproul AB. . 2016. "Full optimisation and sensitivity analysis of a photovoltaic thermal (PV/T) air system linked to a typical residential building." Solar Energy 136: 15-22.

[18] Ibrahim Adnan, Fudholi Ahmad, Sopian Kamaruzzaman, Othman Mohd Yusof, Ruslan Mohd Hafidz. 2014. "Efficiencies and improvement potentiial of building integrated photovoltaic thermal (PIPV) system." Energy Convers Management 77: 527-34.

[19] "FOTO-THERM Thermo-photovoltaic modules;," www.fototherm.com/en/, 2016..

[20] Hou Longshu, Quan Zhenhua, Zhao Yaohua, Wang Lincheng, Wang Gang. 2016. "An experimental and simulative study on a novel

photovoltaic thermal collector with micro heat pipe array (MHPA-PV/T)." Energy Building 124: 60-9.

[21] Zhou Jinzhi, Zhao Xudong, Ma Xiaoli, et al. 2016. "Experimental investigation of a solar driven direct-expansion heat pump system employing the novel PV/micro-channels-evaporator modules ." Applied Energy 178: 484-495.

[22] Jouhara H, Szulgowska-Zgrzywa M, Sayegh MA, et al. 2016. "The performance of a heat pipe based solar PV/T roof collector and its potential contribution in districr heating application." Energy.

[23] P Xu, Zhang Xingxing, Shen Jingchun, Zhao Xudong, He Wei, Li Deying. 2015. "Parallel experimental study of a novel super-thin thermal absorber based photovoltaic/thermal (PV/T) system against conventional photovoltaic (PV) system." Energy Rep 1: 30-35.

[24] Dupeyrat P, Ménézo C, Wirth H, Rommel M. 2011. " Improvement of PV module optical proporties for PV- themal hybrid collector application." Solar Energy M ater Solar Cells 95 (8): 2028-36.

[25] Dupeyrat P, Ménézo C, Rommel M, Henning HM. 2011. "Efficient single glazed flat plate photovoltaic-thermal hybrid collector for domestic hot water system." Solar Energy 85 (7): 1457-68.

[26] Bai Y, Chow TT, Ménézo C, Dupeyrat P. 2012. "Analysis of a hybrid PV/thermal solarassisted heat pump system for sports center water

heating application." Int J Photoenergy , 2012. https://doi.org/10.1155/2012/265838

[27] Bionicol., "Bionicol-Dev a bionic Sol Collect Alum Roll absorber-Proj Status Second year," www.bionicol.eu/, 2010.

[28] Chandrasekar M, Senthilkumar T. 2015. " Experimental demonstration of enhanced solar energy utilization in flat PV (photovoltaic) modules cooled by heat spresders in conjunction with cotton wick structures." Energy 90: 1401-10.

[29] J.C. Shen, Xingxing Zhang a,⇑, Tong Yang a, Llewellyn Tang a, Ali Cheshmehzangi a, Yupeng Wu. 2016. "Characteristic study of a novel cpmpact solar thermal facade (STF) with internally extruded pin-fin flow channel for building integration." Applied Energy 168: 48-64.

[30] J. Hadorn, Solar and heat pump sysytem for residential buildings., John Wiley &Sons, 2015.

[31] S.H.C. IEA, Task 53. 2017. New Generation Solar Cooling & Heating Systems -avaliable. ⟨http://task53.iea-shc.org⟩ [-05-23]. n.d.

[32] P. Stefano, S. Nelson, B. Chris, M. Hatef, L. Per,. 2018. "Techno-economic review of solar heat pump sysytems for residential heating applications." Renew. Sustain.Energy Rev. 81: 22-32.

[33] E Frank, H Michel, S Herkel and R Jorn. Sep.29-Oct 1, . "Systematic classification of comined solar thermal and heat pump systems." Proceedings of the EuroSun 2010 conference. Graz, Austria.

[34] E. Frank, M.Y. Haller, S. Herkel, J. Ruschenburg,. 2010. "Systematic classification of combiende solar thermal and heat pump sysytems." Proceedings of the EuroSun 2010 conference. Graz, Austria,.

[35] J. Ruschenburg, S. Herkel, H.M. Henning,. 2013. " A statistical analysis on market avaliable solar thremal heat pump sysytems." Sol.Energy 95: 79-89.

[36] J. Ruschenburg, S. Herkel,. 2013. A Review of Market-Available Solar Thermal Heat pump sysytems. A Technical Report of Subtask A. IEA SHC Task 44/HPP Annex 38.

[37] "Survey of Energy Resources, World Energy Council," 2007.

[38] Rauschenbach., H.S. n.d. Solar Cell Array Design Handbook: the Principles and Technology of photovoltaic enrgy conversion.

[39] A. Joyce, L. Coelho, J. Martins, N. Tavares, R. Pereira, P. Magalh~aes,. 2011 . "A PV/T and heat pump based trigeneration system model for residential applications,." ISES e Sol. World Congr 11: 1-12.

[40] Ali H.A. Al-Waeli, K. Sopian, Hussein A. Kazemb, Miqdam T. Chaichan,. 2017. "Photovoltaic/Thermal (PV/T) systems: status and future prospects, Renew." Sustain. Energy Rev. 77 : 109-130.

[41] Zhongzhu Qiu, Xiaoli Ma, Xudong Zhao, Li Peng, Samira Ali,. 2016. "Experimental investigation of the energy performance of a novel Micro-encapsulated Phase Change Material (MPCM) slurry based PV/T system, ." Appl. Energy 165: 260-271.

[42] E. Giuseppe, Z. Angelo, D.C. Michele,. 2017. "A heat pump coupled with photovoltaic thermal hybrid solar collectors: a case study of a multi-source energy system." Energy Convers. Manag. 151 : 386-399.

[43] L. Cabrol, P. Rowley,. n.d. "Towards low carbon homes ea simulation analysis of building-integrated air-source heat pump systems. ." Energy and buildings. (https://doi.org/10.1016/j.enbuild.2012.01.019.).

[44] T. Christos, B. Evangelos, M. Georgios, A.A. Kimon, D.A. simakis,. 2016. " Energetic and financial evaluation of a solar assisted heat pump heating system with other usual heating sysytems in Athens." Appl. Therm. Eng. 106: 87-97.

[45] B. Evangelos, T. Christos,. 2017. " Energetic and financial sustainability of solar assisted heat pump heating systems in Europe, ." Sustain. City. Soc. 33: 7-84.

[46] T.P. Maria, B. Evangelos, T. Christos, A.A. Kimon,. 2019. "Financial and energetic evaluation of solar-assisted heat pump underfloor heating systems with phase change materials, ." Applied Thermal and Enginnering 149: 548-564.

[47] P. Stefano, B. Chris, H. Andreas, H. Franz, C. David, et al.,. 2016. "Analysis of system improvements in solar thermal and air source heat pump combisystems,." Applied Energy 173 (1): 606-623.

[48] S. Nikoofard, V.I. Ugursal, M.I. Beausoleil,. 2014. "Economic analysis of energy upgrades based on tolerable capital cost." J. Energy 1 141 (3): 1-6.

[49] P Khagendra Bhandari, M Jennifer J Collier, Randy SA Ellingson,. 2015. " Energy payback time (EPBT) and energy return on energy invested (EROI) of solar photovoltaic systems: a systematic review and meta-analysis." Renew. Sustain.Energy Rev. 47: 133-141.

[50] M. Hosenuzzaman, N.A. Rahim, J. Selvaraj, M. Hasanuzzaman, A.B.M.A. Malek, A. Nahar,. 2015. "Global prospects, progress, policies, and environmental impact of solar photovoltaic power generation." Renew. Sustain. Energy Rev. 41: 284-297.

[51] "Environmental Management e Life Cycle Assessment e Principles and Frame work," 2006.

[52] T.T. Chow. 2010. "A review on photovoltaic/thermal hybrid solar technology, ." Appl. Energy 87: 365-379.

[53] S. Rasoul Asaee, V. Ismet Ugursal, Ian Beausoleil-Morrison,. 2017. "Techno-economic assessment of solar assisted heat pump system retrofit in the Canadian housing stock." Appl. Energy 190: 439-452.

[54] L.G. Swan, V.I. Ugursal, M.I. Beausoleil,. 2013. " Hybrid residential end-use energy and greenhouse gas emissions model e development and verification for Canada,." J Build Perform Simul 6 (1): 1-23.

[55] A.A. Farhat, V.I. Ugursal,. 2010. "Greenhouse gas emission intensity factors for marginal electricity generation in Canada." Int. J. Energy Res. 34 (15): 1309-1327.

[56] Zakaria MA, M.N.A. Hawlader,. 2013. " A review on solar assisted heat pump systems in Singapore." Renew. Sustain. Energy Rev. 26: 286-293.

[57] P Stefano and B Chris. 2016. "Techno-Economic Analysis of a Novel Solar Thermal and Air-Source Heat Pump System." International Refrigeration and Air Conditioning Conference. Paper 1638. .

[58] P Stefano, B Chris, Y Michel. Haller, Andreas Heinz. 2016. "Influence of boundary conditions and component size on electricity demand in solar thermal and heat pump combisystems." Applied Energy 162: 1062-1073.

[59] S Mahmut, S Riffat. 2016. " Solar assisted heat pump systems for low temperature water heating applications: A systematic review. ." Renewable and Sustainable Energy Reviews 55: 399-413.

[60] D Jonas, D Theis, F Felgner, and G Frey. 2017. "A TRNSYS-Based Simulation Framework for the Analysis of Solar Thermal and Heat Pump Systems." Applied Solar Energy 53 (2): 126-137.

[61] J.F. Chen, Y.J. Dai, R.Z. Wang. 2016. "Experimental and theoretical study on a solar assisted CO2 heat pump for space heating. ." Renewable Energy 89: 295-304.

[62] H Li, Y Sun. 2018. "Operational performance study on a photovoltaic loop heat pipe/solar assisted heat pump water heating system. ." Energy and Buildings 158: 861-872.

[63] YH Li, WC Kao. 2017. " Performance analysis and economic assessment of solar thermal and heat pump combisystems for subtropical and tropical region. ." Solar Energy 153: 301-316.

[64] WS Deng, JL Yu. 2016. " Simulation analysis on dynamic performance of a combined solar/air dual source heat pump water heater. ." Energy Conversion and Management 120: 378-387.

[65] C Fraga, P Hollmuller, F Mermoud, B Lachal. 2017. " Solar assisted heat pump system for multifamily buildings: Towards a seasonal

performance factor of 5? Numerical sensitivity analysis based on a monitored case study. ." Solar Energy 146: 543-564.

[66] E Bellos, C Tzivanidis, K Moschos, A Kimon. 2016. " Antonopoulos Energetic and financial evaluation of solar assisted heat pump space heating systems ." Energy Conversion and Management 120: 306-319.

[67] G Hailu, P Dash, AS Fung. 2015. "Performance Evaluation of an Air Source Heat Pump Coupled with a Building-Integrated Photovoltaic/Thermal (BIPV/T) System under Cold Climatic Conditions. ." Energy Procedia 78: 1913-1918.

[68] R. Kamel, N. Ekrami, P. Dash, Alan Fung, Getu Hailu. 2015. "BIPV/T+ASHP: Tech-nologies for NZEBs ." Energy Procedia , 78: 424–429.

[69] RS. Kamel, S Alan. Fung. 2014. "Modeling simulation and feasibility analysis of residential BIPV/T+ASHP system in cold climate—Canada. ." Energy and Buildings 82: 758-770.

[70] C CAO, H Li, G Feng, R Zhang and K Huang. 2016. "Research on PV/T-air source heat pump integrated heating system in severe cold region. ." Procedia Engineering 146: 410-414.

[71] H Li, C Cao, G Feng, R Zhang, K Huang. 2015. "A BIPV/T System Design Based on Simulation and its Application in Integrated Heating System. ." Procedia Engineering 121: 1590-1596.

[72] T Kim, B Choi, YS Han, KH Do. 2018. " A comparative investigation of solar-assisted heat pumps with solar thermal collectors for a hot water supply system. ." Energy Conversion and Management 172: 472-484.

[73] D Zhang, QB Wu, JP Li, XQ Kong. 2014. "Effects of refrigerant charge and structural parameters on the performance of a direct expansion solar assisted heat pump system. ." Applied Thermal Engineering 73: 522-528.

[74] MJ Song, L Xia, N Mao, SM Deng. 2016. "An experimental study on even frosting performance of an air source heat pump unit with a multi-circuit outdoor coil." Applied Energy 164: 36-44.

[75] MJ Song, N Mao, YJ Xu, SM Deng. 2019. "Challenges in and the development of building energy saving techniques, illustrated with the example of an air source heat pump." Thermal Science and Engineering Progress 10: 337-356.

[76] GD Qiu, XH Wei, ZF Xu, WH Cai. 2018. "A novel integrated heating system odf soalr energy and air source heat pumps and its optimal working condition range in cold regions. ." Energy Conversion and Management 174: 922-931.

[77] M Giampaolo, PM Luigi Colombo, R Stefano, F Damiano. 2016. "Tiles as solar air heater to support a heat pump for residential air conditioning. ." Applied Thermal Engineering 102 : 1412-1421.

[78] D Xu, Q Tian, Z Li. 2017. " Energy and exergy analysis of solar integrated air source heat pump for radiant floor heating without water. ." Energy and Buildings 142: 128-138.

[79] D Xu, Q Tian, Z Li. 2017. " Experimental investigation on heating performance of solar integrated air source heat pump. ." Applied Thermal Engineering 123: 1013-1020.

[80] K Bakirci, B Yuksel. 2011. "Experimental thermal performance of a solar source heat-pump system for residential heating in cold climate region. ." Applied Thermal Engineering 31 (2011) 1508-1518 31: 1508-1518.

[81] J Cai, J Ji, Y Wang, W Huang. 2016. " Numerical simulation and experimental validation of indirect expansion solar-assisted multi-functional heat pump. ." Renewable Energy 93: 280-290.

[82] Fraga, C., Mermoud, F., Hollmuller, P., Pampaloni, E., Lachal, B.,. 2015. "Large solar driven heat pump system for a multifamily building: long term in-situ monitoring. ." Solar Energy 114: 427-439.

[83] C Wang, G Gong, H Su, CW Yu. 2015. "Efficacy of integrated photovoltaics-air source heat pump systems for application in Central-south China. ." Renewable and Sustainable Energy Reviews 49: 1190-1197.

[84] F.J. Aguilar, S. Aledo, P.V. Quiles. 2017. "Experimental analysis of an air conditioner powered by photovoltaic energy and supported by the grid. ." Applied Thermal Engineering 123: 486-497.

[85] M. Giampaolo, P.M. Luigi Colombo, R. Stefano, F. Damiano,. 2016. " Tiles as solar air heater to support a heat pump for residential air conditioning, ." Appl. Therm. Eng. 123: 1412-1421.

[86] G Wang, Z Quan, Y Zhao, P Xu, C Sun. 2015. " Experimental study of a novel PV/T- air composite heat pump hot water system. ." Energy Procedia 70: 537-543.

[87] L Ni, D Qv, R Shang, Y Yao, F Niu, W Hu. 2016. ". Experimental study on performance of a solar-air source heat pump system in severe external conditions and switchover of different functions. ." Applied Thermal Engineering 100: 434-45.

[88] F Niu, L Ni, Y Yao, Y Yu, H Li. 2017. " Performance and thermal charging/discharging features of a phase change material assisted heat pump system in heating mode." Applied Energy 206: 784-792.

[89] S.K. Chaturvedi, T.M. Abdel-Salam, S.S. Sreedharan, F.B. Gorozabel. 2009. "Two-stage direct expansion solar-assisted heat pump for high temperature applications. ." Applied Thermal Engineering 29: 2093-2099.

[90] C Wang, G Gong, H Su, Chuck Wah Yu. 2015. "Dimensionless and thermodynamic modelling of integrated photovoltaics–air source heat pump systems." Solar Energy 118: 175-185.

[91] N Omid, MCJ Luis, SF Alan. 2016. " Review of computer models of air-based curtainwall-integrated PV/T collectors. ." Renewable and Sustainable Energy Reviews 63: 102-117.

[92] J Wu, C Chen, S Pan, J Wei, T Pan, Y Wei, Y Wang, X Wang, and J Su. 2013. "Experimental Study of the Performance of Air Source Heat Pump Systems Assisted by Low-Temperature Solar-Heated Water Advances in ." Mechanical Engineering Volume 2013 8.

[93] J Ji, J Cai, W Huang, Y Feng. 2015. "Experimental study on the performance of solar-assisted multi-functional heat pump based on enthalpy difference lab with solar simulator.." Renewable Energy 75: 381-388.

[94] J Cai, J Ji, Y Wang, W Huang. 2017. "Operation characteristics of a novel dual source multi-functional heat pump system under various working modes." Applied Energy 194: 236-246.

[95] E Mohamed, S Riffat, S Omer. 2017. "Low-temperature solar-plate-assisted heat pump: a developed design for domestic applications in cold climate. ." International journal of Refrigeration 81: 134-150.

[96] WZ Huang, J Ji, N Xu, GQ Li. 2016. "Frosting characteristics and heating performance of a direct-expansion solar-assisted heat pump for space heating under frosting conditions. ." Applied Energy 171: 656-666.

[97] WZ Huang, T Zhang, J Ji, N Xu. 2019. " Numerical study and experimental validation of a direct-expansion solar-assisted heat pump for space heating under frosting conditions. ." Energy and Buildings 185: 224-238.

[98] JB Long, RC Zhang, J Lu, F Xu. 2019. "Heat transfer performance of an integrated solar-air source heat pump evaporator." Energy Conversion and Management 184: 626-635.

[99] Y Liu, J Ma, GH Zhou, C Zhang, WL Wan. 2016. "Performance of a solar air composite heat source heat pump system. ." Renewable Energy 87: 1053-1058.

[100] S. Dubey, G.S. Sandhu, G.N. Tiwari,. 2009. "Analytical expression for electrical efficiency of PV/T hybrid air collector." Appl. Energy 86: 697-705.

[101] Gang Wang, Zhenhua Quan, Yaohua Zhao, Peng Xu, Yuying Sun. 2015. "Experimental study of a novel PV/T-air composite heat pump hot water system." Energy Procedia 537-543.

[102] ML Qu, JB Chen, LJ Nie, FS Li, Q Yu, T Wang. 2016. "Experimental study on the operating characteristics of a novel photovoltaic/thermal

integrated dual-source heat source heat pump water heating system." Applied Thermal Engineering 94: 819-826.

[103] G Besagni, L Croci, R Nesa, L Molinaroli. 2019. "Field study of a novel solar-assisted dual-source multifunctional heat pump. ." Renewable Energy 132: 1185-1215.

[104] SX Lu, RB Liang, JL Zhang, C Zhou. 2019. "Performance improvement of solar photovoltaic/thermal heat pump system in winter by employing vapor injection cycle. ." Applied Thermal Enginnering 155: 135-146.

[105] Clara., G. 2016. "Environmental impact assessments of hybrid photovoltaic–thermal (PV/T) systems – A review. ." Renewable and Sustainable Energy Reviews 55: 234-239.

[106] G Clara, A Inger, GH Anne. 2015. "Solar energy for net zero energy buildings – A comparison between solar thermal, PV and photovoltaic–thermal (PV/T) systems ." Solar Energy 122: 986-996.

[107] K. Kramer, H. Helmers,. 2013. " The interaction of standards and innovation: Hybrid photovoltaic–thermal collectors, ." Solar Energy, 98: 434-439.

[108] "https://en.wikipedia.org/wiki/K-epsilon_turbulence_model," [Online].

[109] Y.AldLI, T.Muneer and D. Henderson. 2013. "Solar absorber tube analysis: thermal simulation using CFD." Internaltional Journal of Loe-carbon Technologies 8: 14-19.

[110] He Wei, Zhang Yang, Ji Jie. 2011. "Comparative experiment study on photovoltaic and thermal solar system under natural circulation of water." Applied Thermal Engineering 16 (31): 3369-79.

[111] Charalambous PG, Maidment GG, Kalogirou SA, Yiakoumetti K. 2007. "Photovoltaic thermal (PV/T) collectors: a review." Applied Thermal Engineering 27: 275-86.

[112] Buker Mahmut Sami, Mempouo Blaise, Riffat Saffa B. 2014. "Performance evaluation and techno-economic analysis of a novel building integrated PV/T roof collector: an experimental validation." Energy Building 76: 164-75.

[113] Hassani Samir, Taylor Robert A, Saad Mekhilef C, Saidur R. 2016. "A caseade nanofluid-based PV/T system with optimized optical and thermal properties." Energy 112: 963-75.

[114] Zhang X, Zhao X, Smith S, et al. 2012. "Review of R & D Progress and practical application of the solar photovoltaic/thermal (PV/T) technologies." Renewable Sustainable Energy Reviews 1 (16): 599-617.

[115] Kroiß A, Präbst A, Hamberger S, Spinnler M, Tripanagnostopoulos Y, Sattelmayer T. 2014. "Development of a seawater-proof hybrid

photovoltaic/thermal (PV/T) solar collector." Energy Procedia 52: 93-103.

[116] Farshchimonfared M, Bilbao JI, Sproul AB. 2016. "Full optimisation and sensitivity analysis of a photovoltaic thermal (PV/T) air system linked to a typical residential building." Solar Energy 136: 15-22.

[117] Ibrahim Adnan, Fudholi Ahmad, Sopian Kamaruzzaman, Othman Mohd Yusof, Ruslan Mohd Hafidz. 2014. "Efficiencies and improvement potentiial of building integrated photovoltaic thermal (PIPV) system." Energy Convers Management 77: 527-34.

[118] " www.fototherm.com/en/.," 2016. [Online].

[119] Hou Longshu, Quan Zhenhua, Zhao Yaohua, Wang Lincheng, Wang Gang. 2016. "An experimental and simulative study on a novel photovoltaic thermal collector with micro heat pipe array (MHPA-PV/T)." Energy Building 124: 60-69.

[120] Zhou Jinzhi, Zhao Xudong, Ma Xiaoli, et al. 2016. "Experimental investigation of a solar driven direct-expansion heat pump system employing the novel PV/micro-channels-evaporator modules." Applied Energy 178: 484-95.

[121] Jouhara H, Szulgowska-Zgrzywa M, Sayegh MA, et al. 2016. "The performance of a heat pipe based solar PV/T roof collector and its potential contribution in districr heating application." Energy.

[122] Chandrasekar M, Senthilkumar T. 2015. " Experimental demonstration of enhanced solar energy utilization in flat PV (photovoltaic) modules cooled by heat spresders in conjunction with cotton wick structures." Energy 90: 1401-10.

[123] Xu Peng, Zhang Xingxing, Shen Jingchun, Zhao Xudong, He Wei, Li Deying. 2015. "Parallel experimental study of a novel super-thin thermal absorber based photovoltaic/thermal (PV/T) system against conventional photovoltaic (PV) system." Energy Rep 1: 30-5.

[124] Jingchun Shen a, Xingxing Zhang a,⇑, Tong Yang a, Llewellyn Tang a, Ali Cheshmehzangi a, Yupeng Wub,. 2016. "Characteristic study of a novel cpmpact solar thermal facade (STF) with internally extruded pin-fin flow channel for building integration." Applied Energy 168: 48-64.

[125] K. S. A, "Solar energy engineering: process and sysytem," Elsecier Inc., 2009.

[126] Emmanouil Mathioulakis, George Panaras, Vassilis Belessiotis. 2012. "Uncertaint in estimating the perfoamance of solar thermal systems." Solar Energy 86: 3450-3459.

[127] G. A. J. Çengel Yunus A. 2015. Heat and mass transfer: fundamentals & applications. New York: McGraw-Hill.

[128] G. A. J. Çengel Yunus A, Heat and mass transfer: fundamentals & applications, New York: McGraw-Hill, 2015.

[129] Alejandro Del Amo, Amaya M artinez-Gracia, Angel A.Bayod-Rujula, Marta Canada. 2019. "Performance analysis and experimental validation of a solar assisted heat pump fed by photovaltaic-thermal collectors." Energy (169): 1214-1223.

[130] Can Şener, Ş.E., Sharp, J.L., Anctil, A.,. 2018. " Factors impacting diverging paths of renewable impacting dierging paths of renewable energy: a review." Renwable Suatainable Energy Review (81): 2335-2342.

[131] Guven, G., Sulun, Y. 2017. "Pre-service teachers' knowledge and awareness about renewable energy." Renewable Sustainable Energy Review (80): 663-668.

[132] Ammar H.Elsheikh, Swellam W.Sharshir, Mohamed Abd Elaziz, A.E. Kabeel, Wang Guilan, Zhang Haiou. 2019. "Modeling of solar energy systems using airtificial neural network: a comprehensive review." Solar Energy (180): 622-639.

[133] Chen, Q.F., Du, S.W., Yuan, Z.X., Sun, T.B., Li, Y.X. 2018. " Experimental study on performance change with time of solar adsorption refrigeration system. ." Appl. Therm.Eng. (138): 386-393.

[134] Sharma, A.K., Sharma, C., Mullick, S.C., Kandpal, T.C. 2017. " Solar industrial process heating: a review. ." Renew. Sustain. Energy (78): 124–137.

[135] M. Sardarabadi, M. Passandideh-Fard, S. Zeinali Heris,. 2014. " Experimental investigation of the effects of silica/water nanofluid on PV/T (photovoltaic/thermal units)." Energy (66): 264-272.

[136] S. Dubey, G.S. Sandha, G.N. Tiwari,. 2009. "Analytical expression for efficiency of PV/T hybrid aor collector." Applied Energy (86): 697-705.

[137] A D. Atheaya, A. Tiwari, G.N. Tiwari, I.M. Al-Helal,. 2015. "Analytical characteristic equation for partially covered photovoltaic thermal (PVT) compound parabolic concentrator (CPC)." Solar Energy (111): 176-185.

[138] J. Yazdanpanahi, F. Sarhaddi, M. Mahdavi-Adeli,. 2015. "Experimental investigation of exergy efficiency of a solar photovoltaic thermal (PVT) water collector based on exergy losses." Solar Energy (118): 197-208.

[139] C. Guo, J. Ji, W. Sun, J. Ma, W. He, Y. Wang,. 2015. "Numerical simulation and experimental validation of tri-functional photovoltaic/thermal solar collector." Energy (87): 470-480.

[140] M. Farshchimonfared, J.I. Bilbao, A.B. Sproul*. 2015. "Channel depth, air mass flow rate and air distribution duct diameter optimization of photovoltaic thermal (PV/T) air collectors linked to residential buildings." Renewable Energy (76): 27-35.

[141] Chen Y, Athienitis AK, Galal K. 2010. "Modelling, design and thermal performance of a BIPV/T system thermally coupled with a ventilated

concrete slab in a low energy solar house: part 1, BIPV/T system and house energy concept." Solar Energy 11 (84): 1892-907.

[142] Henning Helmers, Korbinian Kramer. 2013. "Multi-linear performance model for hybrid (C)PVT solar collectors." Solar Energy (92): 313-322.

[143] M.M. Papari, F. Yousefi, J. Moghadasi, H. Karimi, A. Campo,. 2011. " Modeling thermal conductivity augmentation of nanofluids using diffusion neural networks, ." Int.J. Therm. Sci. (50): 44–52.

[144] M. Mohanraj, S. Jayaraj, C. Muraleedharan,. 2015. "Applications of artificial neural networks for thermal analysis of heat exchangers, a review,." Int. J. Therm. Sci (90): 150-172.

[145] Hadi Kalani, Mohammad Sardarabadi, Mohammad Passandideh-Fard. 2017. "Using artificial neural network models and particle swarm optimization for manner prediction of a photovoltaic thermal nanofluid based collector." Applied Thermal Engineering (113): 1170-1177.

[146] F. Ghani, M.Duke, J.K.Carson. 2012. "Estimation of photovoltaic conversion efficiency of a building integrated photovoltaic/thermal (BIPV/T) collector array using an artificial neural network." Solar Energy (86): 2278-3387.

[147] Giorgio Graditi, Sergio Ferlito, Giovanna Adinolfi, Giuseppe Marco Tin, Cristina Ventura. 2016. "Energy yield estimation of thin-film

photovoltaic plants by using physical approach and artificial neural networks." Solar Energy (130): 232-243.

[148] N.Gunasekar, M.Mohanraj, V.Velmurugan. 2015. "Artificial neural network modeling of a photovoltaic-thermal evaporator of a solar assisted heat pumps." Energy (93): 908-922.

[149] Kamthania, D., Tiwari, G.N. 2012. "Performance analysis of a hybrid photovoltaic thermal double pass air collector using ANN." Applied Solar Energy 3 (48): 186-192.

[150] Hamze Ravaee, Saeid Farahat, Faramarz Sarhaddi. 2012. "Artificial neural network based model of photovoltaic thermal (PV/T) collector." The Journal of Mathematics and Computer Science 4 (3): 411-417.

[151] Majed Ben Ammar, Maher Chaabene, Zied Chtourou. 2013. "Artificial neural network based control for PV/T panel to track optimum thermal and electric power." Energy Conversion and Management (65): 372-380.

[152] Tamer Khatib, Ahmed Ghareeb, Maan Tamimi, Mahmoud Jaber, Saif Jaradat. 2018. "A new offline method for extracting I-V characteristic curve for photovoltaic modules using artificial neural networks." Solar Energy (173): 462-469.

[153] Engin Karatep, Mutlu Boztepe, Metin Colak. 2006. "Neural network based solar cell model." Energy Conversion and Management (47): 1159-1178.

[154] Celik, Ali Naci. 2011. "Artificial neural network modelling and experimental verification of the operating current of mono-crystalline photovoltaic modules." Solar Energy (85): 2507-2517.

[155] Francesco Bonanno, Giacomo Capizzi, G.Graditi, Christian Napoli, Giuseppe Marco Tina. 2012. "A radial basis function neural network based approach for the electical characteristics estimation of a photovoltaic module." Applied Energy (97): 956-961.

[156] Sonveer Singh, Sanjay Agarwal, G.N. Tiwari, Deepika Chauhan. 2015. "Application of genetic algorithm with multi-objective function to improve the efficiency of glazed photovoltaic thermal system for New Delhi (India) climate condition." Solar energy (117): 153-166.

[157] Sonveer Singh, Sanjay Agrawal , Arvind Tiwari , I.M. Al-Helal , D.V. Avasthi. 2015. "Modeling and parameter optimization of hybrid single channel photovoltaic thermal module using genetic algorithms." Solar Energy (113): 78-87.

[158] Sonveer Singh, Sanjay Agrawal. 2015. "Parameter identification of the glazed photovoltaic thermal system using Genetic Algorithm–Fuzzy System (GA–FS) approach and itscomparative study." Energy Conversion and Management (105): 763-771.

[159] Gwang-Hee Kim, Jie-Eon Yoon, Sung-Hoon An, Hun-Hee Cho, Kyung-In Kang. 2004. "Neural networkmodel incorporating a genetic algorithm

in estimating construction costs." Building and Environment (39): 1333-1340.

[160] F. Sobhnamayan, F. Sarhaddi , M.A. Alavi , S. Farahat , J. Yazdanpanahi. 2014. "Optimization of a solar photovoltaic thermal (PV/T) water collector based on exergy concept." Renewable Energy (68): 356-365.

[161] Sonveer Singh, Sanjay Agrawal , Rajit Gadh. 2015. "Optimization of single channel glazed photovoltaic thermal (PVT) array using Evolutionary Algorithm (EA) and carbon credit earned by the optimized array." Energy Conversion and Management (105): 303–312.

[162] J. Antonanzas, N. Osorio, R. Escobar,R. Urraca, F.J. Martinez-de-Pison, F. Antonanzas-Torres. 2016. "Review of photovoltaic power forecasting." Solar Energy (136): 78-111.

[163] S. Haykin, Neural networks and learning machines., USA: Pearson, Upper Saddle River,NJ, 2009.

[164] Jani, D.B., Mishra, M., Sahoo, P.K. 2017. "Application of artificial neural network for predicting performance of solid desiccant cooling systems – a review." Renew.Sustain.Energy Rev. (80): 352-366.

[165] Facão, J., Varga, S., Oliveira, A.C. 2004. " Evaluation of the use of artificial neural networks or the simulation fof hybrid solar collectors. ." Int. J. Green Energy 3 (1): 337-352.

[166] Stephan Fischer, Patrick Freg, Harald Druck. 2012. "A comparison between atate-of-the-art and neural network modelling of solar collectors." Solar Energy (86): 3268-3277.

[167] Shile Wang, Ting Zhang. 2019. "Research on innovation path of school ideological and political work based on large data." Cluster Computing (22): 3375-3383.

Appendix: List of publications

Paper:

Xinru Wang, Liang Xia, Chris Bales, Xingxing Zhang, Benedetta Copertaro, Song Pan, Jinshun Wu. A systematic review of recent air source heat pump systems assisted by solar thermal, photovoltaic and photovoltaic/thermal sources. Renewable Energy. Volume 146, 2020 (02) 2472-2487;

Song Pan, Saisai Du, **Xinru Wang***, Xingxing Zhang , Liang Xia, Liu Jiaping, Fei Pei, Yixuan Wei. Analysis and interpretation of the particulate matter (PM2.5 and PM10) concentrations at the subway stations in Beijing, China. Sustainable Cities and Society 45 (2019) 366–377.

Yaxiu Gu, Junwei Wang, **Xinru Wang***, Mohua Li, Song Pan, Guangdong Liu, Wentao Wang, Zexiang Gong. Theoretical analysis of annular elliptic finned tube evaporative condenser based on field measurement. Journal of Thermal Science (Accepted);

Xinru Wang, Liang Xia, Xingxing Zhang, Jinshun Wu, Yixuan Wei, Song Pan, Meng Liu, Zu Wang, Danwei Jiang. Thermal performance of solar collector with a novel absorber plate in PV/T assisted air source heat pump system for an office heating application in Beijing, China. Applied Energy (submitted);

Xinru Wang, Liang Xia, Xingxing Zhang, Jinshun Wu, Yixuan Wei, Song Pan, Zu Wang. Performance study of a solar PV/T assisted air source heat pump system in Beijing, China. Solar Energy (submitted);

Song Pan, **Xinru Wang**, Yixuan Wei, Xingxing Zhang, Guangying Ren, Da Yan, Yong Shi, Jinshun Wu, Liang Xia, Jingchao Xie, Jiaping Liu. Cluster analysis for occupant-behavior based electricity load patterns in buildings: A case study inShanghairesidences, Building Simulation December 2017, Volume 10, Issue 6, pp 889–898;

Fan Zhang, Hasan Fleyeh, **Xinru Wang**, Minghui Lu. Construction site accident analysis using text mining and natural language processing techniques. Automation in Construction 99 (2019) 238–248.

Mengjie Han, Ross May, Xingxing Zhang, **Xinru Wang**, Song Pan, Da Yan, Yuan Jin, LiguoXu. A review of reinforcement learning methodologies for controlling occupant comfort in buildings. Sustainable Cities and Society 51 (2019) 101748.

Mengjie Han, Ross May, Xingxing Zhang, **Xinru Wang**, Song Pan, Da Yan, Yuan Jin. A novel reinforment learning method for improving occupant comfort via window opening and closing. Sustainable Cities and Society 5 (2020) 102247;

Song Pan, YiqiaoLiu, Lang Xie, **Xinru Wang**, Yanping Yuan, Xiaoyu Jia. A thermal comfort field study on subway passengers during air conditioning season in Beijing. Sustainable Cities and Society 5 (2020) 102218.

Yixuan Wei, Haowei Yu , Song Pan, Liang Xia, Jingchao Xie, **Xinru Wang** , Jinshun Wu, Weijie Zhang, Qingping Li. Comparison of different window behavior modeling approaches during transition season in Beijing,China. Building and Environment ,157 (2019) 1–15 .

Book chapter

Xingxing Zhang, **Xinru Wang**, Xudong Zhao. Solar system design and energy performance assessment approaches. In book: advance energy efficiency technologies for solar heating, cooling and power generation. DOI: 10.1007/978-3-030-17283-1_12.

Xudong Zhao, Chuangben Wen, Xingxing Zhang, Zhangyuan Wang, **Xinru Wang**. Study of a novel liquid vapour separator incorporated gravitational loop heat pipe. In book: recent advances in heat pipes. DOI: 10.5772/intechopen.86048

Patent

Xinru Wang et al. The software for prediction of the performance of PV/T collector (2020SR0469830) (in Chinese)

Xinru Wang et al. The software for prediction of the performance of PV/T collector with half-stable conditions (2020SR0090613) (in Chinese)

Xinru Wang et al. The software for prediction of the particle matters in subway stations (2019SR0926051) (in Chinese)